

FAÇADE INTERNET OF THINGS (FIOT): A HUMAN-SENSING, TWO- FAÇADE
COMMUNICATION APPROACH TO ACHIEVE GLARE REDUCTION,
OPTIMIZED DAYLIGHTING, AND SOLAR ENERGY COLLECTION

A Dissertation

by

RANIA LABIB

Submitted to the Office of Graduate and Professional Studies of
Texas A&M University
in partial fulfillment of the requirements for the degree of

DOCTOR OF PHILOSOPHY

Chair of Committee,	Mark Clayton
Co-Chair of Committee,	Ann McNamara
Committee Members,	Stephen Caffey Michael O'Brien
Head of Department,	Robert Warden

December 2019

Major Subject: Architecture

Copyright 2019 Rania Labib

ABSTRACT

The use of large glazed façades in buildings can cause a disabling glare that can impair the vision of the occupants of surrounding buildings. In order to avoid glare, building occupants tend to close their blinds and depend on artificial lighting, thus increasing lighting-based energy consumption. Solar reflections can also overheat surrounding areas and so negatively impact the thermal comfort of occupants in surrounding buildings.

To resolve the various issues caused by reflective façades, this research study proposes the Façades Internet of Things (FIoT), a model that facilitates the communication between two building facades, which can adapt to human occupancy and weather conditions in order to reduce glare, to optimize indoor daylighting, and to maximize solar energy collection.

Although communication between different building elements within the same building is extensively studied by researchers, the proposed FIoT is the first novel approach that enables communication between building elements, in this case building facades, in two different buildings.

To examine the performance of the proposed FIoT framework, computer-based glare, daylighting, and solar radiation simulations of two buildings and the simulations of a

virtual Wireless Sensor Network (WSN) that connects both buildings are carried out. Both buildings face one another, and one building is fitted with the proposed façade that is installed on front of the existing facade. Glare is examined from 15 views inside the building that faces the reflective façade. Simulations confirmed that glare is greatly reduced by employing a FIoT to dynamically adjust the surfaces; the average occurrences of intolerable glare from all 15 views in one month (December) decreased from 40% of the time to 0.87%.

FIoT not only eliminated glare but also improved the daylighting performance inside the building, increasing both the daylighting uniformity ratio and the illuminance levels. Through usage of the proposed workflow, the lighting uniformity ratio (LUR) increased on December 21, between 8:00 and 17:00, from 0.24–0.29 to 0.34–0.45. Additionally, the hourly average illuminance values improved by 88–268% during the winter solstice.

Finally, compared to traditional vertical BIPV, FIoT-enabled BIPV façade elements increased the amount of solar radiation falling on them by 190–250% during the winter solstice and by 300–520% during the summer solstice.

DEDICATION

I dedicate this to my father who passed away last year, the man who instilled in me a strong work ethic and a love of learning. I know that he is looking down on me.

I dedicate this to my mother who taught me hard work and dedication.

I dedicate this work to my awesome husband Nagi; his encouragement and support of me goes beyond what words can adequately express.

To my precious son John, and my beautiful daughters Judy and Julia, thank you for your understanding when I was distracted or not fully present for you when writing this dissertation.

ACKNOWLEDGEMENTS

I would like to thank my committee chair, Dr. Clayton, and my co-chair Dr. McNamara for their kind support and their insightful comments. I am quite appreciative of both to serve on my dissertation committee on such short notice.

I am appreciative of Prof. O'Brien, an excellent design professor, for his continuous support and for sharing with me his tremendous experience in building facade design.

I am grateful to Dr. Caffey, an excellent mentor, for his great support and his invaluable feedback that opened my eyes to new research avenues for future work.

Thanks also, go to my friends and colleagues and the department faculty and staff for making my time at Texas A&M University a great experience.

Finally, thanks to my family for their encouragement and their patience and love.

CONTRIBUTORS AND FUNDING SOURCES

Contributors

This work used the Extreme Science and Engineering Discovery Environment (XSEDE), which is supported by National Science Foundation grant number ACI-1548562

Through allocation ID TG-CDA160011.

I thank Martin Kandes for his assistance with submitting batch jobs to the XSEDE platform, which was made possible through the XSEDE Extended Collaborative Support Service (ECSS) program.

.

Funding Sources

This research received no specific grant from any funding agency in the public, commercial, or not-for-profit sectors.

TABLE OF CONTENTS

	Page
ABSTRACT	ii
DEDICATION	iv
ACKNOWLEDGEMENTS	v
CONTRIBUTORS AND FUNDING SOURCES.....	vi
TABLE OF CONTENTS	vii
LIST OF FIGURES.....	x
LIST OF TABLES	xiii
CHAPTER I INTRODUCTION AND LITERATURE REVIEW	1
Introduction.....	1
Literature Review	5
Negative Impacts of Solar Reflections.....	6
Decreased Workers’ Performance.....	6
Increased Errors and Task Times Leading to Reduced Economic Returns	7
Dependence on Artificial Lighting Leading to an Increase in Energy Consumption	10
Visual Discomfort	11
Increase in Indoor Air Temperature Leading to an Increase in Cooling Loads ...	12
Microclimate Change	12
Vegetation Burn Caused by Solar Reflections	14
Driving Performance	15
Melting and Damaging of Building Materials Caused by Solar Reflections	15
Research Objectives	16
CHAPTER II DAYLIGHTING AND GLARE	17
Introduction to the History of Daylighting Design	17
The Energy Crisis and Daylighting	21
Daylighting Benefits	21
Daylighting and Green Building Codes	23
Introduction to Glare	25

Glare Indices	26
CHAPTER III INTERNET OF THINGS AND SMART FACADES.....	30
Introduction to Smart Cities, IoT, WSN, and Smart Façades	30
The Benefits of Using the IoT in Buildings and Cities.....	32
Sensors and Actuators to Achieve Human-centered Comfort.....	32
Decreased Energy Consumption	34
Data Collection and Profiling.....	35
The Emergence of Smart Building Façades.....	38
Wireless Sensor Networks	40
The Labor cost and maintenance of WSN.....	41
Literature Review Summary	44
CHAPTER IV METHODOLOGY	47
Introduction to Methodology	47
The Proposed Façade and Wireless Sensor Network.....	49
Stage One: The Geometric Model and Glare Analysis.....	51
Preparation of the Geometric Model	51
Glare Simulations	55
Key Challenges in Large-Scale Glare Simulations	60
Automating Glare Simulations, Parallel Computing, and Results Analysis	61
Visualizing Glare Simulations Results.....	67
Stage Two: Glare Elimination, Daylighting, and Solar Energy Optimization.....	68
Glare Elimination	69
Sunlight Tracking.....	69
Computer Vision Recognition.....	71
Improving Daylighting Performance.....	73
Solar Energy Collection Optimization	74
Stage Three: Wireless Sensor Network Design	74
CHAPTER V VALIDATION.....	80
Introduction	80
Glare Reduction.....	80
Improvement in Daylighting Performance.....	86
Solar Energy Collection	92
CHAPTER VI CONCLUSIONS AND DISCCUSION.....	96
Conclusion.....	96
Study Limitations	98
Discussion and Future Studies	99

REFERENCES.....	102
APPENDIX A THE XSEDE HIGH PERFORMANCE COMPUTING ENVIRONEMNT.....	114
APPENDIX B PYTHON CODE	119

LIST OF FIGURES

	Page
Figure 1 The architecture of WSN	41
Figure 2 Methodology Workflow	48
Figure 3 The proposed facade. a) The façade elements rotate around the X-axis (angle a) and around the Z-axis (angle b). b) Examples of different façade configurations.	50
Figure 4 The modeled tower (blue), the 3-floor building (red), and the context building (brown)	54
Figure 5 The properties of the glazing used in this study in Optics	58
Figure 6 The wavelength of the reflective glazing that is used in this study	58
Figure 7 A screenshot of the Linux-based program, Optics2Rad, which is used to convert the Optics output to a radiance material definition.....	59
Figure 8 The execution of a batch simulation job on a computer, as opposed to its execution in an HPC environment.....	62
Figure 9 Executing thousands of image-based glare simulations for all 15 views with Ladybug and a custom Python script.....	65
Figure 10 The resulting HDR images for all 15 views on December 17 at 13:00. Glare sources are highlighted in Magenta	66
Figure 11 False color images of the resulting HDR renderings for all 15 views, on December 17 at 13:00. Luminance values (cd/m ²) are illustrated in colors. ...	67
Figure 12 Example of the HTML glare heatmaps of two views in the small buildings. The maps represent DGP values of every HOY between 8:00 and 18:00.....	68
Figure 13 A custom Python-based Grasshopper component to calculate all HOY when the sunlight falls of the reflective façade	70
Figure 14 The custom-made component eliminates all sunlight being blocked by surrounding buildings, which work as shading contexts. In this image, blocked sunlight is shown in blue, while actual sunlight falling on the façade is shown in orange.....	71

Figure 15 A rendered view with the reflective façade assigned a green color to be used for image analysis with OpenCV module library.....	72
Figure 16 Images that have a DGP value over 0.35 and that occurred at an hour when the sun hits the reflective façade are further analyzed by means of OpenCV for Python. The output is stored in an SQL database.	73
Figure 17 An example of the Python script workflow and the wireless sensor network design at a specified HOY in Room 1 in the tower. The execution of the script results on moving the façade elements in front of Room 1, as is shown in the boxes highlighted in green. The sensors and the SQL input are fed to the WSN, shown in dashed blue lines, and the WSN output is shown in red dashed lines.	76
Figure 18 The simulation of the WSN with virtual sensors and actuators. The WSN is simulated through the use of Node Red, which is hosted on IBM’s Watson platform. a) A node to start the flow; b) a sub-flow that contains a virtual set of sensors (partially illustrated in the upper box); c) A connection the SQL database; d) a connection to an online live weather app; e) a connection to the Python script; and f) a sub-flow that contains the output of the Python script that contains a set of rotation angles that are fed to a set of virtual actuators (partially illustrated in the lower box).....	78
Figure 19 Boxplot that shows the DGP values of the hourly simulations between 8:00 and 18:00 through the month of December of all 15 views in the base case three-story building.....	83
Figure 20 Boxplot that shows the DGP values of the hourly simulations throughout the month of December between 8:00 and 18:00 for all 15 views in the three-story building with the proposed façade and the WSN system installed	85
Figure 21 The illuminance grid in the base case from 8:00 to 16:00 on December 21 ...	88
Figure 22 The illuminance grid in the proposed case with the WSN and smart facade from 8:00 to 16:00 on December 21	90
Figure 23 Minimum, maximum, and average illuminance of both the base case and the proposed case with the WSN and smart façade installed between 8:00 and 17:00 on December 21	91
Figure 24 LUR values of both the case study and the proposed WSN and smart façade between 8:00 and 17:00 on December 21.....	92
Figure 25 The range (minimum and maximum) of the direct solar radiation falling on the proposed façade surfaces by changing both angles around the X-axis	

and Z-axis on December 21 from 8:00 to 17:00, compared to the amount of solar radiation falling on a traditional vertical BIPV.....	93
Figure 26 The range (minimum and maximum) of the direct solar radiation falling on the surfaces by changing both angles around the X-axis and Z-axis on June 21 from 8:00 to 17:00, compared to the amount of solar radiation falling on a traditional vertical BIPV	95
Figure 27 The technical specifications of the XSEDE HPC platform	114
Figure 28 The status of computing jobs progress on 1000 nodes accessed through an SSH interface	115
Figure 29 A list of bash files that contain Radiance commands	116
Figure 30 The computing resources that are available to the author through XSEDE, over 15000 of computing hours were used for the purpose of this research study (shown in the red box), this is equal to about two years of computing time	117
Figure 31 Example batch job that is submitted to the XSEDE platform, the batch job facilitated running 1000 tasks parallelly on individual computing nodes	118

LIST OF TABLES

	Page
Table 1 Glare regions and daylight glare index	27
Table 2 Glare regions and DGP	28
Table 3 A comparison between the annual and the point-in-time glare calculation methods.....	57
Table 4 Radiance material properties of the buildings' materials.....	60
Table 5 DGP minimum, maximum, median, quartile 1, quartile 3, and the interquartile range values for all 15 base case views between December 1 to 31 from 8:00 to 18:00	82
Table 6 The percentage of different glare type occurrences for the total daylight hours in December in the base case and the total number of glare occurrences when the DPG is higher than 0.35	83
Table 7 DGP values in the case study with the proposed façade and WSN system installed. The values consist of minimum, maximum, median, quartile 1, quartile 3, and the interquartile range values for all 15 views between December 1 and 31 from 8:00 to 18:00	85
Table 8 The percentage of different glare type occurrences for the total daylight hours in December in the case study with the proposed façade and WSN installed and for the total number of glare occurrences when the DPG is higher than 0.35	86
Table 9 Minimum, maximum, and average illuminance, and the LUR of the base case study from 8:00 to 17:00 on December 21	87
Table 10 Minimum, maximum, and average illuminance, and the LUR of the proposed WSN and smart facade from 8:00 to 17:00 on December 21	89
Table 11 The amount of solar radiation falling on a traditional vertical façade with BIPV and the range of solar radiation falling on the proposed façade surfaces through the use of different rotation angles on December 21 between 8:00 and 17:00	93
Table 12 The amount of solar radiation falling on a traditional vertical façade with BIPV and the range of solar radiation falling on the proposed façade	

surfaces through the use of different rotation angles on June 21 between
8:00 and 17:0095

CHAPTER I

INTRODUCTION AND LITERATURE REVIEW

Introduction

Reflective glazing is a popular architectural element that is widely used in building façades, especially tall buildings in urban settings. The modern architectural style, which employed full glazed building façades, remains a source of inspiration for architects around the world, despite significant variations in daylight availability and thermal requirements across different climatic regions. The growing preference to use large glazed façades in buildings, regardless of geographical location or climatic region, causes severe visual discomfort due to the reflection of sunlight falling on buildings' surfaces. These intense reflections can cause a disabling glare, which can impair the vision of surrounding buildings' occupants and prevent them from performing their daily tasks. A 2014 research study that examined glare in a residential building caused by sun reflections off a nearby commercial building façade covered in photovoltaic panels concluded that solar reflections can cause a disabling glare for 30 minutes up to 72 days a year and for over an hour for up to 34 days a year [1].

In order to avoid glare, building occupants tend to close their blinds and depend on artificial lighting, thus increasing lighting energy consumption that is estimated to account for 25 to 40% of commercial buildings' total energy consumption [2].

Solar reflections caused by reflective façade materials not only cause glare, but can also overheat surrounding areas, negatively impacting the thermal comfort of both pedestrians and the occupants of surrounding buildings. Consequently, an increase in building cooling capacity is necessary to mitigate the problem of overheated spaces caused by solar reflections [3–5].

In addition to the growing use of full glazed façades in urban areas, architects and designers have been increasingly incorporating building-integrated photovoltaics (BIPVs) into their designs. BIPVs are photovoltaic units that have solar collection capabilities; they can be used to replace traditional building envelope materials, such as roofs, and façades [6]. They are frequently incorporated into the construction of new buildings and used to retrofit existing building façades. One factor in BIPVs' popularity is that their initial cost may be partially offset by a reduction in the cost of other cladding materials, as well as their ability to generate some of the electricity used in the building. Another advantage of using BIPV modules is that their installations can earn up to three Leadership in Energy and Environmental Design (LEED) credits, making them highly desirable for architects and clients [7]. In terms of reflectivity, BIPV panels behave like glazed building façades, causing glare when sunlight reflects off the modules and into surrounding buildings.

An example of reflective building materials causing glare is a new installation of a PV array with 2,478 panels at a Massachusetts airport. This array has caused severe specular

reflections that affect the visibility of aircraft on the taxiway. It has also caused a disabling glare, resulting in difficulties viewing computer screens inside the airport control tower [8]. Similarly, a 42-story high-rise building in Dallas, TX (the Museum Tower) was fitted with a full glazed façade, which has caused intense specular reflections into the Nasher sculpture museum. The problem has caused glare, cases of extreme heat inside the museum, and even damage to the sculptures on display, many of which have had to be moved away to protect them from damage from the reflected sun rays. Although museum officials have spent three years and more than \$1 million working on possible solutions, no feasible approaches have yet been found [4,9,10]. To combat the situation in the meantime, the Nasher Sculpture Museum has installed internal blinds which has negatively impacted its lighting conditions. The Nasher Museum's garden has also been affected by the solar reflections caused by the museum tower's façade. Specifically, these solar reflections have created hot spots in both exposed and shaded sections of the garden. Daily readings by Museum officials have recorded temperatures at those hot spots approximately 40 degrees higher than the air temperature [11].

To resolve the various issues, such as glare and thermal discomfort, caused by reflective façades in urban areas, this research study proposes the Façades Internet of Things (FIoT), a novel model of communicating building façades designed to use embedded intelligence enabled through a set of built-in microcontrollers and sensors that collect occupancy data and data from the surrounding environment (e.g. weather, temperature,

and lighting levels). To avoid reflecting sunlight off one building and onto another, two communicating façades will share their collected data, including occupancy data, and then change their form accordingly in order to re-direct sunlight away from occupants' view, thereby eliminating disability glare and thermal discomfort. The proposed FIoT framework could serve as a model for improving future smart cities, which have gained the interest of researchers and urban designers and the support of governmental entities around the world for the past two decades.

Recently, researchers have been examining the use of Internet of Things (IoT) to facilitate the automation of complex tasks in buildings based on real-time data that is collected through various sensors [12]. Some researchers demonstrated that IoT not only facilitated the automation of complex tasks but also enabled the communication between different building elements within one building, thus, transforming traditional buildings into smart ones [13,14].

Based on the literature review on the negative impact of the solar reflections in urban settlements, it is evident that buildings' facades have an impact not only on their occupants but also on each other; therefore, it is crucial to examine the effect of retrofitting façade with new IoT technologies on other building facades.

The literature review on IoT technologies and smart facades shows that researchers have been integrating IoT technologies in building to address various issues in buildings while

treating building facades as individual entities regardless of the surrounding buildings [15,16]. While this approach can serve the purpose of addressing the targeted issue in the studied building, it can cause severe negative impact on other surrounding buildings' facades. Thus, this research study introduces a novel approach that has never been examined before (based on the research literature conducted by the author). The proposed FIoT approach takes into consideration the impact of manipulating one facade's elements while carefully examining consequences this can have on another façade by facilitating communication between both facades via WSN.

Future studies are needed to expand the capabilities for such a communication model in order to adapt to climate change, technology advancement, and accelerated urban growth. An expanded section on future studies is included in chapter IV.

Literature Review

In addition to visual and thermal problems, the abundant use of reflective façade materials in dense urban areas can lead to various other problems, such as microclimate change, vegetation burns, poor indoor daylighting, and the melting of building materials. The following sections will discuss the various problems caused by solar reflections. Next, two subsequent sections will introduce the IoT and its benefits and then introduce smart façades.

Negative Impacts of Solar Reflections

In addition to causing visual and thermal discomfort, solar reflections can have a negative impact on the surrounding environment. For example, sun rays bouncing off reflective materials can contribute to vegetation burn, damage building materials, and alter local regions' microclimates [3]. The following sections explain in detail the negative impacts of solar reflections in urban areas on building occupants, outdoor pedestrians, and the environment.

Decreased Workers' Performance

Discomfort glare impairs visual performance and well-being, leading to premature fatigue, headaches, blurred vision, eye strain, and bad moods [17,18]. Glare problems can worsen in office environments requiring frequent and extended computer usage. The growing use of various digital technologies in offices can create substantial challenges for office occupants as they attempt to process information and perform visual tasks throughout the day. Kuratorium et al. stated that workers switch views among manuscripts, their keyboards and their computer monitors up to 30,000 per day [19]. Creating a visually comfortable office environment could help reduce the strain on these workers' eyes and ultimately increase their productivity.

In a 1959 study, Hopkinson concluded that when the eye is subjected to intolerable glare, the pupil not only contracts, but varies in diameter, dilating and contracting irregularly every few seconds. This can cause eye strain and fatigue that may reduce

workers' performance [20]. Similarly, a 2014 study concluded that subjective evaluations of discomfort glare were highly correlated with eye movement and pupil constriction. Severe glare discomfort increased the speed of eye movement and increased pupil constriction. The study results suggested that the correlation between discomfort glare and physiological responses represents an objective way to characterize and evaluate discomfort glare that may overcome the problems of conventional subjective evaluations [21].

In addition to eye strain and fatigue, discomfort glare contributes to bad moods and poor relaxation [22]. These issues, in turn, can ultimately reduce workers' performance and negatively affect economic returns.

Increased Errors and Task Times Leading to Reduced Economic Returns

In commercial built environments, workers' visual discomfort caused by glare can negatively impact their performance, leading to lower economic returns. A 1985 study conducted by Garcia and Wierwille at Virginia State University concluded that glare increased the time required to read a relatively simple paragraph displayed on a computer screen. When task difficulty was measured by subjective ranking, glare was found to increase the amount of time required to read relatively easy passages. Other findings included a general increase in reading time and a decrease in the proportion of correct answers with increases in task difficulty for both subjective and objective rankings of difficulty [23].

Glare has been a major problem in airports, where intense sun reflections bouncing off reflective surfaces, such as solar arrays, cause disabling glares that temporarily blind airport workers. For example, a new installation of a PV array with 2,478 panels at a Massachusetts airport has caused severe specular reflections that affect the visibility of the aircraft on the taxiway. It has also caused a disabling glare, limiting workers' ability to view computer screens inside the airport control tower [8]. The negative impacts of glare on the work environment have undesirable effects that can lead to economic losses.

To avoid glare, employees close their blind and depend on artificial lighting which in turn transform interior spaces into unpleasant environments. Spaces with no daylight have been linked to seasonal affective disorder SAD [24]

In addition to eye strain and fatigue, discomfort glare contributes to bad moods and poor relaxation [22]. These issues, in turn, can ultimately reduce workers' performance and negatively affect economic returns.

Goetzel et al. have studied the economic effect of some health issues that employees face during work; some of the issues that he studies include headaches/migraine, hypertension, sadness/depression [25]. As discussed earlier, glare has been found to directly cause headaches and hypertension, and indirectly causing seasonal affective disorder that leads to sadness and depression. Therefore in the next section I will focus

on explaining Goetzel's results in relation to three issues; headaches, hypertension, and sadness.

Goetzel et al. reported that based on surveys performed by private and governmental institutions that sadness, hypertension, and migraines are three of the top 10 conditions that contribute to an economic loss in work setting. Those conditions contributed to the following (estimated cost was based on 240 work days/per year, 8 hours/day and a \$23.25 hourly salary):

- High absenteeism rates; which are estimated to be as high as 22.8%, 0.9%, and 10.1% respectively and an average annual dollar impact (per employee per year) of \$4,741, \$170, and \$1,988 respectively.
- Presenteeism, which is working while sick, rates, are estimated to be as high as 24.5%, 10.4%, and 28.5% respectively. And an average annual dollar impact (per employee per year) of \$6,720, \$3,210, and \$ 9,120 respectively.

Conversely, if we assume that 50% of our 40 employees that occupy both buildings in the proposed study (one employee per room) suffer one of the conditions mentioned above the yearly dollar impact can range from \$67,600 to \$229,220.

Dependence on Artificial Lighting Leading to an Increase in Energy Consumption

Disabling glares and glares that cause discomfort can negatively impact building occupants. Therefore, in order to avoid glare, occupants tend to turn to artificial lighting in their interior spaces. However, a great amount of energy can be saved by using daylight rather than artificial lighting, since such a shift can reduce heating and cooling loads.

In the 1960s, energy consumption was not a huge concern. For example, buildings were sometimes designed without light switches, since it was believed that it was more economical to leave lights on all the time [26]. The role of energy consumption in buildings was completely ignored until the energy crisis of 1973, when the countries of the Organization of Petroleum Exporting Countries (OPEC) raised their energy prices. In response to this crisis, passive solar technologies emerged and were soon adapted. Furthermore, architects began to show interest in using sunlight as a major light source to reduce energy demands [27].

The US Department of Energy (DOE) reported that the residential sector's lighting use in 2010 represented 9.6% of total energy consumption [2]. In terms of energy, this amounts to approximately 23.8 billion kWh in one year. In other words, in 2010, lighting in residential buildings produced approximately 137 billion tons of carbon dioxide. When it comes to the commercial sector, the same report shows even bigger numbers. The commercial sector's lighting use in 2010 was estimated to be 17.1% of total energy

consumption, which is equal to 29.1 billion kWh and 183.6 tons of carbon dioxide.

Interestingly, the report also states that there has been a 3% reduction in energy use and a 6.6% reduction in carbon dioxide emissions from lighting consumption in commercial buildings since 2008. This improvement is due to the efforts of recently founded green building movements and the set of newly implemented energy codes and legislations.

Visual Discomfort

Glare is a visual sensation caused by extreme brightness resulting from intense sunrays bouncing off reflective surfaces. There are two types of glare: discomfort glare and disability glare. The former is a sensation of annoyance or even pain induced by bright sources, and the latter is a temporary blinding caused by intense brightness [28].

In a recent study performed by a group of researchers led by Suk, a large group of human subjects was interviewed in different exterior scenes surrounding a glazed building. Later, the interviews were compared with 84 High Dynamic (HDR) images, which are images that contain high range of luminance values in each pixel. The HDR images were taken to analyze the existing glare in the exterior setting. A statistical analysis confirmed that intolerable, disturbing, perceptible, and imperceptible glares existed in multiple exterior locations around the façade; the human subjects reported experiencing the disturbing (14%), perceptible (36%), and imperceptible (50%) glares across all locations [29].

Increase in Indoor Air Temperature Leading to an Increase in Cooling Loads

Intense solar reflections bouncing off nearby building façades not only cause glare and visual discomfort, but can also cause heat gains, leading to thermal discomfort and increased cooling loads. Cooling loads are significant in commercial buildings, and more than one-third are due to solar heat gains through windows [30,31].

A 42-story high-rise museum in Dallas, Texas, was fitted with a large array of PV panels on its façade. These panels caused intense specular reflections into the adjacent Nasher Sculpture Museum, resulting in glare and extreme heat gain inside the museum. These issues, in turn, damaged the sculptures in display, forcing sculptures to be moved away from the window to protect them from further damage. Museum officials spent three years and more than \$1 million working on possible solutions to the problem [4].

Similarly, in a 2016 study, a group of researchers led by Suk worked to quantify the exterior glare caused by a glazed building. Suk documented the existence of thermal discomfort, noting that “In front of the bakery, the authors have experienced not only serious visual discomfort but also excessive thermal discomfort from the reflected sunlight. Inside the bakery, the reflected sunlight penetrated very deep into the space with a low incident angle with potential problems to customers inside” [29].

Microclimate Change

Solar reflections caused by reflective building materials can lead to thermal and visual changes to the surrounding microclimate, making pedestrians uncomfortable in outdoor

spaces. For example, one research study examined the effects of the solar reflections and glare caused by the Walt Disney Concert Hall (WDCH) on the nearby microclimate. The WDCH, which was designed by Frank Gehry, has a curved skin composed of convex and concave surfaces. The majority of the building's skin is made of brushed stainless steel, but the Founders Room and the marquee for the California Institute of the Arts Roy and Edna Disney California Arts Theater (REDCAT) are made of polished stainless steel. In addition to using infrared thermography to measure heat gains around the building, the researchers embedded data loggers in the surrounding sidewalk. Upon analyzing the digital images and the readings of the data loggers, the researchers found a noticeable increase in the ground surface temperature in the vicinity of the REDCAT marquee. Furthermore, a digital glare simulation confirmed that the building's skin caused both discomfort and disability glares among pedestrians at various times of the year [3,32].

A study performed at the Swiss Federal Institute of Technology Zurich (ETHZ) confirmed that solar reflections off of building façades in urban canyons can change the microclimate, thereby increasing energy demands in surrounding buildings [33]. The authors noted that, “[d]ue to multiple reflections more solar and thermal radiation is absorbed in the façades of buildings in street canyons than at façades of stand-alone buildings.” In order to address the effects of the solar reflections, the radiation exchange between urban surfaces was examined. In street canyons, the net radiation on building façades, which is the sum of solar and long-wave radiation, including multiple

reflections, is higher than that on façades of stand-alone buildings. Therefore, façade surface temperatures are higher in urban than in rural areas. These higher temperatures can directly cause higher space cooling demands. The researchers confirmed that cooling demands for buildings affected by solar reflections were up to 500% higher.

Vegetation Burn Caused by Solar Reflections

An additional concern relating to reflected solar energy is the potential negative impact on plant life. It is commonly known that vegetation is able to sustain excessive sunlight exposure during the growing season by regulating its temperature via evaporation from leaves or convection to the air to prevent physical damage [34]. However, some research studies have shown that modifying daylight exposure patterns in laboratories can have a negative impact on vegetation [35]. For instance, the solar reflections bouncing off the "C-Curve", a 2007 sculpture by the British artist Anish Kapoor, have caused physical damage to surrounding grass. The sculpture is made of stainless steel and shaped like a giant letter C lying sideways on the ground. The outer surface is convex. Together, the shape and optical properties of the sculpture's outer surface create intensely concentrated sunlight reflections that cause severe patches of burnt grass [36]. In 1977, Simms likened the sculpture to the mirrors reportedly used by the ancient Greek mathematician Archimedes to concentrate rays of sunlight and burn the ships of an invading Roman fleet, an ancient methodology called the "death ray" [37]

Driving Performance

Glare not only affects the visual performance of building occupants, but also causes extreme visual discomfort to drivers, potentially leading to drivers' fatigue and poor driving performance. Furthermore, disability glares caused by direct sunlight or solar reflections can create distractions that can cause road accidents [38,39].

In a 1999 study examining the effect of glare on drivers' performance, the authors found that drivers initiated left turns at a significantly smaller safety margin when a glare was present. The authors also confirmed that the percentage of turns made in front of an oncoming vehicle was significantly higher in glare conditions than in non-glare conditions [39]. In another 2002 study, a team of researchers led by Theeuwes examined the effect of glare on drivers' performance. The study concluded that the presence of a glare source reduced speed by approximately 2 km/h and led participants to make more steering wheel reversals. Additionally, when participants were exposed to a source of glare while driving, they occasionally missed targets, such as wooden poles on the side of the road [38].

Melting and Damaging of Building Materials Caused by Solar Reflections

Direct reflections of solar energy from smooth surfaces, such as window glass, and diffuse reflections from rough surfaces, such as polished metal, may heat vinyl siding surfaces to the point of wrapping [40].

Research Objectives

This research study intends to mitigate the problems caused by solar reflections in an urban context, such as glare and heat gain. This research study proposes a responsive human-sensing building façade that aims:

- a) To establish a framework of communications between façades via an FIoT .

- b) To reduce glare in interior spaces to increase daylighting performance and reduce dependence on artificial lighting and ultimately decrease energy consumption and improve worker's productivity.

- c) To increase the performance and functionality of building façades employing BIPVs to achieve higher solar energy harvesting without causing glare to surrounding buildings' occupant.

CHAPTER II

DAYLIGHTING AND GLARE

Introduction to the History of Daylighting Design

The built environments in which we live, work, or play shelter us from nature, yet they affect our health and our environment in many different ways. Some of the ways that buildings adversely affect the environment include creating air pollution, exhausting natural resources such as water, producing massive amounts of landfill, and increasing energy consumption. Therefore, many organizations around the world have created various green building codes or sets of rules to encourage sustainable construction methods. These codes often address many areas related to construction impacts on the environment, with a major focus on saving energy.

According to the U.S. Department of Energy [41], using actual daylight to illuminate the interiors of commercial buildings to reduce the use of artificial lighting can save between 25%–40% of building energy costs.

Energy savings can be maximized through the utilization of daylight for lighting interior spaces, especially with respect to lighting designs for buildings mainly occupied during the day, such as schools and offices. This can be achieved by the careful design of daylighting; however, architects and engineers need to be properly and fully informed early in the design process, first, in order to recognize and balance a number of factors

that can affect lighting design and, second, to optimize the use of daylight without unexpected problems, such as glare and overheating.

Daylighting has been used in one way or another by all ancient civilizations. To the ancient Egyptians, the sun represented light, warmth, and growth. They even worshipped the sun god Ra, who was often represented by the midday sun [42]. The importance of the sun in the ancient Egyptian's lives and their religious beliefs regarding the sun influenced their architectural designs and their town planning as well. The Karnak Temple, located on the eastern bank of the Nile in Egypt, illustrates the integration of daylighting in buildings that are designed by ancient Egyptian architects. According to Hamlin, the Karnak Temple was oriented to face the North-South axis so that natural light could fill the open courts at the temple. However, the covered area needed an extra source of illumination. Clerestory windows were implemented under the high raised roof (80 feet high) in the main hall, thereby allowing natural light to enter while maintaining the secrecy and the privacy of the space [43].

The Romans provide another example of an ancient civilization utilizing daylight in their architectural design. The Roman basilicas had high-ceiling interior spaces that are thermally comfortable in climates where it can grow quite hot in summer. In addition to facilitating thermal comfort, clerestory windows were used to allow for better daylight penetration into these spaces.

As Boubarki has noted, “during the mid-eighteenth century, the beginning of the Industrial Revolution, Western Europe witnessed economic and social changes demands for housing increased due to the large influx of people led to overcrowded and unsanitary residential developments in many cities in countries of Western Europe.” To fulfill the overwhelming demand for housing in urban areas, architects had to produce cheap and quick solutions that lacked basic sanitary needs; one such need is daylight in buildings. These unsanitary living conditions led to outbreaks of cholera, typhus, and other deadly diseases across parts of industrialized western Europe. The lack of sunlight in buildings was not the direct cause of these outbreaks, but it did contribute to the spread of disease [44].

In the nineteenth century, planners and architects, being concerned about the horrible living conditions across Europe, hastened to find solutions; importantly, they started to integrate apertures in their design to allow for daylight and air into buildings. The importance of sunlight in building design was emphasized when Dr. Finson, who won the Noble Prize in 1903, discovered that sunlight can cure a form of tuberculosis, and he created a method of ultraviolet therapy to cure lupus vulgaris [44].

In the early twentieth century, architects realized the need for sunlight, and since new innovations in construction allowed large spans in buildings, architects could design buildings with large openings for windows. As Boubekri has noted: “Le Corbusier, one of the most well-known architects of the modern movement, once said that in addition to

the three dimensions of any building there is a fourth dimension called nature, which brings sunlight and fresh air to building occupants” [44]. Le Corbusier’s statement is reflected in all of his work. One residential project he designed is La Villa Savoye at Poissy, France, where he introduced the free façade and the liberal plan, where most walls are no longer load-bearing, which, in turn, allows for wider openings for windows and for more natural light inside the building.

Architects were encouraged to use the free façade with a tremendous amount of glazing without the careful utilization of daylight design, thus rendering the buildings uncomfortable in terms of thermal comfort and forcing engineers to design giant, energy-consuming heating plants or cooling plants to remedy the problem [44]. Glare was also a problem caused by these huge glazing areas [45]

In the late mid-twentieth century, many architects excluded daylight from their designs and replaced it with fluorescent lights; building professionals even argued that daylight was a luxury that could be disregarded [46]. In 1936, one author for the *Architectural Record* noted: “science has advanced to the point where artificial lighting can be a competitor to daylighting” [26]. Around the 1950s, researchers discovered a relationship between illumination levels and people’s productivity, and workplaces, such as offices and schools, were then designed with artificial light that provided illumination as high as 1200 LUX on work surfaces, without regard for energy costs or illumination quality. In the late 1970s, designers started considering daylight during the energy crisis; however, it was not until more recently, around the 1990s, when professionals started to realize the

great benefits of daylight and started integrating daylighting in most new building designs as a desired source of lighting.

The Energy Crisis and Daylighting

Energy consumption in buildings was completely disregarded until the energy crisis of 1973, when the countries which comprised the Organization of Petroleum Exporting Countries (OPEC) raised their prices. Passive solar technologies emerged and were soon adapted. With this growing concern, architects showed an interest in using sunlight as a major light source to reduce some of the energy demands [45].

A great amount of energy can be saved through the use of daylight in lighting buildings in order to reduce artificial lighting consumption and, therefore, reduce heating and cooling loads [38, 39]. Daylighting not only saves energy but also increases worker productivity, which, in turn, increases the economic value of happy workers [49].

Daylighting Benefits

Daylight has been proven to benefit both physical and psychological health in human beings [50]. A study by the Rensselaer Lighting Research Center has suggested that our biological clocks are regulated by the light levels and wavelengths typical of daylight and, furthermore, that changes to this cycle can affect our circadian rhythms, thus causing fatigue [51]. One interesting fact is that daylight spectrum therapy can be used to treat seasonal affective disorder (SAD), which is caused by the lack of daylight in winter

in northern climates. Lack of light causes an increase in the production of melatonin (the hormone that makes us sleepy at night), and a reduction of serotonin (a lack of serotonin causes depression) [51].

The relationship between daylight and the performance of students in schools was discussed in two studies. The first study, which was completed in 1999 by the Heschong Mahone Group, has found that students in classrooms with the highest levels of daylight performed 7% to 18% higher on standardized tests than those with the lowest. In San Juan Capistrano, California, the students with the most daylighting in their classrooms were found to progress 20% faster on mathematics tests and 26% faster on reading tests over the course of a year than those in classrooms with the least daylighting. The study also talked about the quality of daylight as compared to artificial lights in terms of distribution, the absence of flicker, better spectral distribution, and highlighting on three-dimensional objects. Teachers even reported that children with attention deficit disorder (ADD) performed better in daylight classrooms [52]. In another study of 90 Swedish elementary school students, researchers tracked their behavior, health, and cortisol (a stress hormone) levels over the course of a year in four classrooms with varying daylighting levels. The results have indicated that working in classrooms without daylight may upset the students' basic hormone patterns, and this, in turn, may influence their abilities to concentrate or cooperate and may also have an impact on annual body growth and absenteeism ultimately [53].

Daylighting and Green Building Codes

In the wake of the energy crisis and the greater need for substantial reduction in energy consumption, many organizations around the world have adapted some sort of green building codes to ensure sustainable building methods and healthy indoor environments in new and existing buildings. With many studies arguing for the benefits of daylight in buildings, these organizations have also set certain rules for daylighting in buildings.

The American Society of Heating, Refrigerating & Air-Conditioning Engineers (ASHRAE) is an international organization founded in 1894. Their latest building code, termed *Standard 189.1-2009*, has recommended that the design for a building project should demonstrate an illuminance of at least 30 footcandles (fc) (300 lux) on a plane 3 ft (1 m) above the floor, within 75% of the area of the daylight zones [54].

In March 2000, The U.S. Green Building Council (USGBC) developed the Leadership in Energy and Environmental Design (LEED) rating system. LEED promotes sustainable building and development practices through a suite of rating systems that recognize projects that are implementing strategies for better environmental and health performance (USGBC, 2009). LEED requires daylighting in two credits. Under the Indoor Environmental Quality Credit 8.1, which has four options, one option is to achieve daylight illuminance levels of a minimum of 30 fc (300 lux) and a maximum of 300 fc (3000 lux) in a clear-sky condition on September 21 at 9 a.m. and 3 p.m. Under Credit 8.2, LEED requires a direct line of sight to the outdoor environment via vision

glazing between 30 and 90 inches (0.8 and 2.3 meters) above the finished floor for the building occupants in 90% of all regularly occupied areas [55]

In Europe, green building ratings have been developed in many countries. The British rating system, called the Building Research Establishment Environmental Assessment Method (BREEAM), was developed by the BRE Group. BREEAM sets the standards for best practices in sustainable building design, construction, and operation in the UK and in more than 190 countries around the world. Under the health and well-being category, BREEAM allows 4–6 credits for good daylighting practices, including daylight factors, glare control, and illumination levels, depending on the type of building [56].

In the UK, the Chartered Institution of Building Services Engineers (CIBSE) has established Lighting Guide 10 (LG10-1999), which broadly places average daylight factors into three categories:

- Average daylight factor under 2% – not adequately lit – artificial lighting will be required.
- Average daylight factor between 2% and 5% – adequately lit, but artificial lighting may be in use for part of the time.
- Average daylight factor over 5% – well lit – artificial lighting generally not required except at dawn and dusk, but glare and solar gain may cause problems [57].

Another widely used European rating system is the French rating system called Haute Qualité Environnementale (High Quality Environmental) (HQE). HQE rates building's rooms as "good," "efficient," or "very efficient," based on the daylight factor calculation studies for each room. The final building rate is the highest rate obtained in 80% of the rooms [58].

In the Middle East, a rating scheme for new buildings has been developed, called the Pearls Rating System. It was created by the Abu Dhabi Urban Planning Council's Estimada. According to the Council's websites, the Pearls Rating System requires one of the following daylight designs in buildings [59]:

Demonstrate a minimum daylight illuminance of 250 lux on the working plane (762 mm from the finished floor level) for a percentage of the occupied area, as follows:

- One credit point: 50% of the occupied area
- Two credit points: 75% of the occupied area

Introduction to Glare

Increased luminance contrasts in the field of human view can lead to a visual sensation called glare; this can impair or disable vision. Glare can cause a range of maladies from eye irritation, which is known as discomfort glare, to temporary blindness, which is referred to as disability glare [51, 51, 52]

Glare Indices

There are many glare indices that are used for the purposes of glare analysis. One of the oldest indices is the Daylight Glare Index (DGI), which is an index used to evaluate daylight discomfort glare. The Daylight Glare Index is calculated as per Equation 1:

Equation 1. This equation is used to calculate the DGI index

$$DGI = 10 \log 0.478 \sum_{i=1}^n \frac{L_s^{1.6} \Omega^{0.8}}{L_b + 0.07 \omega^{0.5} L_s}$$

In this equation, the symbols represent the following information:

- 1) L_s entails source luminance in cd/m^2
- 2) L_b entails average background luminance in cd/m^2
- 3) ω entails angular size of the source in steradians as seen by the eye
- 4) Ω entails solid angle subtended by the source, modified for the effect of the position of the observer in relation to the source in steradians [62]. Table 1 shows the glare regions and their related Daylight Glare Index.

Table 1 Glare regions and daylight glare index

Zone	Region	DGI
Discomfort zone	Intolerable	>28
	Just intolerable	28
	Uncomfortable	26
	Just uncomfortable	24
Comfort zone	Acceptable	22
	Just acceptable	20
	Noticeable	18
	Just perceptible	16

DGI has some limitations because it is based on experiments with uniform light sources, and for this reason it is not reliable when glare is caused by non-uniform light sources.

Researchers have tried to overcome DGI's limitations by developing new daylight indices, such as the J-index and the Predicted Glare Sensation Vote (PGSV). The J-index defines visual comfort through a measurement of the difference between the maximum possible visual acuity (A_{max}) and the visual acuity which the person can actually reach (A) in a given illumination condition [63].

One of the most recent, most promising methods to measure daylight glare is Daylight Glare Probability (DGP), developed by Wienold and Christoffersen (2006) and based on laboratory studies in daylit spaces in two different locations (in Freiburg, Germany, and Copenhagen, Denmark). In order to assess glare, the study tested 72 different objects under various daylighting conditions. DGP is defined by the following mathematical equation (Equation 2)

Equation 2. The equation used to calculate the DGP index

$$DGP = 5.87 \times 10^{-5} E_v + 9.18 \times 10^{-2} \log \left(1 + \sum_j \frac{L_{s,j}^2 \omega_{s,j}}{E_v^{1.87} P_j^2} \right) + 0.16$$

In equation 2, the symbols represent the following information:

- 1) L_s is the luminance of the source (cd/m²)
- 2) DGP is the daylight glare probability
- 3) E_v is the vertical illuminance at eye level (lux)
- 4) ω_s is the solid angle of the source (sr)
- 5) P is the Guth position index.

Table 2 Glare regions and DGP

Region	DGP
Intolerable	45–60
Disturbing	40–45
Perceptible	35–40
Imperceptible	30–35

The DGP showed a remarkably high correlation with the user response regarding glare perception [64]. Table 2 Glare regions and DGP) shows glare regions and their related Daylight Glare Probability.

DGP can be calculated with a new tool called Evalglare, which was developed by Jan Wienold at the Fraunhofer Institute for Solar Energy Systems in Freiburg, Germany. The software calculates the daylight glare probability (DGP), as well as other glare indices, such as Unified Glare Rating (UGR), Daylight Glare Index (DGI), Visual Comfort Probability (VCP), and CIE Glare Index (CGI) [56, 57, 57–60].

Visual Comfort Probability (VCP) was developed by the LESO group at EPFL during the spring of 1991, and it is defined as the percentage of people who will find a certain scene (viewpoint and direction) comfortable with regards to visual glare [70]. A VCP rating of 85, for example, indicates that 85% of the occupants in a room would not be bothered by direct glare.

CHAPTER III

INTERNET OF THINGS AND SMART FACADES

Introduction to Smart Cities, IoT, WSN, and Smart Façades

According to the United Nations' Department of Economic and Social Affairs, more than half of the world's population lives in urban areas. Furthermore, of this population, 74% and 82% live in Europe and North America, respectively [71]. This urbanization is expected to continue to grow. Therefore, it is critical to ensure the sustainability of new urban developments. In order to mitigate the problems caused by rapid urbanization, various government agencies have introduced smart city initiatives to support the use of smart computing technologies to transform existing cities into smart ones. For example, the U.S. Department of Transportation provided \$40 million in funding to Columbus, Ohio, to transform its traffic system, which experienced elevated levels of traffic congestion and car accidents following a 1% growth in the city's population in 2016 alone [72]. Another example is the Canadian "Smart Communities" initiative, which includes the Ottawa "Smart Capital" project. This project aims to improve local business, government, and community use of connected resources [73].

A smart city relies on a various computing technology that can be applied on top of its existing infrastructure. Smart computing within cities involves a network of integrated hardware and software that provides real-time, real-world data to help people make

informed decisions for optimized living conditions. The rapid increase of information and communication technologies (ICTs) has become a key driver of smart city initiatives [74]. ICTs have been rapidly growing thanks to the growth of such devices as smartphones, sensors, and cameras connected to the internet, which are estimated to reach 50 billion in 2020 [75]. Consequently, a wide-ranging Internet of Things (IoT) ecosystem is rapidly growing to connect real-world objects like buildings, cities, cars, and people to the Internet via networks of sensors and microcontrollers capable of collecting massive amount of real-time data, such as building occupancy patterns, indoor air quality conditions, lighting conditions, local weather, occupancy count, temperature, etc. This enormous amount of data facilitates extensive opportunities and venues for reducing buildings' energy consumption and increasing occupants' thermal and visual comfort through the integration of smart IoT-controlled systems, such as HVAC controls for remote HVAC activation and management and smart power meters to manage peak and off-peak electricity usage.

Although, in recent years, the IoT has been used to automate tasks within the context of urban areas in an effort to design smart cities, there has been a significant lack of efforts to use the IoT to enable communication among buildings to achieve automated tasks based on a human-centric approach [76]. Additionally, there is a lack of studies taking advantage of the IoT's capabilities to address solar reflections through a human-centric approach. Therefore, it is necessary to introduce such an approach as an example for future IoT innovations to improve humans' comfort in their urban environments.

The Benefits of Using the IoT in Buildings and Cities

In recent years, the availability of a wide range of low-cost sensors, microcontrollers, and actuators, along with the abundance of existing wireless networks, has enabled an increase in IoT-based technologies within cities [77]. This growth in the IoT, in turn, has facilitated the automation of complex tasks, such as HVAC operations and lighting levels, within the built environment. Additionally, IoT-connected buildings are capable of sensing their occupants' behavioral patterns, allowing humans to optimize the built environment for better comfort. Furthermore, it is possible to use IoT services to connect any device or sensor to IoT-connected buildings and to leverage big data analytics to make sense of the resulting information. With such tools and approaches, processes can be immediately fine-tuned and automated without the need for human intervention.

Sensors and Actuators to Achieve Human-centered Comfort

Recent trends in IoT technologies have focused on sensing human behaviors and connecting humans to the digital world. These trends have led to new and revolutionary smart sensing capabilities that can not only sense human locations, but also sense human behaviors and even predict humans' future schedules and tasks using smart data analytics. Today, the sensing of human behaviors and occupancy patterns can be achieved in real-time through networks of sensors and embedded devices that facilitate human-centered designs in which building occupants passively and actively participate in the IoT system [47]. Thanks to the rapid development of human-centric IoT systems,

communications between people and things (building elements) are becoming a huge asset in smart environments, since such systems make it possible to quickly assess people's interactions with building elements to achieve maximum comfort and minimal consumption.

Several IoT-based approaches for human-centered systems have been demonstrated to improve occupants' comfort and reduce energy consumption. For example, in their research study entitled "Thermovote: Participatory Sensing for Efficient Building HVAC Conditioning," Erickson and Cerpa detailed the design of a new technology that uses a smartphone application to collect subjective thermal comfort data and control an HVAC system [12]. This study, which took place on one floor of a university research building, recruited a total of 39 human subjects who reported comfort data through their phones. Later, these data were pushed to the HVAC system to achieve real-time control. Over a five-month test interval, the authors achieved HVAC energy savings of 10.1% and a satisfaction rate of 100%. Similarly, in 2013, Erickson et al. utilized an occupancy estimation system comprising a 22-node wireless camera, a 40-node Passive InfraRed (PIR) wireless sensor network, and image processing algorithms and classification techniques to accurately detect occupants' transitions in order to determine optimal cooling or heating strategies for human comfort while minimizing ventilation requirements [78]. The researchers concluded that the proposed IoT system achieved a significant energy savings of 26% while maintaining conditioning effectiveness over a period of four weeks. They further estimated that the system could achieve annual

energy savings of 30% compared to standard strategies. A return on investment (ROI) analysis further showed that the cost of the new IoT system could be recouped in approximately 6 to 10 months.

IoT-based systems that facilitate human-centric approaches are also considered an asset in the healthcare industry, where rapid user input is crucial for triggering real-time actions that could save lives. Kim et al. developed a Radio-Frequency Identification (RFID) tag that could be used to monitor the location and other important health information of elderly patients living in care homes [79]. The tag provides indoor location sensing and tracking, then sends the collected information, along with timestamps, to a network server for further analysis. The server couples the sensing and tracking data with the elderly patients' personal health status, such as their movement patterns and exercise durations. Such information could significantly improve the quality of patient health care. For example, such a system could be set to trigger a warning message when a movement is not detected for a pre-set period.

Decreased Energy Consumption

In a 2006 report, the California Energy Commission confirmed that smart windows, including smart glass and responsive shading equipment, could reduce peak electric loads by 20 to 30% in many commercial buildings and increase daylighting benefits throughout the U.S. The report further suggested that smart windows could improve comfort and enhance productivity in both residential and commercial buildings [80].

Cooling and heating commercial spaces consume an enormous amount of energy. HVAC equipment typically consumes at least 40% of a commercial building's energy [41]. Many buildings' HVAC systems consume even higher proportion of energy to oversized HVAC equipment. Oversized HVAC systems in commercial buildings may not be able to sufficiently reduce output to provide consistent operations, resulting in cold air dumps that can lead to poor thermal comfort in the conditioned spaces [81]. IoT networks of sensors and actuators using a human-centered approach have been proven to achieve personalized cooling and heating conditions that can significantly reduce HVAC energy consumption [80]. By implementing an IoT system that allowed real-time changes to HVAC operations based on occupants' feedback, Erickson and Cerpa were able to reduce HVAC-related energy consumption by 10.1% [12]. Similarly, by utilizing a network of IoT node sensors, such as PIR sensors and cameras, to detect occupants' transitions between spaces, Erickson et al. reduced energy consumption related to heating, cooling, and ventilation loads by approximately 26% over a period of four weeks and expected a 30% energy savings annually [78]. Based on these examples, IoT-controlled building management systems are clearly able to satisfy energy efficiency requirements while considering user comfort.

Data Collection and Profiling

Computer science research has already proposed and demonstrated extensive models for the representation of the tracking and profiling data collected by building sensors [82–

85]. The collected sensor data can be analyzed to predict occupants' behaviors and transitions within the built environment. The resulting information could support decision-making and the development of recommendations for future building retrofitting in order to improve existing building performance and maximize energy savings.

Sensor-collected data can be used to monitor indoor air quality to drive various HVAC operations. A group of researchers from the University of Southern California proposed an occupancy estimation model based on a combination of non-intrusive sensors capable of detecting indoor temperature, humidity, CO₂ concentration, light, sound, and motion. The sensor data were processed in real time to estimate the number of occupants in a given space. Field tests carried out in two shared lab spaces for 20 consecutive days reported an overall detection rate of up to 87.62%. These results indicate the ability of the proposed system to monitor the occupancies of multi-occupancy spaces in real time, thereby supporting demand-driven HVAC operations [84].

Sensor-collected data can also be very useful for studying and predicting pedestrian behaviors across large cities. For example, a team of researchers led by Yoshimura at the Sensible City Lab at the Massachusetts Institute of Technology (MIT) proposed a framework for modeling and analyzing the dynamics of pedestrian behaviors in the shopping environment in order to examine the relationship between pedestrian behaviors and the features of the shopping environment. The researchers collected the MAC

addresses of pedestrians' smartphones by planting five Bluetooth sensors (nodes) to detect the presence and movements of pedestrians between places in the historical center of Barcelona, Ciutat Vella, Spain. By analyzing the collected data, researchers were able to accurately determine the time pedestrians spent in different areas of the historical center in relation to different shopping events, such as seasonal sales. For example, the researchers found that, during discounted Saturdays, pedestrians actively explored different places, rather than limiting their stay to smaller areas [83].

Extensive computer science research has confirmed the advantages of using IoT technologies in building design to track building occupants' behaviors. Some computer science researchers have already demonstrated extensive models for data representation. For example, one recent study discussed the integration of IoT technologies, such as WIFI-based monitoring, camera-based tracking, and counting, into sensor networks. The study's findings confirmed the feasibility of using such IoT technologies to collect data to monitor building occupants to achieve better building energy performance. The authors noted that, "[w]ith the goal of using minimal hardware and software costs, future smart buildings have a great potential to save energy by employing smart control strategies on HVAC through the help of data collected via IoT" [86]. It is clear that the various data collected by sensors, such as temperature, occupancy, air quality, and other building-related data, could be an invaluable asset for modifying built and urban environments to create more comfortable and energy efficient human-centered living spaces.

The Emergence of Smart Building Façades

The rapid development of applications of IoT technologies and the abundance of cheap microcontrollers, sensors, and actuators have enabled the transformation of traditional building skins into intelligent skins capable of sensing humans and their surrounding environments and intelligently transforming or changing themselves accordingly. Recent research studies have proposed smart building façades comprising a variety of individually controlled façade elements based on IoT systems. For example, in 2014, Yekutieli and Grobman introduced a responsive façade model with an embedded IoT-based system comprising interior and exterior sensors for collecting information on interior and exterior lighting conditions. Although the proposed façade was tested for improving lighting conditions, the authors noted that other types of sensors could be added to collect data on other environmental conditions, such as wind speed, temperature, occupants' movements, etc. The façade was divided into multiple grids, each comprising elements that could be automatically operated using a set of actuators (in this case, motors) to adapt to different exterior lighting environments and maximize interior daylighting penetration and availability. Both the sensors and actuators were part of a larger IoT system based on a network of Arduino devices, sensors, and actuators [15].

Similarly, Jange et al. proposed a responsive façade prototype that used embedded sensors to collect a variety of information, such as the location of the sun in the sky and the level of daylighting entering the interior space. The collected data were stored in an

MSQL server and then sorted and sent to a virtual model in Rhino. Based on the collected data, the responsive façade panels changed form to reduce or increase the size of built-in window apertures. The paper demonstrated that the use of IoT-embedded hardware and software can not only facilitate the complex tasks of collecting, storing, and analyzing data, but also control the size of a façade aperture based on real-time daylighting and sun location data [16]. Additionally, this research demonstrated that a small IoT-controlled prototype can be synced to a virtual three-dimensional model for testing and simulations: an approach that can be considered an invaluable asset in high-performance building design. Thus, the development and integration of IoT-based systems to control façade elements have proven to facilitate the automation of complex tasks based on real-time data collected through various sensors, thereby transforming traditional building façades into intelligent building components.

A review of literature suggests that although there is an ongoing research focus on smart façades, the possibility of designing a façade that not only senses human occupancy and environmental properties, but also communicates with other façades, has not yet been investigated. Communication between façades may help to resolve many of the issues that arise in urban areas where tall buildings are built in close proximity, such as the glare and heat gains resulting from reflective glazing and cladding that can affect both building occupants and outdoor pedestrians and increase urban heat and adversely affect the microclimates of surrounding areas.

Wireless Sensor Networks

The number of devices connected to the Internet is estimated to reach 50 billion in 2020 [77] exceeding the number of people inhabiting our planet which is estimated to be 7.7 billion [71]. Due to evident rapid growth of internet-connected devices, an Internet of Things (IoT) ecosystem has emerged to facilitate the process of connecting real-world objects like buildings, cities, household appliances, and most importantly humans to the Internet via microcontrollers and sensors that collect and stream various sets of data from our surrounding environments such as, temperature, light levels, wind speed and people's movement. The Internet of Things has enabled everyday objects that are not considered non-electronic to connect to the Internet as well as connect to each other; those objects include cloth, food, roads, cars,.....etc. The rapid growth of the IoT system has led to the availability of a wide array of cheap low-power wireless solutions using low-cost microcontrollers and sensors.

The system proposed in this research study takes an advantage of abundance of such low cost microcontrollers and sensors to conceive a low-power hardware Wireless Sensor Network (WSN) architecture that is able to collect and transmit data between its own sensor nodes and to the Internet to optimize the thermal and visual performance of the indoor spaces. In addition to anticipated improvement in indoor spaces, the system can be easily manipulated by plugging extra outdoor sensors to improve outdoor environments for better pedestrians' thermal comfort and glare-free driving experience. Although, this study conceives of the system and provide evidence for its utility, future

work must be conducted to implement such a system. Figure 1 shows a simplified setup of a WSN that is installed on two building façades.

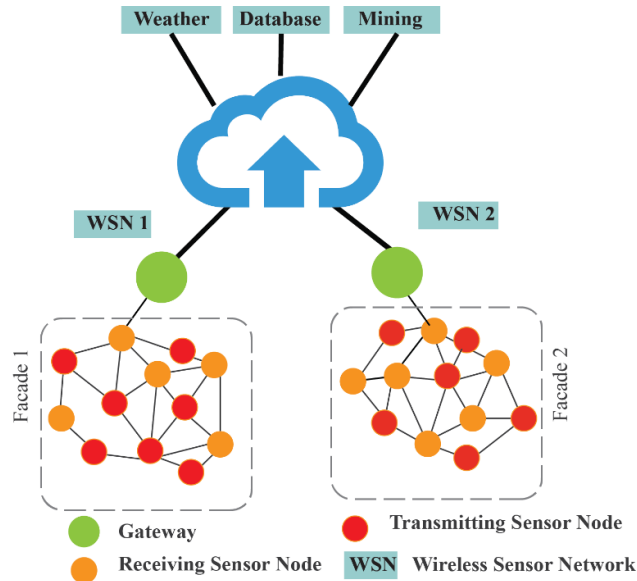


Figure 1 The architecture of WSN

The Labor cost and maintenance of WSN

Traditional wired networks have some disadvantages such as reduced mobility, and high installation costs. On the contrary, Wireless Sensor Networks are an effective alternative to deploy IoT solutions, considering their flexibility, scalability, and low-cost hardware architecture. [87] One huge advantage of WSN is the elimination of cables that were previously required to power sensors in traditional wired networks. Therefore, the hardware and installation costs for a large number of sensors in large projects such are greatly reduced by wireless technologies leading to reduced labor cost. In 2000,

Kaiser and Potite, early pioneers of WSN systems, wrote in their article entitled “Wireless integrated network sensors”:

“WSN opportunities depend on the development of a scalable, low-cost, sensor-network architecture. Such applications require delivery of sensor information to the user at a low bit rate through low-power transceivers. Continuous sensor signal processing enables the constant monitoring of events in an environment in which short message packets would suffice. Future applications of distributed embedded processors and sensors will require vast numbers of devices. Conventional methods of sensor networking represent an impractical demand on cable installation and network bandwidth” [88].

It is evident that WSN is considered a low-cost system due to its low-cost hardware setup that facilitated streaming data wirelessly without the need to a large amount of cables, thus greatly reducing the cost of the labor that was previously needed to install wired systems.

The upfront cost of IoT systems hardware and installation is likely to be recouped over time considering that it achieves occupant comfort and energy saving. In 2013, Erickson et al. utilized an occupancy estimation system comprising a 22-node wireless camera, a 40-node Passive InfraRed (PIR) wireless sensor network, and image processing algorithms and classification techniques to accurately detect occupants’ transitions in order to determine optimal cooling or heating strategies for human comfort while

minimizing ventilation requirements. A return on investment (ROI) analysis further showed that the cost of the new IoT system could be recouped in approximately 6 to 10 months [78].

One advantage of WSN is scalability; WSN can be modified to adapt to new changes, for example adding new sensors to nodes, adding new nodes, or adding a cluster of nodes that communicate to their own gateway [89]. Therefore, the proposed system can be adjusted in the future to collect more data by adding more sensors in order to perform more tasks such as optimizing HVAC and lighting control, collecting occupancy information to enhance security systems. Additionally, all tasks can be accessed remotely from the cloud facilitating easy access to the system by facility managers, maintenance official, and even parts providers.

Maintenance and labor are a major driver of new technology adoption. However, their cost is often less significant when compared to the benefits achieved by the entire system, and cost of the entire solution. A great Return on Investment is expected when using the proposed system due to the use of WSN, which proves to be a scalable system that can expand to mitigate future changes. Furthermore its accessibility makes the system maintenance and labor cost redeemable in a short time.

WSN accessibility over the cloud exponentially reduces the maintenance labor due to the easy access to the system from remote locations. Maintenance officials can easily

monitor the performance of the entire system, allowing them to perform maintenance tasks for the whole system or even for one node at a time. Additionally, cloud accessibility allows for quickly troubleshooting the system and quickly locating the node/sensor causing the error.

Literature Review Summary

As discussed in the previous sections, solar reflections caused by reflective façades in dense urban areas can have a negative impact on building occupants, causing visual and thermal discomfort that can ultimately increase worker errors, harm work health, and decrease work performance. Additionally, reflected sunlight entering interior spaces can cause heat gains, that can increase cooling loads.

Solar reflections affect not only building occupants, but also outdoor pedestrians and drivers. For example, solar reflections bouncing off glazed façades have been shown to contribute to the urban heat island effect, increasing air temperatures and causing outdoor thermal discomfort. These intense reflections have also been found to cause disability glares for drivers, resulting in road accidents. This issue, in particular, has prompted researchers and scientists to work on solution to prevent glare in urban areas within drivers' views.

Damage to building materials and outdoor vegetation as a result of intense solar reflections has also been a problem in areas where building façades are covered with

highly reflective glazing. In some cases, spots where sunlight is reflected have recorded temperatures 40°F higher than surrounding air temperatures. This significant rise in temperature can cause severe vegetation burns.

Considering the various negative impacts of solar reflections on people, buildings, vegetation, surrounding environments, and the microclimate, it is crucial to address solar reflections and find a solution to improve occupant comfort and energy efficiency in buildings and urban environments. In this context, IoT-based systems support a human-centric approach that facilitates real-time actions based on user inputs.

New technology can help to create responsive environments that sense human living patterns and adapt to environmental occupants. Indeed, the proliferation of IoT-based systems in general, and human-centric approaches in particular, supports new opportunities for the development of smart ecosystems that facilitate user interaction and connectivity with the surrounding built environment.

There is an ongoing research focused on smart façades. Specifically, researchers have been working on using IoT-based devices to help transform traditional static façades into dynamic smart ones. Some researchers have incorporated sets of sensors into façade prototypes in order to collect data on various conditions, such as lighting levels.

Although such façade designs can help increase building performance, they do not

necessarily achieve maximum occupant comfort because they fail to sense and recognize human needs. Furthermore, such smart façades can encounter problems caused by other nearby buildings, such as sunlight bouncing off reflective façades. Facilitating communications among façades may help to overcome these issues and mitigate many of the problems that arise in urban areas.

CHAPTER IV

METHODOLOGY

Introduction to Methodology

The research employed software simulation to explore the methods for a FIoT and the possible benefits of reducing glare, increasing energy generation, and reducing energy consumption. The workflow of the research study consisted of three stages, as is shown in Figure 2. In the first stage, two buildings were modeled: an 11-floor tower that has a reflective façade and a 3-floor building whose occupants experience a glare problem caused by the façade of the tower. Later, glare analysis is carried out to determine which patches of the façade are causing glare and at which hour of the year (HOY) those panels cause glare to the residents of the 3-floor building. All the data collected in this phase is stored in an SQL database.

To design the proposed dynamic human-sensing façade, a set of daylighting, glare, and solar energy collection simulations was carried out in the second phase. The results of the simulations help determine the position of the different façade elements at each HOY in which the façade can eliminate glare and increase both daylighting performance and energy collection by the tower building. As with the previous phase, data extracted from the simulation results are stored in the same SQL database.

Lastly, in the third phase, a computer program was developed to simulate management of the proposed façade and the wireless sensor network (WSN) that would be embedded in both building facades. The program scrutinizes the database for hourly information regarding the buildings' existing conditions, optimized conditions, and sensors' inputs, which consist of occupancy patterns, sun positions, and weather conditions.

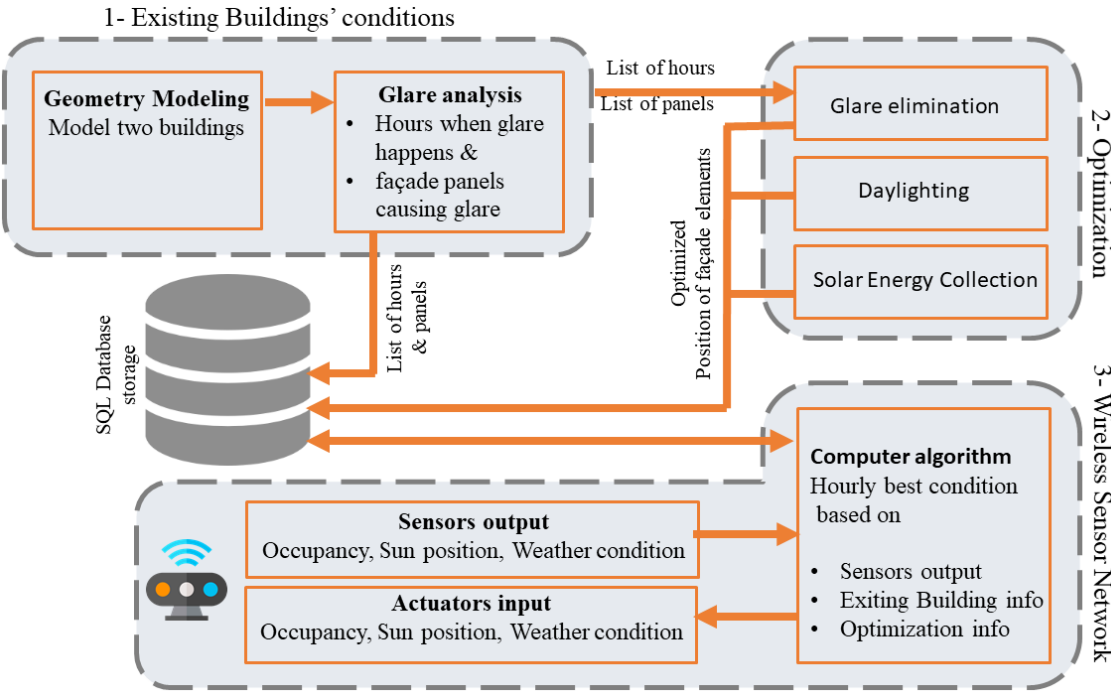


Figure 2 Methodology Workflow

The Proposed Façade and Wireless Sensor Network

In order to eliminate glare caused by the tower's reflective façade, this research study examines a façade design that has embedded intelligence enabled by a WSN to collect various data such as human occupancy patterns, weather conditions, sun positions, and illuminance levels on the façade. Unlike a façade with fixed elements to solve issues caused by glare, this façade has elements that change positions on an hourly basis, controlled by the information that is both collected by sensors and building simulations to maximize all three conditions: a glare-free environment, daylighting performance, and solar energy collection. The proposed façade can sense both the occupants and the surrounding environment through an embedded WSN.

The proposed façade is placed in front of the existing building façade at a distance of 3 ft, and it consists of *building-integrated photovoltaics* (BIPV) reflective elements that rotate around two axes: an X and a Z axis. (Figure 3). The reflective elements redirect sunlight so that glare is eliminated in the 3-floor building, while maximizing daylighting conditions inside the tower building. Reflecting the sunlight upward toward the interior ceiling leads to distribution of the light back to areas that are further from the windows; this improves the uniformity of illuminance levels inside the room, and, additionally, this change can contribute to diffusing direct light for improving the quality of indoor lighting and for reducing glare inside the tower.

When buildings are not in use (that is, no occupancy is detected by the embedded sensors), such as during weekends, the reflective elements follow the sun's position to maximize solar energy collection.

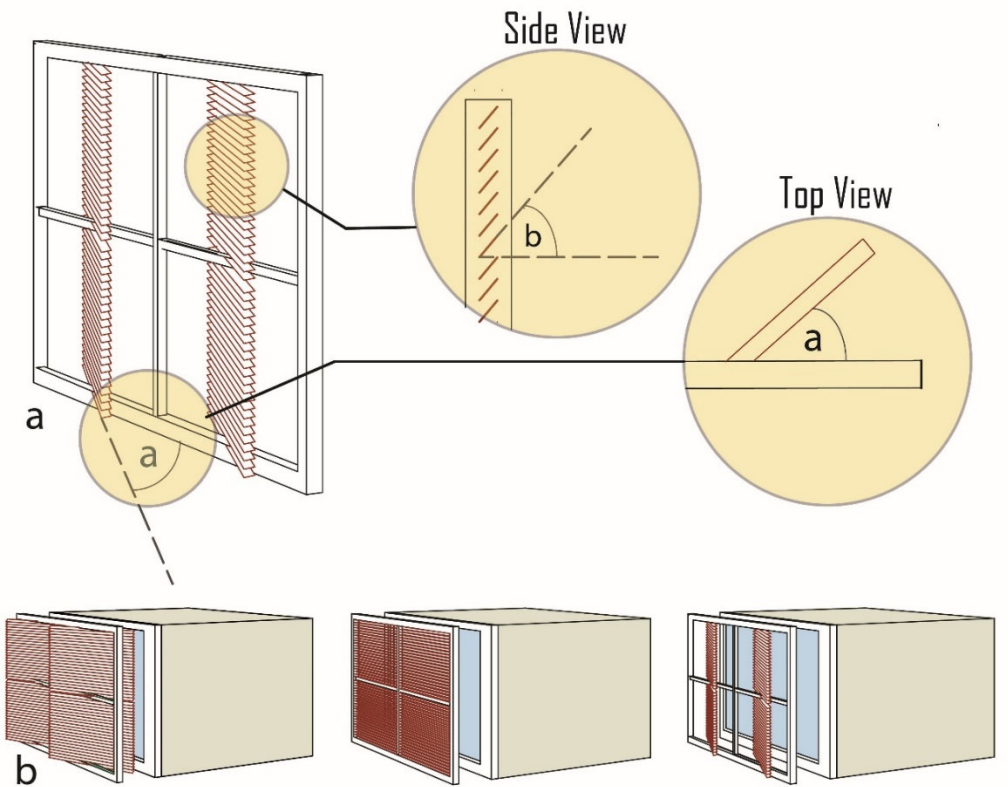


Figure 3 The proposed facade. a) The façade elements rotate around the X-axis (angle a) and around the Z-axis (angle b). b) Examples of different façade configurations.

The angles of rotation around the X and Z axis of the reflective elements are determined on an hourly basis by a computer algorithm that calculates the rotation angles that yield an optimized building condition, based on data that is collected by the WSN and from existing buildings' performance simulations. Such data contains HOY, occupancy patterns, weather conditions, and sun positions.

Stage One: The Geometric Model and Glare Analysis

Preparation of the Geometric Model

In order to analyze glare caused by reflection facades, a case study of two buildings is considered for this research study. A geometric model of both buildings was created with Rhinoceros 3D, which is a modeling software [90]. The location of the buildings was set to Houston, Texas, in the United States. The latitude of Houston is 29.76°N , the longitude is -95.36°W , and its elevation is 80 ft (24.4 m) above sea level.

In the modeled buildings, the façade of one of the buildings is considered to be a glare-causing surface due to its high reflectivity property and its orientation towards south while the other building is analyzed for glare caused by the sun reflected off the glare-causing façade.

In order to establish a realistic scenario of both buildings, many buildings across Houston were surveyed by means of Google Maps. This step was necessary in order to estimate the height and width of tower buildings that typically exist in urban areas around Texas as well as the typical width of major streets where tall buildings exist in those areas, such as in the downtown parts of Houston, Dallas, and Austin.

Some of the buildings that were surveyed include:

1- The ExxonMobil Building (formerly the Humble Building), which was built in 1963 in Houston. At that time, it was the tallest building located west of the Mississippi River, at 606 ft (185 m). It remained the tallest building west of the Mississippi until 1965, when Elm Place was built in Dallas, Texas [91]. The ExxonMobil building is 44 floors high and is located at 800 Bell Street, which is 141.6 ft (43.2 m) wide.

2- The Wesleyan apartment building, located at 2929 Wesleyan, Houston. The apartment tower was built in 2015, has 40 floors, and is 533 ft (162.5 m) high. It is considered the tallest residential tower in Houston [92].

3- Museum Tower is the 15th tallest structure in Dallas. It is located at 1918 North Olive Street, Dallas, Texas. It stands 604 ft tall and has 42 floors. The distance between the Museum Tower and the buildings across the street was measured using Google Maps. The measured distance is 195.3 ft (59.6m) [93].

4- The Heritage Plaza is located at 1111 Bagby, Houston, Texas. The tower has 53 floors. Standing at 762 feet (232 m), the tower is the 5th tallest in Texas and the 79th tallest in the U.S. [94]. The street where the tower is located is 123.1 ft (37.5m) wide.

5- KPMG Centre is located at 717 Harwood in Downtown Dallas, Texas. The building height is 481 feet (147 meters), and it has 34 floors. The street where the building is located is 78.4 ft (23.9m) wide [95].

The surveyed buildings contain between 53 and 34 floors, and the street width where these buildings are located ranges from 195 to 78 ft (60 to 24 m). For the purpose of this study, the tower is modeled with 30 floors and a height of 295 ft (90 m), and the street width between the modeled tower and the smaller building is 125 ft (38 m), which is considered the average street width in urban settings across Texas.

Surveying buildings around the downtown areas of Houston, Dallas, and Austin is crucial for estimating a building/tower height and street width and, thus, for constructing a geometric model with the aim of carrying out different building performance simulations. It was determined to use building height and street width for this simulation that was comparable to the obtained information from the surveyed buildings.

In this research study, a geometric model of two buildings, namely, a tower and another small building, were modeled in Rhino, a 3D modeling environment [96] (Figure 4) The

two buildings do not represent actual buildings, but rather typical or representative buildings from the Texas urban context. The tower consists of 11 floors, and it is 108 ft (33 m) tall and 59 ft (18 m) wide. Each floor has seven rooms that are 16 x 13 ft (5 x 4 m) with a ceiling height of 9.8 ft (3 m). The smaller building consists of three floors, and it is 29.5 ft (9 m) tall and 42.7 ft (13 m) wide. Each floor has five rooms that are 16 x 13 ft (5 x 4 m) with a ceiling height of 9.8 ft (3 m). The street width between both buildings is 98.5 ft (30 m) (Figure 4). The reflective façade is oriented toward the south.

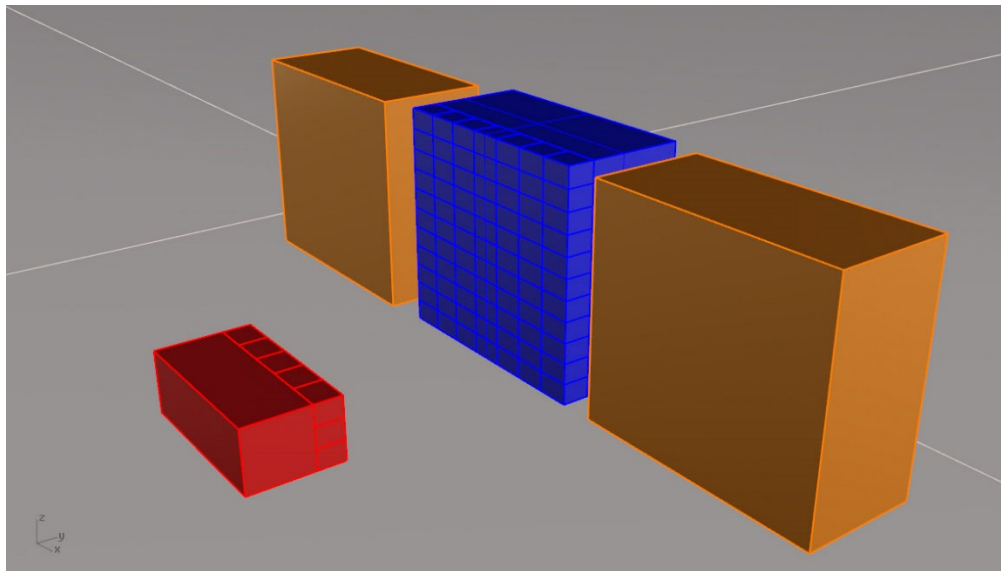


Figure 4 The modeled tower (blue), the 3-floor building (red), and the context building (brown)

Glare Simulations

A view inside each room in the small building is created at a height of 5'6" and is located in the center of the room as one looks toward the reflective building façade. The total number of views is 15. In order to assess and quantify glare caused by the reflective façade, each view is analyzed further to obtain the DGP value for each hour of the year. Several glare indices have been developed over the past decade to assess glare in views within interior spaces; however, it was determined that DGP is the most suitable metric to use for this study. DGP was developed by Wienold and Christoffersen and based on laboratory studies in daylit spaces in two different locations (Freiburg, Germany, and Copenhagen, Denmark) in order to assess glare. The study tested 72 different objects under various daylighting conditions. DGP showed a remarkably high correlation with users response regarding glare perception [97].

There are two ways for calculating the DGP values for every hour: the annual glare simulations, which is widely used for annual glare simulations, and the point-in-time glare simulations, which are typically used to calculate DGP for one hour. The former employs Daysim for calculations, which uses a simplified sky position and divides the sky into patches; in addition, it cannot handle radiance materials that have bidirectional reflection and transmission descriptions (BRTDs) [98,99]. The latter uses Radiance, a ray-tracing daylighting simulation engine [100] for DGP calculations; it also uses a continuous sky that is positioned accurately based on the HOY, and it is capable of handling radiance materials that have BRTD functions. The yearly method is fast. It

takes between one to four hours to complete and yields only one file that has a list of DGP values for every hour in the entire year.

Unlike the yearly method, the point-in-time method is slow because it takes 3 to 6 seconds to complete the calculation for each hour and, thus, a total of about 3.6 to 7.3 hours to calculate glare for every daylight hour in the entire year, and a total of 54 hours to 109.5 hours are required to investigate glare for all 15 views . Additionally, running the hourly method produces one result file per hour and a total of about 4380 files; this makes analyzing the results of the simulations a cumbersome process. Although the point-in-time method is not as time efficient and easy as the annual method, it does produce accurate results due to the engine and sky method it employs. For these reasons, the point-in-time method was chosen for this research. Table 3 compares both glare-calculation methods.

Table 3 A comparison between the annual and the point-in-time glare calculation methods

	Annual Glare	Point-in-Time Glare
Engine	Daysim	Radiance
Sky Type	Sky divided into patches	Sky is continuous
Sky Position	Simplified	Accurate
BRTDfunc	Cannot handle BRTD	Can handle BRTD
Results Files	1 file	3650
Process Time	1–3 hours	3.6- 7.3 hours
HDR Image	No	Yes

For the purpose of running glare, daylighting, and solar radiation simulations, the Radiance material properties that are used to model the reflective façade are obtained from the Optics program, a program which was developed by a group of researchers at the Berkeley Lab [101]. Optics holds a large database of commercially available glazing materials produced by a wide array of manufacturers around the world. It facilitates the export of material property into a Radiance material that can be used for simulations. For this study, a commercially available, solar-control glazing was used; the glazing has a high light-reflectance value that helps in solar gain reduction. Figure 5 and Figure 6 show screenshots of used glazing proprieties inside the Optics program.

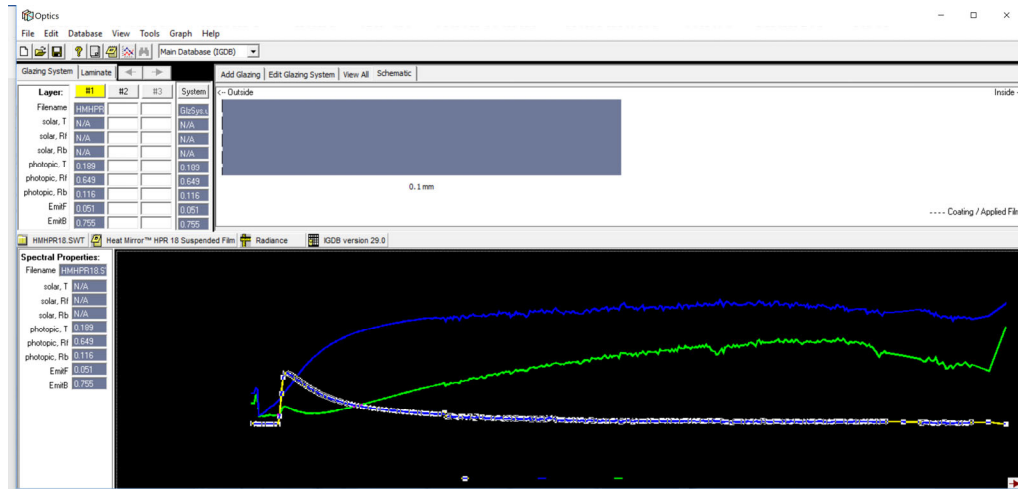


Figure 5 The properties of the glazing used in this study in Optics

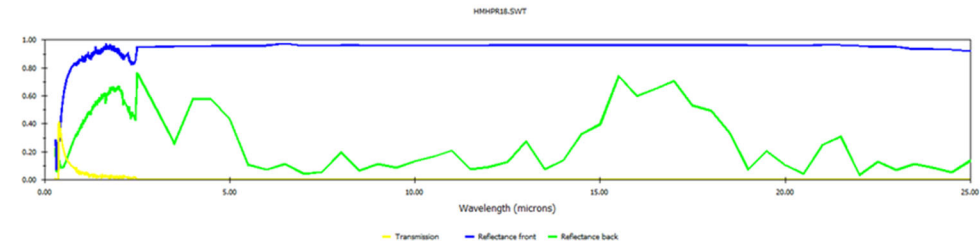


Figure 6 The wavelength of the reflective glazing that is used in this study

Although Optics exports the material properties into a Radiance-friendly format, the glazing material that was chosen for this study has a BRTD function that rendered the exported properties challenging to employ in Radiance simulations; thus, Optics2Rad, which is a Linux-based package, was used to convert Optics output into a Radiance-friendly material definition that could be utilized in the glare simulations (Figure 7).


```
rania@DESKTOP-67RVHDN: /usr/local/radiance/bin
rania@DESKTOP-67RVHDN: /usr/local/radiance/bin$ export PATH=$PATH:./usr/local/radiance/bin
rania@DESKTOP-67RVHDN: /usr/local/radiance/bin$ export RAYPATH=./usr/local/radiance/lib
rania@DESKTOP-67RVHDN: /usr/local/radiance/bin$ optics2rad HeatMirrorHMHPR18.rad
# Output generated by ./optics2rad from HeatMirrorHMHPR18.rad
#
# FileName= HMHPR18.SWT
# Product Name= Heat Mirror HPR 18 Suspended Film
# NFRC ID= 1507
# Manufacturer Name= Southwall Technologies, Inc.
# Glazing Type= Coated
# Coated Side= Front
# Transmittance= 0.189
# Front Reflectance= 0.649
# Back Reflectance= 0.116
# Thickness(mm)= 0.076
# Appearance= Reflective
#
void BRTDfunc HeatMirrorHMHPR18
10
    rR_bronze rG_bronze rB_bronze
    0.131*tR_bronze 0.197*tG_bronze 0.341*tB_bronze
    0 0 0
    window.cal
0
15 0 0 0 0 0 0 0 0
    0.745 0.636 0.4
    0.163 0.1 0.092
rania@DESKTOP-67RVHDN: /usr/local/radiance/bin$
```

Figure 7 A screenshot of the Linux-based program, Optics2Rad, which is used to convert the Optics output to a radiance material definition

The visual light reflectance (VLR) and the visual light transmittance (VTR) of other building materials such as the ceiling, the floor, and the wall that are used in the simulations are listed in Table 4.

Table 4 Radiance material properties of the buildings' materials

Building Element	Tower Building	Three-Story Building
Interior walls	20% reflectance	20% reflectance
Glazing VLT	80% transmittance	80% transmittance
Glazing VLR	65% ref/BRTD	5% reflectance
Floor	20% reflectance	20% reflectance
Ceiling	80% reflectance	80% reflectance
WWR	100%	100%
Frame-to-window ratio	15%	15%

Key Challenges in Large-Scale Glare Simulations

Performing such large-scale hourly glare simulations is cumbersome due to the intensive computing power required to carry out the enormous numbers of simulations. This results in various challenges, which might ultimately hinder the simulation process.

Some of the challenges are as follows:

- **Time limitation.** In addition to accuracy, the point-in-time glare simulation process produces a high dynamic range (HDR) photo that is crucial for utilizing an image-based glare calculation for accurately locating facade panels that can cause glare and for observing the times they cause glare [94, 95]. Over the past decade, HDR photos have been used by many researchers to analyze glare [8, 22, 96, 96–99]. Therefore, it was determined to use the

point-in-time calculation method in this research. When one considers the enormous amount of time needed to complete the point-in-time method for each view (which is approximately 7.3 hours and, thus, a total of 109.5 hours for all 15 views). the implementation of all the simulations would take over a year to complete.

- **Simulation preparation and storage.** It is challenging to prepare large-scale simulations due to the need to handle numerous files. The files must be organized, uniquely named, and finally stored on a local hard drive, which can become troublesome due to the large size of the files.
- **Data analytics and visualization.** The amount of data from the glare simulation processes is usually exceedingly large. Hence, it is almost impossible to open the numerous files that contain the results in order to analyze and visualize the data. Additionally, the results are often in a raw format, and, thus, additional calculations are needed to convert the data into a readable format that a regular user can interpret in the context of the daylighting performance of the examined strategy.

Automating Glare Simulations, Parallel Computing, and Results Analysis

It is evident that glare simulations are time-consuming and often require significant computing resources. Therefore, an alternative cloud-based, high-performance computing (HPC) environment can be most beneficial when one is running hundreds of simulations. An HPC environment consists of thousands of computer nodes, each of

which can be used individually to compute a task, thereby facilitating the processing of thousands of tasks that can run in parallel (Figure 8).

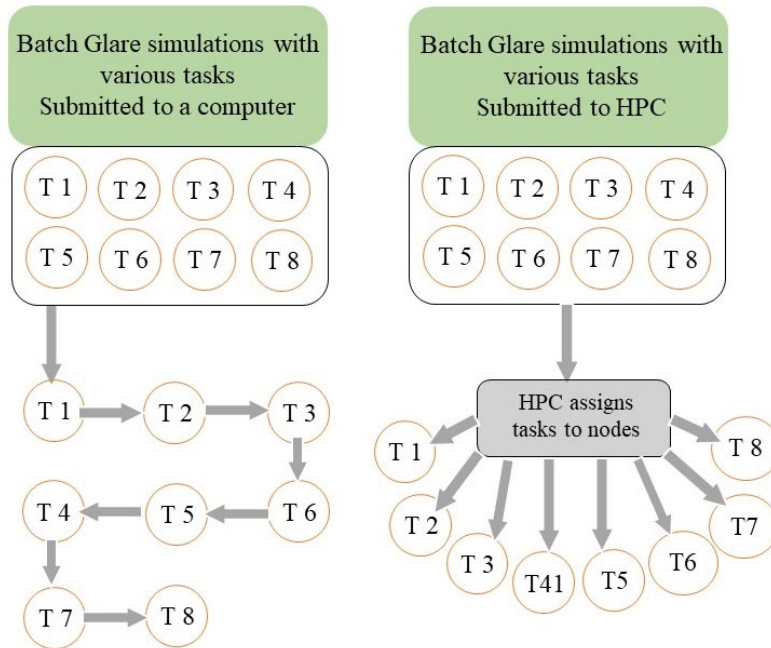


Figure 8 The execution of a batch simulation job on a computer, as opposed to its execution in an HPC environment

Initially, the use of HPC was hindered by many obstacles, such as the high cost of the hardware and maintenance. However, many companies have introduced cloud-based, HPC solutions, which have enabled researchers to rent clusters of computing nodes in order to carry out their research tasks without having to purchase equipment or pay

maintenance fees. Thus, on-demand, cloud-based HPC provides an economical solution (Zhai et al. 2011).

Although many research studies have demonstrated the benefits of modern computational environments, which provide vast amounts of computational resources (Thain, et al. 2005; Pérez-Lombard, et al. 2008), in the field of building performance simulations, the benefits of cloud-based modern computing environments have not been fully examined.

This study utilizes the Extreme Science and Engineering Discovery Environment (XSEDE), which is a cloud-based HPC environment that serves scientists and researchers in the U.S. (Towns et al. 2014). Images from the high-performance computing environment's user portal and the SSH interface are attached in Appendix A

To automate the process of preparing simulation files that are needed to run glare analysis on the HPC environment, a Python script was written in order to automate the creation of Radiance commands for every daylight hour (08:00 to 18:00) through the entire year, to automate the creation of writing bash scripts to be used on a Linux-based supercomputer (bash scripts are a special format for the HPC environment), to extract the DGP value from thousands of result files, to visualize the values, and to download the results HDR images to the local computer if desired. The script can be executed from within any Python IDE environment, the Windows DOS environment, or the

Grasshopper environment, which can ease the process for a regular user (the non-programmer).

In order to write Radiance files for simulations, Ladybug and Honeybee were used for initial glare studies for only one hour during the day. Later, the aforementioned Python script (Appendix B-1) created the same set of Radiance files but replaced the command line so as to reflect a different sky file (for each year). This process produced 3,650 files for each view, with a total of 54,750 files. Finally, the script facilitated the creation of Linux-based commands that are often called *bash commands*. This step was necessary to run the simulation with Radiance, which is installed on a supercomputer via the XSEDE platform, a high-performance computing facility for researchers and scientists working on research that is funded by the National Science Foundation (NSF) [108].

After individual bash scripts were created, another Python script (Appendix B-2) was used to automate the process of uploading the files to the supercomputer in a user-specified directory. The last step was to execute the bash file so that it could run on the supercomputer side. The files were executed in one batch run by means of 1,000 parallel, single-core nodes (the number of nodes allowed per one batch run); thus, in each node, a group of about 57 simulations was run. These 57 simulations took less than three hours to complete. Because all simulations ran simultaneously on parallel nodes, the whole processing time took less than three hours. This process would have normally taken

about 2,860 hours to complete; this equates to 118 days or 4 months until completion on one computer (Figure 9).

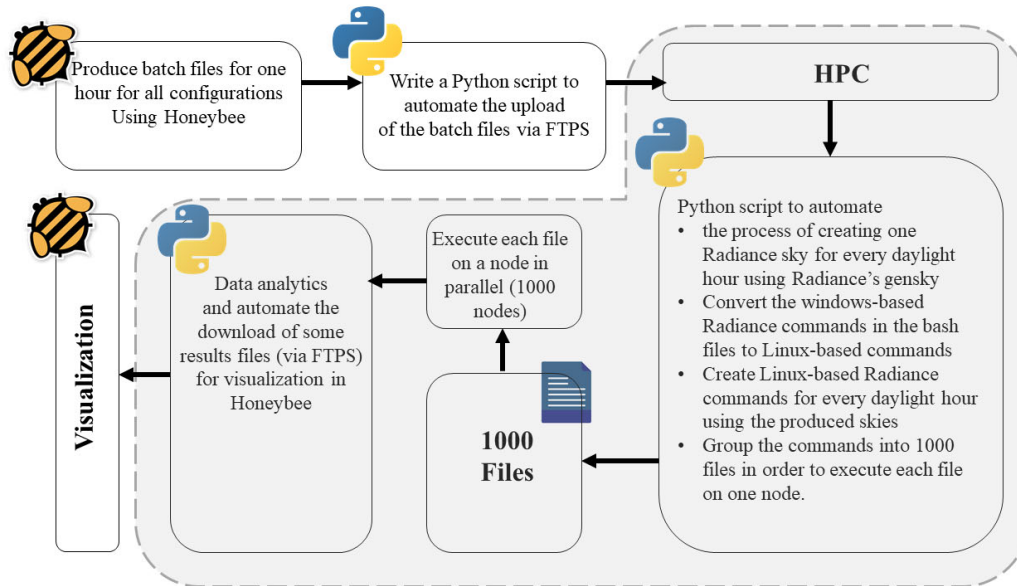


Figure 9 Executing thousands of image-based glare simulations for all 15 views with Ladybug and a custom Python script

By default, Radiance usually highlights glare sources through a random color; this can be problematic, however, when one analyzes the images later using computer vision recognition technology such as OpenCV. In order to mitigate this problem, a custom Python-based Grasshopper component was made, on the basis of the Honeybee component used to create HDR images. This custom component contains an Evalglare command, with an addition of a *(-u)* option that is used to force Radiance to reveal all

glare sources by means of one user-defined color. The (-u) option is usually followed by the RGB values of the desired color. In this research study, the color magenta was chosen with an RGB value of (255, 0, 255) [55, 83].

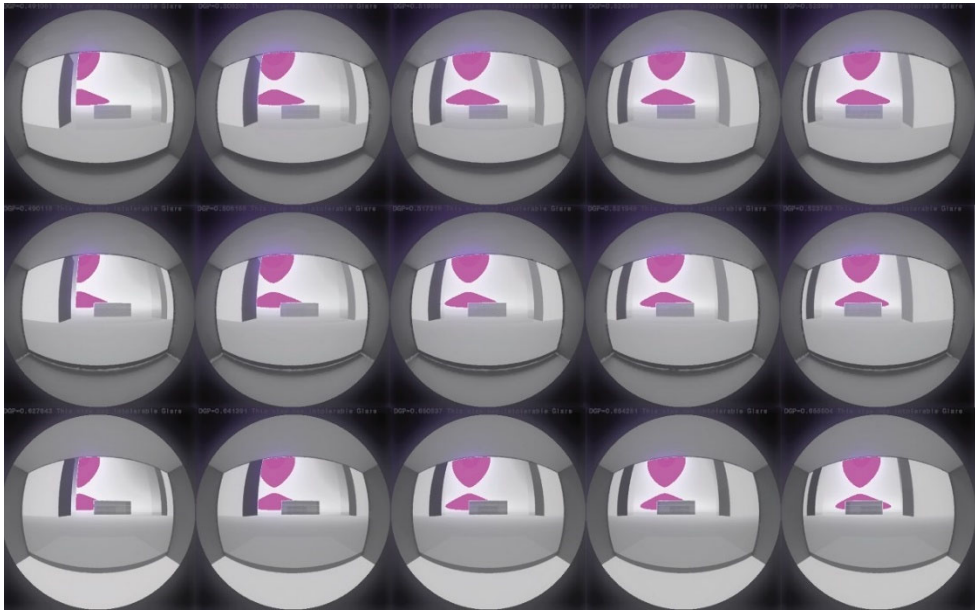


Figure 10 The resulting HDR images for all 15 views on December 17 at 13:00. Glare sources are highlighted in Magenta

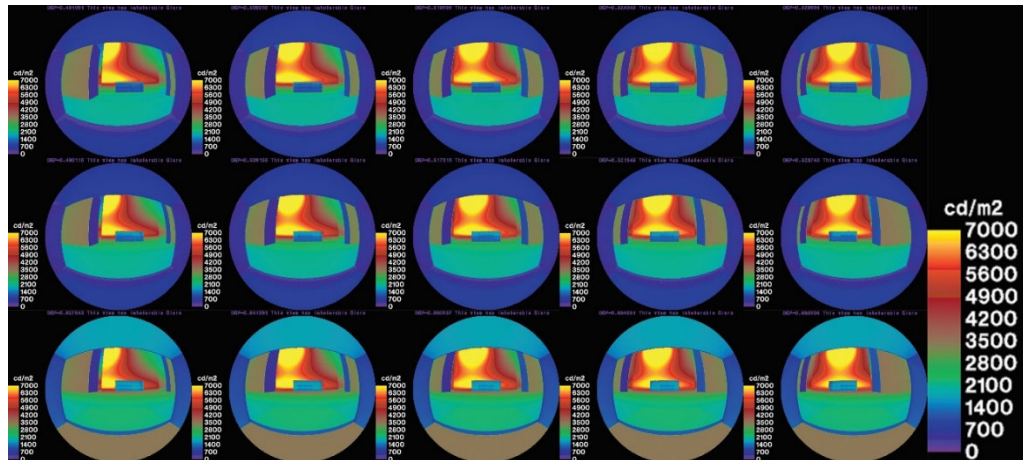


Figure 11 False color images of the resulting HDR renderings for all 15 views, on December 17 at 13:00. Luminance values (cd/m²) are illustrated in colors.

Visualizing Glare Simulations Results

Results of the glare analysis were stored in almost 54,000 files. It was impossible to open the files manually to collect data. Therefore, a custom Python script with embedded HTML and Javascript was written in order to collect such data and to create annual heatmaps that represent the DGP values for every hour of the year between 8:00 and 18:00. The created heatmaps are interactive HTML graphs that facilitated the ability to quickly read the DGP value by allowing one to hover over the desired HOY (Figure 12).

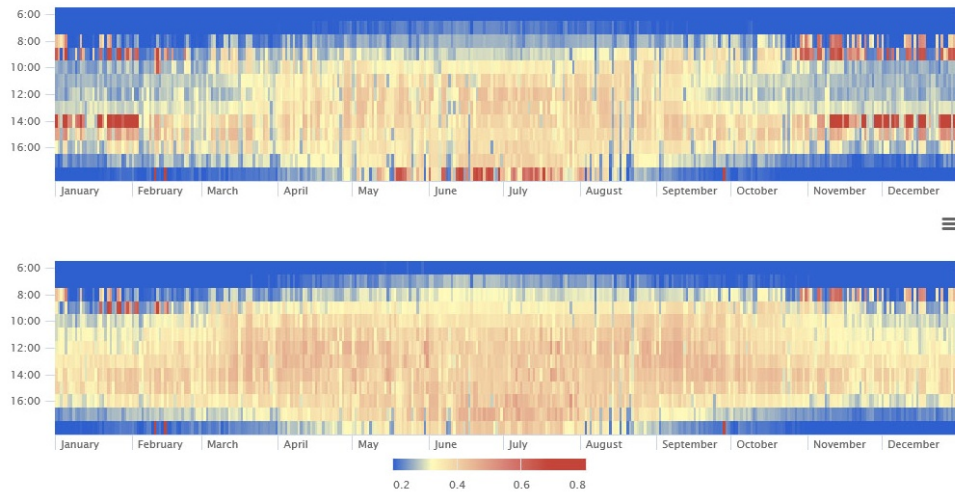


Figure 12 Example of the HTML glare heatmaps of two views in the small buildings. The maps represent DGP values of every HOY between 8:00 and 18:00

Stage Two: Glare Elimination, Daylighting, and Solar Energy Optimization

During this stage, further analysis was performed to examine the initial glare results that were carried out in stage one. This process is crucial for locating the patches of the façade that are recognized as glare sources at every HOY.

During this stage, daylighting and Radiation simulations were performed for every HOY in order to calculate the rotation angles that could yield the best indoor daylighting condition in the tower and the maximum amount of solar energy collected by the proposed façade system.

Glare Elimination

In order to eliminate glare caused by the tower façade, a two-step process is carried out. The first step is used to recognize if the glare is caused by the tower façade or by other scene elements such as direct sunlight. This step is necessary for glare elimination because it enables the proposed façade to recognize if the sun is falling on the tower's facade at a specific hour; therefore, the proposed façade can reposition its elements so as to avoid reflecting sunlight to the examined building.

In addition to the previous step, another step was carried out through use of a computer vision recognition algorithm for locating the patches of the façade that cause glare at each HOY in each room view.

Through key information that is to be fed to the proposed façade, such as sensor input and weather conditions, the information obtained in this phase through the two-step process is crucial in order to recognize what time of the day glare is being caused by the tower's façade and, second, which patches of the façade cause glare in which room in the examined three-story building.

Sunlight Tracking

Although the initial analysis revealed glare during the year, some glare might have been caused by direct sunlight or by sunlight reflection off building elements in the scene apart from the reflective façade. However, in this research study, only glare caused by

the reflective façade is examined further. In order to identify which glare is caused by the reflective façade, a custom Grasshopper component was created with Python (Appendix B-4) (Figure 13, and Figure 14). The component examines the HOY when the sun hits the reflective facade. When the component was run, Python stored all the hours that the sun hits the facade into a list for later access. In addition to determining when the sunlight falls on the reflective façade, the component also eliminates all sunlight blocked by surrounding buildings, which work as shading contexts (Figure 13).

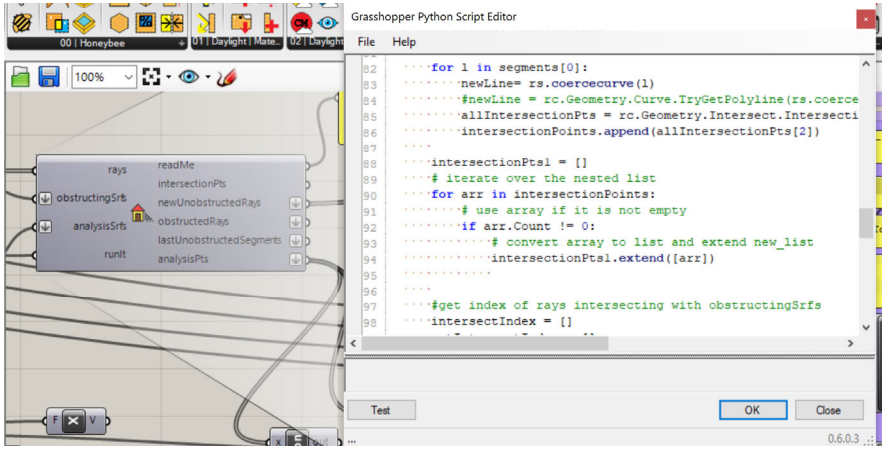


Figure 13 A custom Python-based Grasshopper component to calculate all HOY when the sunlight falls of the reflective façade

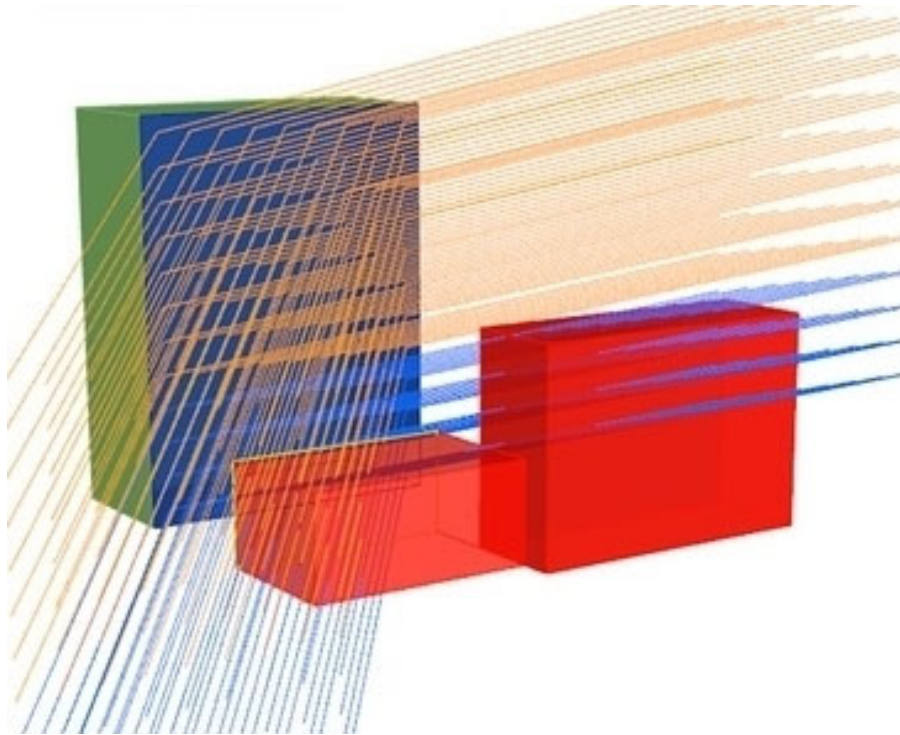


Figure 14 The custom-made component eliminates all sunlight being blocked by surrounding buildings, which work as shading contexts. In this image, blocked sunlight is shown in blue, while actual sunlight falling on the façade is shown in orange.

Computer Vision Recognition

Upon the completion of sunlight tracking, a list of HOY when the façade causes glare is obtained. If an image of each HOY in this list has a DGP value of over 0.35, then the image is further analyzed to accurately calculate the patches of the façade that cause glare at that hour. Image analysis is performed with OpenCV (Open Source Computer Vision Library), an open source computer vision and machine learning software library [109], which was incorporated into a custom-made python script to analyze all the

images with a DGP value over 0.35. For the purpose of analyzing the HDR images, 15 views were rendered by means of a green façade and plain non-reflective materials for any other objects in the scene; those images were then used as a reference for the OpenCV-based script to recognize the façade location, which is rendered in green with RGB values of 0, 255, 0 (Figure 15). The script outputs the HOY and the façade panels that cause glare at each of these hours (See Figure 16 and Appendix B-5).

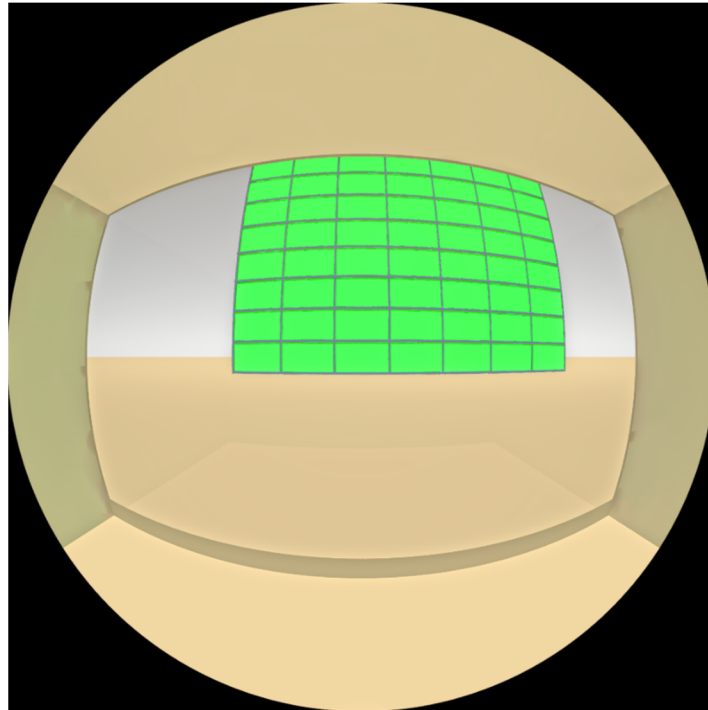


Figure 15 A rendered view with the reflective façade assigned a green color to be used for image analysis with OpenCV module library.

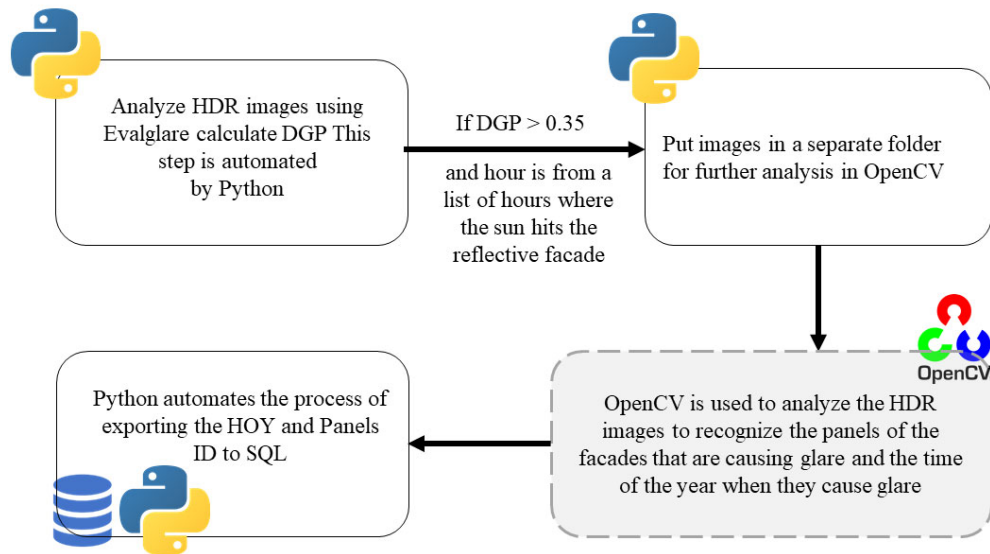


Figure 16 Images that have a DGP value over 0.35 and that occurred at an hour when the sun hits the reflective façade are further analyzed by means of OpenCV for Python. The output is stored in an SQL database.

Improving Daylighting Performance

The total number of hourly daylighting simulations for all 252 configurations is 919,800. It is obvious that the simulation process is time-consuming; therefore, an HPC-based approach that is similar to the one used for glare simulation was adapted for the daylighting simulations. This Python-based approach automated the process of sorting, organizing, preparing, and executing the simulations on a high-performance computing cluster in a few hours. The process would have normally taken 10 months to complete on a single reference computer equipped with an i7-7700HQ processor with a processing speed of 2.80 GHz (up to 3.80GHz with Turbo Boost technology) and 16 GB of RAM.

The daylighting performance simulations were carried out to determine the best position of the reflective elements that contribute to the improvement of the daylighting conditions inside the tower building.

Solar Energy Collection Optimization

In order to collect the maximum amount of energy during every daylight hour during the year, it is crucial to calculate the optimized X-axis and Z-axis rotation of the elements that make up the proposed smart façade that facilitates the maximum amount of solar energy collection.

The same approach performed for daylighting simulations was applied to solar radiation simulation, where nearly a million of hourly solar radiation simulations were performed in order to determine the optimized X-axis and Z-axis rotation angles that could facilitate maximized solar energy collection.

Stage Three: Wireless Sensor Network Design

Both buildings, the tower and the three-story building, were modeled as fitted with WSNs that were linked to microcontrollers connected to the Internet. Connecting the microcontrollers to the Internet facilitates the instant exchange of information between the two façades, as well as allowing the façades to communicate with other online plugins that can provide real-time feedback on various aspects, such as weather conditions and sun positions. Another advantage of connecting the microcontrollers to the Internet

is to enable instant, remote access to the smart system by maintenance officials and the building occupants as well.

In order to organize the data collected by the sensors from both façades, a custom Python script controlled the microcontroller (which acts as gateways to pass information from the sensors and actuators to the Internet—and vice versa). This script enables the microcontrollers to control the movable elements of the proposed façade layer based on the various elements, such as the HOY, occupancy data in the room where elements are placed, weather conditions, and the occupancy data in the three-story building where glare is experienced at that time.

For example, at a specific time, the microcontroller can send a signal to the elements of the proposed façade in front of the spots categorized as glare-causing areas during that time of the day in order to reflect the sun away from the occupied rooms in the three-story building with views that are affected by those glare-causing areas. If no occupancy is detected, the elements can be adjusted to maximize daylighting in the tower. In addition to eliminating glare, the integration of BIPVs into the proposed façade can also support the harvesting of solar energy. The BIPV elements rotate on two axes in order to follow the sun and achieve maximum energy collection whenever possible without contributing to the glare issue. Figure 17 shows an example of results from my executing the Python script at a specific HOY in one room in the tower, as well as the workflow of the WSN input and output.

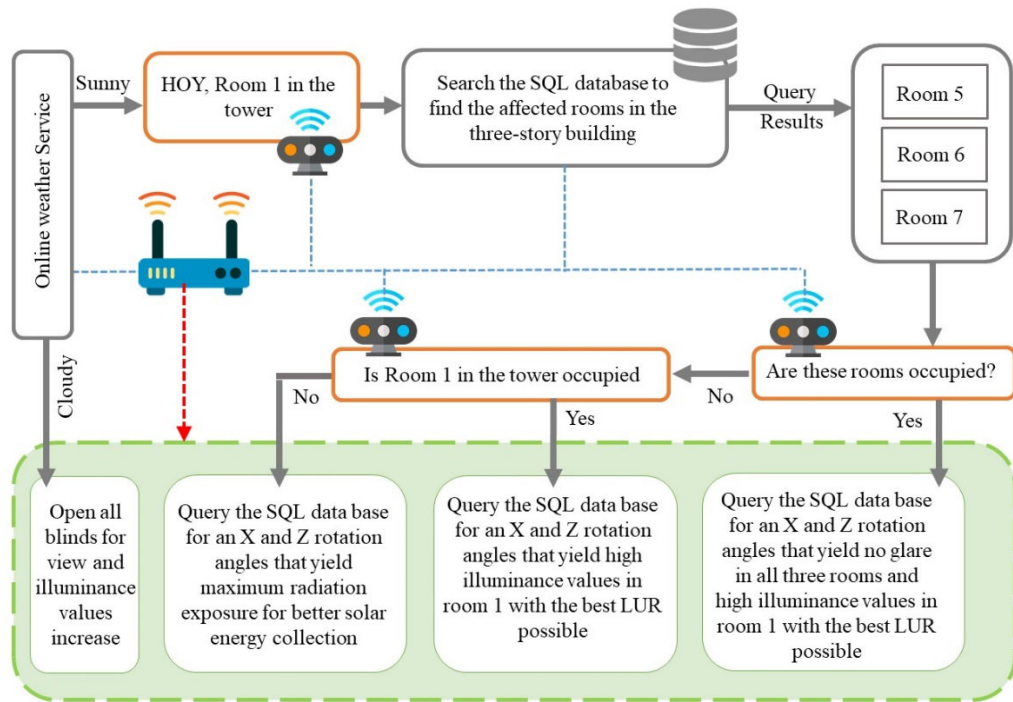


Figure 17 An example of the Python script workflow and the wireless sensor network design at a specified HOY in Room 1 in the tower. The execution of the script results on moving the façade elements in front of Room 1, as is shown in the boxes highlighted in green. The sensors and the SQL input are fed to the WSN, shown in dashed blue lines, and the WSN output is shown in red dashed lines.

The Python script was tested with a virtual IoT platform hosted on IBM’s Watson platform, which is an online platform that can facilitate the design of IoT-enabled systems. Additionally, it enables one to test virtual devices such as sensors and actuators for WSN design by means of a visual programming environment called *Node Red* that can facilitate the simulations of sensors and actuators that constitute a WSN.

Occupancy sensors' outputs are crucial for simulating the performance of a proposed dynamic façade by indicating when action must be taken to accommodate occupants; however, the output of the sensors is not available until the installation of the proposed façade and the WSN. To overcome such a problem, the simulation of the sensors in Node Red is used as an alternative solution. The simulation of the occupancy sensors was produced with the random function in Node Red, which outputs either 0 or 1 for each room in the building. Later, the output can be interpreted with a Python code that translates the number "0" to a vacant room and the number "1" to an occupied room. The Python code is designed to force the status of all rooms to become "vacant" during the weekend.

To design the proposed WSN and test its sensors' outputs and actuators, input blocks that contain JavaScript and Python codes were added and connected to each other in order to create flows in Node Red environment (Figure 18

The Node Red flow starts by feeding simulated occupancy data to a set of virtual sensors; the output of these sensors, weather data, and a connection to the SQL database are all fed to the Python script. The script outputs a set of rotation angles that are needed to move the various facades elements. Later, the rotation angles are used for validating the effectiveness of the proposed façade and the WSN system.

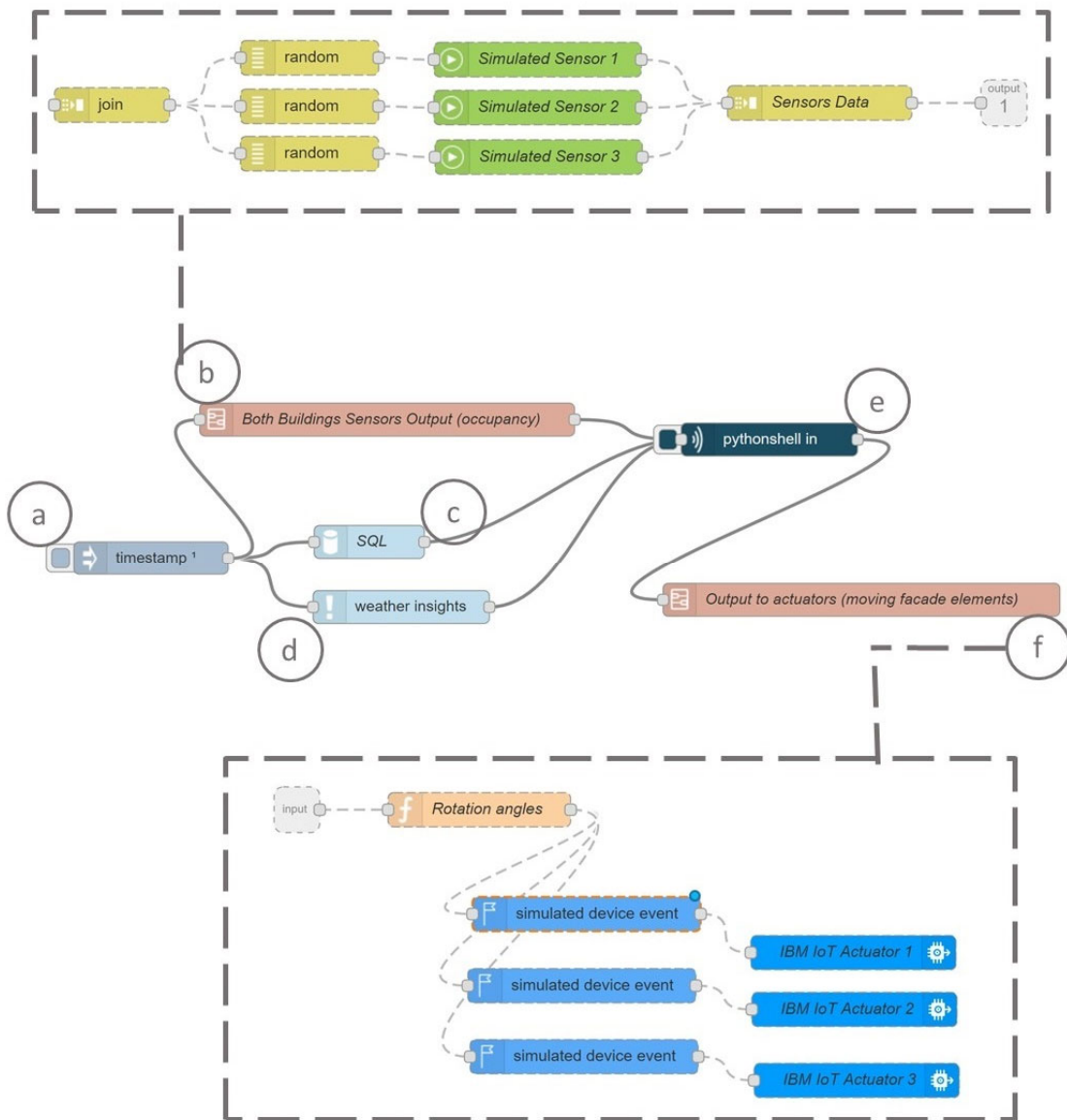


Figure 18 The simulation of the WSN with virtual sensors and actuators. The WSN is simulated through the use of Node Red, which is hosted on IBM’s Watson platform. a) A node to start the flow; b) a sub-flow that contains a virtual set of sensors (partially illustrated in the upper box); c) A connection the SQL database; d) a connection to an online live weather app; e) a connection to the Python script; and f) a sub-flow that contains the output of the Python script that contains a set of rotation angles that are fed to a set of virtual actuators (partially illustrated in the lower box)

As shown in Figure 18 the flow contains the following nodes in order:

- a) A node to start the WSN flow.
- b) A sub-flow that contains virtual sensors that are fed with simulated occupancy data.
- c) A connection to the SQL that contains the results of glare, daylighting, and solar radiation simulations results.
- d) A connection to an online live weather platform.
- e) A connection to the Python file that has a custom script.
- f) The rotation angles resulting from running the WSN and the Python script.

CHAPTER V

VALIDATION

Introduction

In order to validate the workflow and the effectiveness of the proposed WSN-enabled façade, the daylighting and glare performance of the base case are simulated, and the results are compared to the results of the performance simulations of the base case with the proposed WSN-enabled façade installed. Additionally, solar radiation collected by the proposed façade is analyzed through the use of computer simulations to calculate the hourly solar energy collection.

The simulations of the base case before and after the installation of the proposed smart façade are carried out for the winter, specifically during the month of December when the sun is low in the sky, thus causing glare problems.

Glare Reduction

Glare incidents inside all 15 rooms in the three-story building are examined by performing hourly glare simulations for the base case, which contains both buildings without the installation of the proposed façade and the WSN. Glare analysis is carried out for all 15 views within the three-story building between the hours of 8:00 and 18:00. The views in the first floor are named “1a,” “1b,” “1c,” “1d,” and “1e,” the views in the

second floor are named “2a,” “2b,” “2c,” “2d,” and “2e,” and in the third floors the view are called “3a,” “3b,” “3c,” “3d,” and “3e”.

As I noted in Chapter 1, DGP values that are:

- Larger than 0.45 show an incident of intolerable glare.
- Between 0.40 and 0.45 show an incident of disturbing glare.
- Between 0.35 and 0.40 show an incident of perceptible glare.
- Between 0.30 and 0.35 show an incident of imperceptible glare.

Glare simulations results show DGP values of all 15 views. The total number of DGP values in the data are 5,115 (15 views x 11 hours x 31 days in December). The median of the DGP values ranges from 0.32 to 0.47, and the median of the upper half of the DGP values is from 0.48 to 0.61. The median of half of the DGP values in six views is above 0.35. (see Table 5)

As shown in Table 6, glare is experienced in all views ($DGP > 0.35$) where glare incidents occur at least 42% and for up to 83% of the daylight hours in January. All views experience perceptible glare between 1% and 32% of the time, disturbing glare between 4% and 27% of the time, and intolerable glare between 13% and 67% of the time in January. For example, view 2c experiences perceptible glare for 109 hours in December, which equates to 32% of the total hours in January, disturbing glare for 92 hours, which equates to 27% of the total hours in January, and intolerable glare for 44

hours, which equates to 13% of the total hours in January. Overall number of hours when glare is experienced in this view equates to 186 hours in January. (Figure 19)

Table 5 DGP minimum, maximum, median, quartile 1, quartile 3, and the interquartile range values for all 15 base case views between December 1 to 31 from 8:00 to 18:00

View	Min	Q1	Median	Q3	Max	IQR
1a	0.06	0.19	0.32	0.59	0.68	0.40
1b	0.20	0.28	0.36	0.56	0.65	0.29
1c	0.30	0.38	0.47	0.51	0.85	0.13
1d	0.30	0.36	0.40	0.53	0.67	0.17
1e	0.22	0.25	0.41	0.61	0.69	0.36
2a	0.06	0.19	0.29	0.61	0.70	0.42
2b	0.20	0.28	0.35	0.54	0.64	0.26
2c	0.30	0.37	0.45	0.48	0.61	0.11
2d	0.30	0.35	0.40	0.52	0.65	0.17
2e	0.22	0.24	0.40	0.61	0.69	0.36
3a	0.06	0.19	0.32	0.61	0.71	0.42
3b	0.20	0.28	0.35	0.59	0.66	0.31
3c	0.30	0.38	0.47	0.52	0.66	0.14
3d	0.31	0.37	0.41	0.55	0.66	0.18
3e	0.22	0.25	0.42	0.61	0.70	0.35

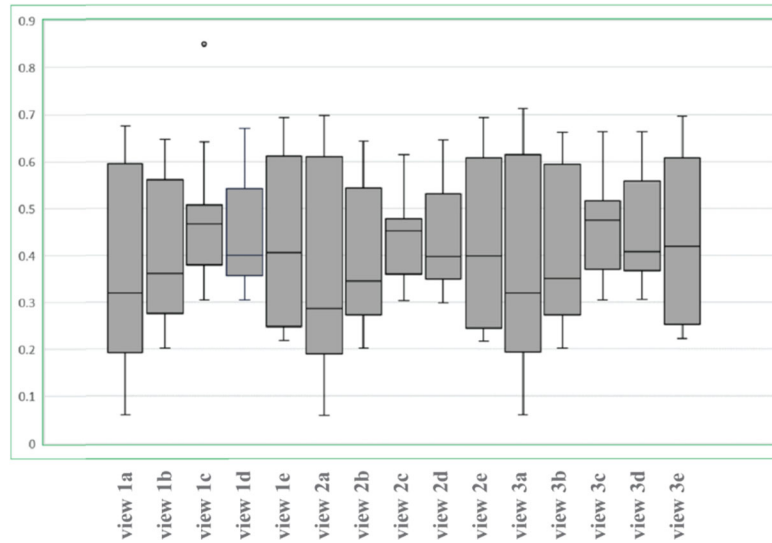


Figure 19 Boxplot that shows the DGP values of the hourly simulations between 8:00 and 18:00 through the month of December of all 15 views in the base case three-story building.

Table 6 The percentage of different glare type occurrences for the total daylight hours in December in the base case and the total number of glare occurrences when the DPG is higher than 0.35

View	Impercep.	perceptible	disturbing	intolerable	occurrences
1a	58%	1%	4%	37%	42%
1b	45%	2%	13%	40%	55%
1c	24%	34%	25%	17%	76%
1d	19%	31%	24%	26%	81%
1e	26%	1%	4%	67%	72%
2a	49%	9%	11%	31%	51%
2b	45%	2%	13%	40%	55%
2c	28%	32%	27%	13%	72%
2d	17%	30%	24%	29%	83%
2e	28%	3%	8%	61%	72%
3a	47%	6%	13%	34%	53%
3b	41%	5%	13%	41%	59%
3c	27%	32%	21%	20%	73%
3d	20%	29%	22%	29%	80%
3e	28%	5%	12%	55%	72%

Glare simulations are carried out over again for all 15 views; however, this time simulations are performed with the proposed façade installed, and its elements are rotated based on the angles that are produced by running the virtual WSN workflow in Node Red, and these angles are fed to the virtual actuators (in this case, motors to rotate the façade elements). The results of this set of the glare simulations are shown in Table 7.

The median of the DGP values ranges from 0.20 to 0.32, and the median of the upper half of the DGP values ranges from 0.30 to 0.38. The median of half of the DGP values in all views is between 0.8 and 0.13.

As shown in Table 8, glare is experienced in all views ($DGP > 0.35$) for only 4.06% to 10.44% of the time in January. All views experience perceptible glare from 1.16% to 4.64% of the time, disturbing glare from 0.1% to 2.0% of the time, and only one view suffered from intolerable glare for 0.87% of the time in January. For example, view 1d experiences perceptible glare for 13 hours in December, which equates to 2.61% of the total hours in January, disturbing glare for 6 hours, which equates to 1.74% of the total hours in January, and intolerable glare for 0% of the total hours in January. Overall number of hours when glare is experienced in this view equates to 19 hours in January. (see Table 8 and Figure 20)

Table 7 DGP values in the case study with the proposed façade and WSN system installed. The values consist of minimum, maximum, median, quartile 1, quartile 3, and the interquartile range values for all 15 views between December 1 and 31 from 8:00 to 18:00

Labels	Min	Q ₁	Median	Q ₃	Max	IQR
1a	0.15	0.18	0.20	0.30	0.40	0.11
1b	0.10	0.22	0.26	0.34	0.38	0.12
1c	0.14	0.25	0.31	0.38	0.45	0.13
1d	0.12	0.23	0.32	0.37	0.40	0.13
1e	0.08	0.23	0.25	0.31	0.41	0.08
2a	0.06	0.18	0.20	0.30	0.41	0.12
2b	0.10	0.22	0.26	0.31	0.36	0.10
2c	0.13	0.24	0.30	0.36	0.43	0.12
2d	0.11	0.23	0.31	0.36	0.37	0.13
2e	0.08	0.22	0.25	0.30	0.41	0.08
3a	0.05	0.18	0.20	0.28	0.741	0.10
3b	0.10	0.22	0.26	0.34	0.63	0.12
3c	0.14	0.25	0.31	0.38	0.39	0.12
3d	0.12	0.24	0.33	0.37	0.39	0.13
3e	0.09	0.23	0.25	0.31	0.41	0.08

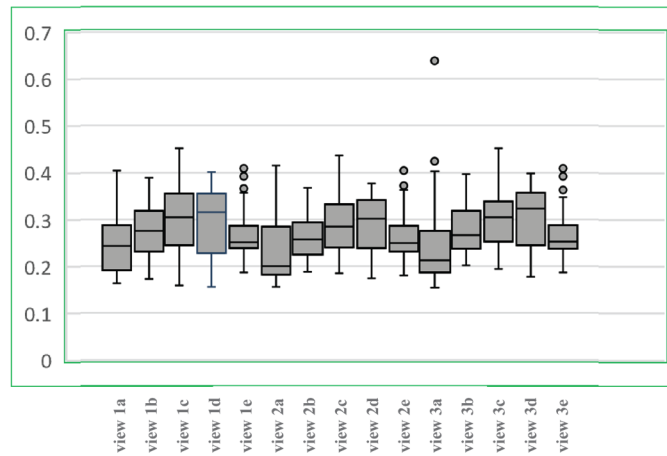


Figure 20 Boxplot that shows the DGP values of the hourly simulations throughout the month of December between 8:00 and 18:00 for all 15 views in the three-story building with the proposed façade and the WSN system installed

Table 8 The percentage of different glare type occurrences for the total daylight hours in December in the case study with the proposed façade and WSN installed and for the total number of glare occurrences when the DPG is higher than 0.35

View	Impercep.	perceptible	disturbing	intolerable	occurrences
1a	2.90%	6.09%	4.64%	0.00%	13.63%
1b	2.61%	1.45%	0.00%	0.00%	4.06%
1c	3.19%	3.48%	1.74%	0.00%	8.41%
1d	3.77%	2.61%	1.74%	0.00%	8.12%
1e	3.77%	2.32%	0.00%	0.00%	6.09%
2a	2.61%	3.77%	0.00%	0.00%	6.38%
2b	5.80%	0.87%	0.00%	0.00%	6.67%
2c	2.32%	0.87%	0.00%	0.00%	3.19%
2d	4.93%	3.77%	1.74%	0.00%	10.44%
2e	5.80%	1.74%	2.03%	0.87%	10.44%
3a	2.90%	2.61%	0.00%	0.00%	5.51%
3b	6.09%	1.74%	1.74%	0.00%	9.57%
3c	2.90%	2.32%	1.16%	0.00%	6.38%
3d	2.32%	1.45%	1.16%	0.00%	4.93%
3e	5.80%	1.16%	1.74%	0.00%	8.70%

Improvement in Daylighting Performance

Daylighting simulations of one office were carried out on December 21. The result includes the illuminance values (in lux) over a horizontal work plane that consists of 500 grid points; the work plane was placed 2.4 ft (about 75 cm) above the office floor. Calculations of the LUR ratio were carried out as well. LUR is defined as the ratio between the minimum illuminance and the average illuminance [28,56]. It is recommended in commercial buildings to have an LUR of 0.3 or higher for better daylight interior spaces. The higher the LUR value is, the better visual comfortability is in daylight areas due to the improved daylighting uniformity leading to less glare[28].

The initial set of daylighting simulations was performed to analyze the daylighting performance of one office in the tower without the installation of the WSN and the smart façade. The daylighting simulations were carried out for the winter solstice (December 21) between 8:00 and 17:00. The results are shown in Table 9 and Figure 21. The LUR values are below the threshold that was previously discussed: the LUR values range from 0.24 and 0.29. The average illuminance values range from 104 lux to 2,262 lux, the minimum illuminance values range from 30 lux to 613 lux, and the maximum illuminance values range from 223 lux to 4,366 lux.

Table 9 Minimum, maximum, and average illuminance, and the LUR of the base case study from 8:00 to 17:00 on December 21

Hour	Min	Max	Avg.	LUR
8	30	223	104	0.29
9	58	456	226	0.26
10	320	1343	957	0.26
11	367	2809	1311	0.28
12	444	3301	1829	0.24
13	613	4366	2262	0.27
14	572	3981	2132	0.27
15	453	3115	1605	0.28
16	335	2325	1174	0.29
17	153	1099	554	0.28

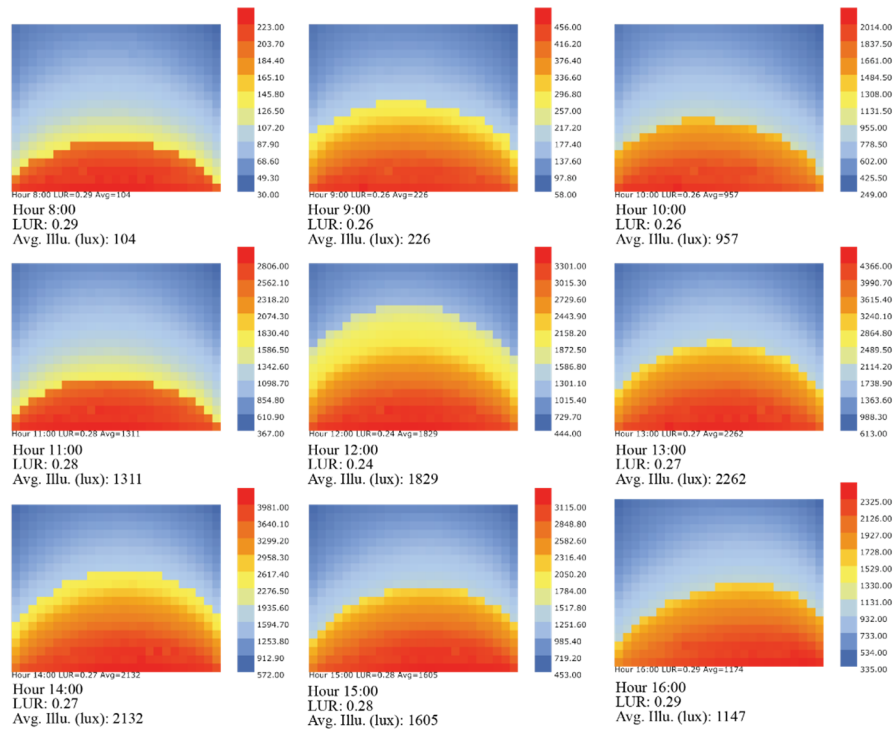


Figure 21 The illuminance grid in the base case from 8:00 to 16:00 on December 21

The second set of daylighting simulations was performed to analyze the daylighting performance of one office in the tower with the installation of the WSN and the smart façade. The results are shown in Table 10 and Figure 22. The LUR values are all above the recommended threshold of 0.3. The LUR values range from 0.34 and 0.45. The average illuminance values range from 279 lux to 2,559 lux, the minimum illuminance values range from 96 lux to 1,243 lux, and the maximum illuminance values range from 480 lux to 4,370 lux.

Table 10 Minimum, maximum, and average illuminance, and the LUR of the proposed WSN and smart facade from 8:00 to 17:00 on December 21

Hour	Min	Max	Avg.	LUR
8	96	480	279	0.34
9	101	495	280	0.36
10	431	2047	1188	0.36
11	644	2646	1594	0.4
12	744	3360	1815	0.4
13	1243	4370	1753	0.45
14	1005	4077	2559	0.39
15	374	1855	993	0.38
16	259	1190	669	0.39
17	219	937	519	0.42

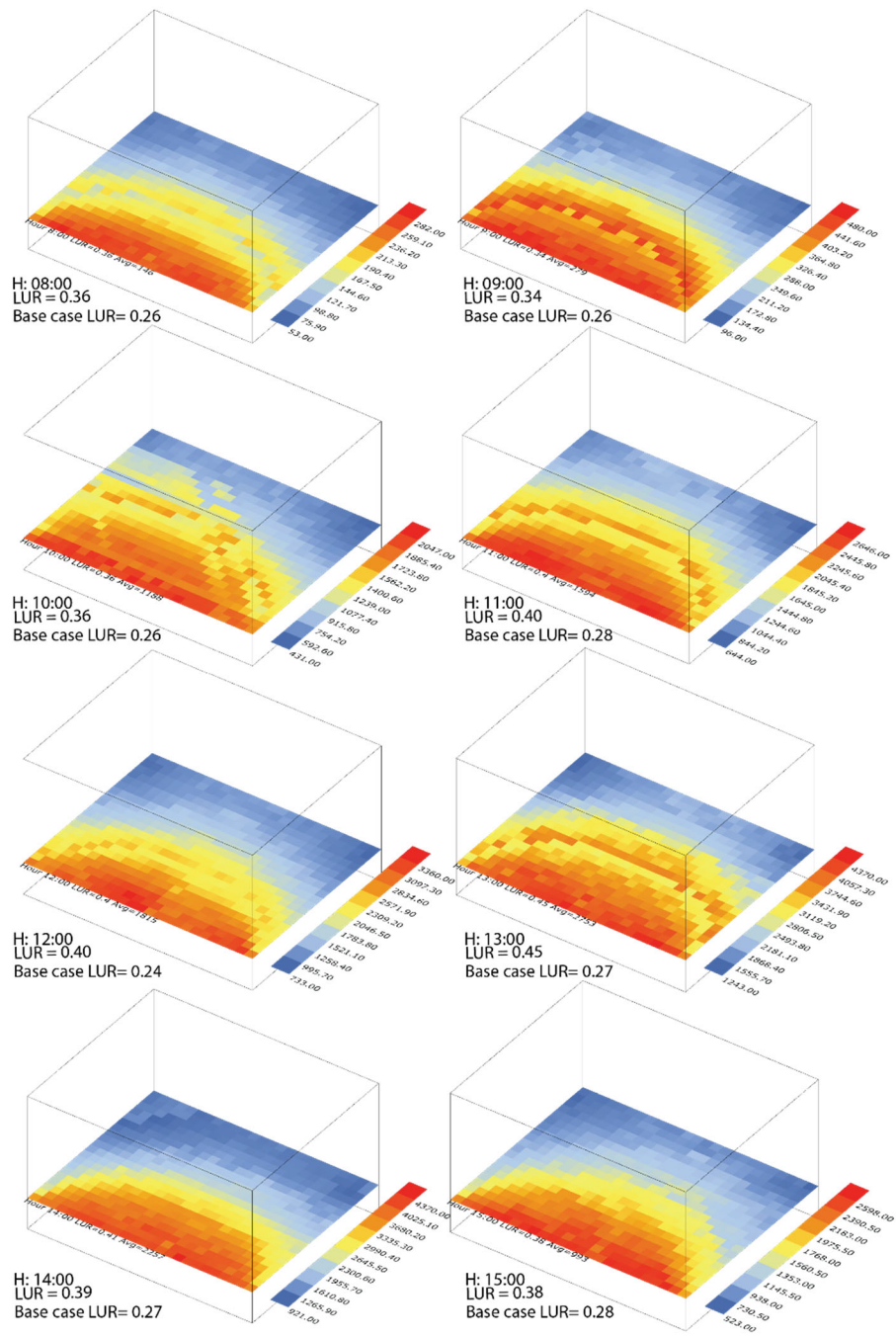


Figure 22 The illuminance grid in the proposed case with the WSN and smart facade from 8:00 to 16:00 on December 21

Figure 23 shows a comparison between the minimum, maximum, and average illuminance values of the proposed smart façade and of the base case between 8:00 and 17:00 on December 21. Although sometimes the average illuminance values in the office room decreased with the installation of the proposed WSN and the smart façade, the LUR was greatly improved, thus leading to a better daylit room with a uniform daylight for visually comfortable spaces. For example, at hour 15:00 the average illuminance value dropped from 1,605 lux to 993 lux after the installation of the WSN and the smart façade. However, the LUR increased by about 60%, from 0.28 to 0.45 (see Figure 24).

Figure 24 shows the increase of the LUR values after the installation of the WSN and the smart façade. The increase in the LUR ranges from 24% to 60%, thus leading to a boost in all LUR values above the minimum recommended threshold of 3.0.

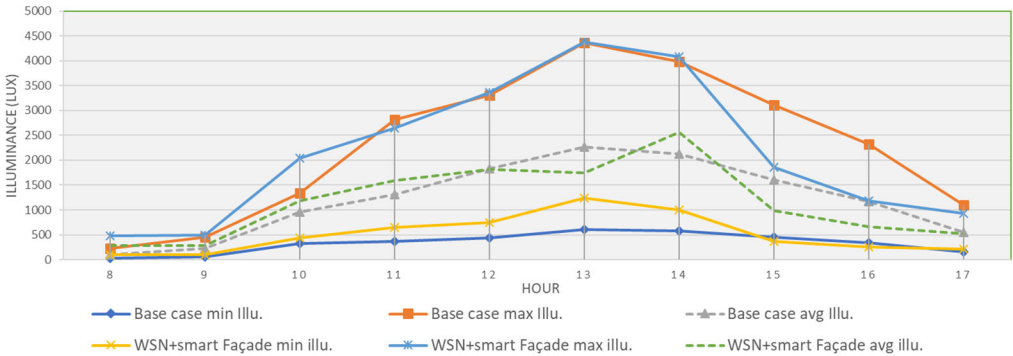


Figure 23 Minimum, maximum, and average illuminance of both the base case and the proposed case with the WSN and smart façade installed between 8:00 and 17:00 on December 21

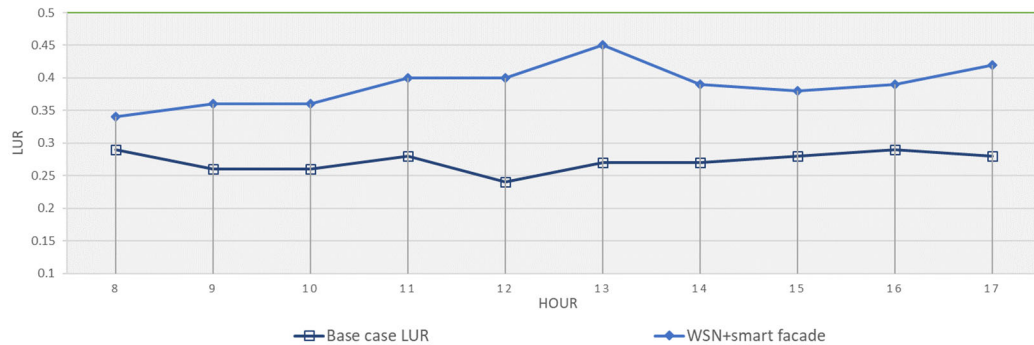


Figure 24 LUR values of both the case study and the proposed WSN and smart façade between 8:00 and 17:00 on December 21

Solar Energy Collection

Python was used to extract solar radiation data from the results of the radiation simulations. The amount of solar radiation falling on the blind surfaces varies according to the rotation angles of the blind system. The data extracted represents the amount of direct solar radiation that is falling on the proposed façade surfaces on both the summer and winter solstice (June 21 and December 21).

The range of the amount of direct solar radiation falling on the proposed facade surfaces resulting from changing the façade system angles varies greatly; for example, on Dec 21, the minimum amount of solar radiation collected by the proposed façade at different hours during the day (from 8:00 to 17:00) ranges from 9 to 40 wh/m², while the maximum amount collected ranges from 19 to 118 wh/m². Therefore, changing the proposed system angles leads to an increase of solar collection between 211% and

295%. Additionally, the results were compared with the solar radiation collected by a traditional vertical façade with BIPV; the comparison shows that the solar radiation collected by the vertical façade on December 21 from 8:00 to 17:00 ranges from 10 to 46 wh/m². The results indicate that the performance of the proposed façade increases the solar radiation collection from 190% to 256%; for example, at 13:00, the amount of radiation collected by a traditional vertical façade with BIPV is 143 wh/m², while the solar radiation collected by the proposed façade with the optimized angles is 326 wh/m², which equates to a 228% increase (see Figure 25 and Table 11).

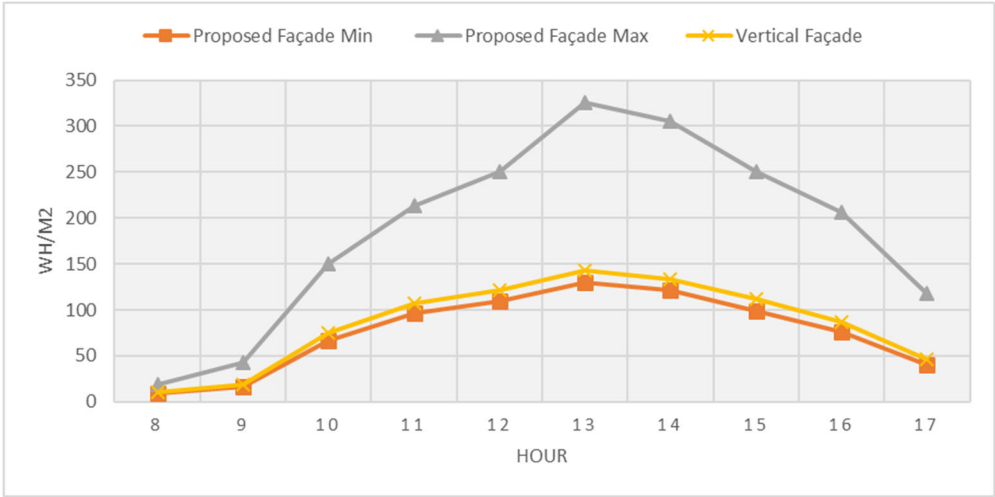


Figure 25 The range (minimum and maximum) of the direct solar radiation falling on the proposed façade surfaces by changing both angles around the X-axis and Z-axis on December 21 from 8:00 to 17:00, compared to the amount of solar radiation falling on a traditional vertical BIPV

Table 11 The amount of solar radiation falling on a traditional vertical façade with BIPV and the range of solar radiation falling on the proposed

**façade surfaces through the use of different rotation angles on December 21
between 8:00 and 17:00**

December 21 Hour	Proposed Façade Min (wh/m ²)	Proposed Façade Max (wh/m ²)	Vertical Façade w/BIPV (wh/m ²)
8	9	19	10
9	17	43	19
10	67	150	75
11	97	213	107
12	110	250	122
13	130	326	143
14	121	305	134
15	99	250	112
16	76	206	87
17	40	118	46

Similarly, on the summer solstice (June 21), changing the proposed façade angles leads to a solar radiation collection with minimum values from 77 to 90 wh/m² and with maximum values from 559 to 650 wh/m², which equates to an increase from 722 to 725% in solar collection when optimized angles are used. Furthermore, optimized angles yield an increase in solar radiation collection of between 300 and 520%; for example, on June 21 at 12:00, the amount of solar radiation collection by a traditional vertical BIPV is 183 wh/m², compared to 957 wh/m² when the proposed façade with the optimized angles is used (see Figure 26 and Table 12).

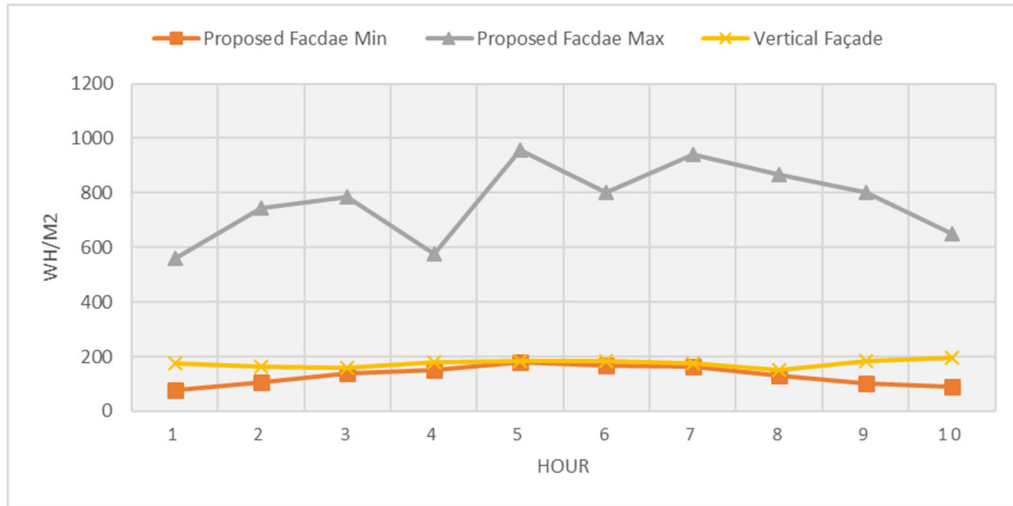


Figure 26 The range (minimum and maximum) of the direct solar radiation falling on the surfaces by changing both angles around the X-axis and Z-axis on June 21 from 8:00 to 17:00, compared to the amount of solar radiation falling on a traditional vertical BIPV

Table 12 The amount of solar radiation falling on a traditional vertical façade with BIPV and the range of solar radiation falling on the proposed façade surfaces through the use of different rotation angles on June 21 between 8:00 and 17:00

June 21 Hour	Proposed Façade Min (wh/m ²)	Proposed Façade Max (wh/m ²)	Vertical Façade w/BIPV (wh/m ²)
8	77	559	175
9	106	742	164
10	138	786	157
11	151	576	180
12	180	957	183
13	168	800	185
14	164	940	177
15	131	867	152
16	101	801	183
17	90	650	197

CHAPTER VI

CONCLUSIONS AND DISCCUSION

Conclusion

The WSN has facilitated glare elimination based on occupancy and on the results of glare analysis; however, some rooms are not always occupied or do not experience glare all the time. Accordingly, the proposed façade has introduced a dynamic solution to address daylighting performance and solar energy collection when glare elimination is not needed due to lack of room occupancy or simply because the view does not experience glare at a specific HOY. Furthermore, the proposed workflow has facilitated views whenever overcast weather is detected, the views were maximized through the rotation of the façade elements in order to allow maximum daylight and views.

Based on the results discussed in Chapter V, it is evident that the proposed façade with the integrated WSN on both buildings improves daylighting performance and solar radiation collection, and it eliminates glare caused by reflective facades.

Applying the proposed façade and the WSN that is installed on both buildings leads to the elimination of glare caused by the tower's reflective façade; for example, in December, when the sun is at a low angle, the overall hours when glare is experienced are reduced from 186 hours to 19 hours for one view on the second floor. Although, some glare still exists, this is caused by the bright scene due to the low angle of sun. The

proposed façade and the WSN contributed to the reduction of the overall glare in all 15 views in December when all the views experience perceptible glare between 1% and 32%, disturbing glare between 4% and 27% of the time, and intolerable glare between 13% and 67% of the time in January. The proposed framework leads to an elimination of glare caused by sunlight reflection, which, in turn, leads to a reduction in glare where all views experience perceptible glare from 1.16% to 4.64% of the time, disturbing glare from 0.1% to 2.0% of the time, while only one view suffered from intolerable glare, 0.87% of the time in December. As noted earlier, some glare still exists in some views due to the low angle of the sun leading to a bright scene.

The proposed workflow not only eliminated glare but also improved the daylighting performance inside the examined tower by improving the daylighting uniformity ratio and the illuminance levels. Through the proposed workflow, the lighting uniformity ratio improved on December 21 between 8:00 and 17:00 from 0.24–0.29 to 0.34–0.45, thus leading to the increasing of the LUR above the recommended minimum threshold of 0.30.

In addition to improving the LUR, using the workflow improved the average illuminance values from 88% to 268% (increasing the average illuminance values from 104–2262 lux to 279–2559 on the winter solstice from 8:00 to 17:00).

Finally, the proposed framework increased the amount of solar energy collection by optimizing the façade's elements tilt in both the XY and XZ directions, thereby leading to a maximized energy production. On the winter solstice between 8:00 to 17:00, the proposed façade leads to an increase in the amount of solar radiation falling on the façade's elements of 190–250%, compared to the use of BIPV on a traditional vertical façade. In summer between 8:00 to 16:00, the amount of solar radiation collected by the proposed façade increased by 300–520%, compared to BIPV on a traditional vertical façade.

Study Limitations

In dense urban areas, solar reflections can be caused by multiple glazed building façades in a given area. However, for the purposes of this research study, the proposed FIoT model does not consider the reflections caused by other buildings surrounding the two buildings under investigation. Instead, the proposed research project focuses on the application of the proposed FIoT model to the façades of two buildings: one causing solar reflection and one affected by the solar reflection.

Although offices in commercial buildings can be occupied by more than one worker situated in different positions within each room, this study assumed that all the rooms along the perimeter of the façade of the building have only one occupant. Furthermore, to emulate the worst-case scenario, the occupant is assumed to face the window. This one occupant's view was examined for the glare analysis.

Discussion and Future Studies

Considering the various negative impacts of solar reflections on people, buildings, vegetation, the surrounding environments, and the microclimate, it is crucial to find a solution to improve occupant comfort and energy efficiency in buildings and urban environments. In this context, IoT-based systems support a human-centric approach that facilitates real-time actions based on user inputs. This can help to create responsive environments that sense human living patterns and that can adapt to environmental occupants. Indeed, the proliferation of IoT-based systems, in general, and human-centric approaches, in particular, supports new opportunities for the development of smart ecosystems that can facilitate user interaction and connectivity with the surrounding built environment.

There is ongoing research focus on smart façades. Specifically, researchers have been working on using IoT-based devices to help transform traditional static façades into dynamic smart ones. Some researchers have incorporated sets of sensors into façade prototypes in order to collect data on various conditions, such as lighting levels.

Although such façade designs can help increase building performance, they do not necessarily achieve maximum occupant comfort because they fail to sense and recognize human needs. Furthermore, such smart façades can encounter problems caused by other nearby buildings, such as sunlight bouncing off reflective façades. Facilitating communications among façades may help to overcome these issues and may mitigate many of the problems that arise in urban areas.

Further studies are needed to address the limitations that were previously discussed. For example, the solar reflection of various surfaces in the urban scene were not taken into consideration. This can be addressed in future studies by examining the expansion of the existing WSN for installation on various building facades and other surfaces.

Furthermore, in the last couple of decades, urban development has been growing in an accelerated manner causing the constant construction of new buildings. In such case, the expansion of existing WSN might not be the optimal solution, therefore, further studies are needed to examine the advantage of other emerging technologies such as Artificial Intelligence (AI) that can mitigate such a problem. The study of AI is beyond the scope of this dissertation; however, it is notable that AI can be beneficial in teaching a façade to adapt and sense newly built buildings without the need to expand the existing WSN. AI can also be beneficial in addressing climate change due to global warming by teaching the façade to adapt to new climatic patterns.

It is worth mentioning that the FIoT model depends on collecting occupancy data.

However, safety and privacy concerns continue to hinder implementing such a model.

Other factors that act as barriers to fully integrating the FIoT in the built environment include social, legal, and cultural aspects. Further work is needed to further investigate these issues.

Although, it is evident that the proposed FIoT model reduced glare and improved building conditions, the major contribution from this study is the introduction of a novel FIoT approach that enabled communication channels between two facades.

REFERENCES

- [1] W.J. Brotas Luisa, Solar reflected glare affecting visual performance, in: Proceedings of 8th Windsor Conference: Counting the Cost of Comfort in a Changing World Cumberland Lodge, 2014: pp. 10–13.
- [2] J.D. Kelso, Buildings Energy Databook, Departemet of Energy, 2011.
- [3] M. Schiler, E. Valmont, Microclimatic Impact: Glare around the Walt Disney Concert Hall, in: Proceedings of the International Solar Energy Society Conference, 2005: pp. 6–12.
- [4] Council on Tall Buildings and Urban Habitat, “Oculi Solution” to Museum Tower Glare Rejected, (2012).
<http://www.ctbuh.org/News/GlobalTallNews/tabid/4810/Article/165/language/en-US/view.aspx> (accessed December 10, 2017).
- [5] T. Tsoutsos, N. Frantzeskaki, V. Gekas, Environmental Impacts from the Solar Energy Technologies, Energy Policy. 33 (2005) 289–296. doi:10.1016/S0301-4215(03)00241-6.
- [6] H. Hammer, Potential and Feasibility of PV for Commercial Buildings in Norway and Its Effect on Building Certification Schemes, 2014.
<http://researchrepository.murdoch.edu.au/24197/>.
- [7] S. Kubba, LEED v4 Practices, Certification, and Accreditation Handbook: Second Edition, 2015. doi:10.1016/C2015-0-00887-5.
- [8] J.A. Jakubiec, C.F. Reinhart, Assessing Disability Glare Potential Due to Reflections from New Constructions : A Case Study Analysis and Recommendations for the Future, Transportation Research Record. (2014) 1–12. doi:10.3141/2449-13.
- [9] M. Granberry, S. Thompson, G. Jacobson, Museum Tower hires technical firm to help solve glare dispute | News | Dallas News, (2014).

<https://www.dallasnews.com/news/news/2014/04/02/museum-tower-hires-technical-firm-to-help-solve-glare-dispute> (accessed December 10, 2017).

- [10] R. Stott, Search Ends for Solution to Museum Tower’s Glare Problems at Nasher Sculpture Center, (2015). <https://www.archdaily.com/773066/search-ends-for-solution-to-museum-towers-glare-problems-at-nasher-sculpture-center> (accessed December 10, 2017).

- [11] C. Birnbaum, Museum Tower: “attack” on the Nasher Sculpture Center’s garden, building & art | The Cultural Landscape Foundation, (2012). <https://tclf.org/blog/museum-tower-attack-nasher-sculpture-centers-garden-building-art> (accessed December 10, 2017).

- [12] V.L. Erickson, A.E. Cerpa, Thermovote: Participatory Sensing for Efficient Building HVAC Conditioning, in: Proceedings of the Fourth ACM Workshop on Embedded Sensing Systems for Energy-Efficiency in Buildings (BuildSys ’12), 2012: pp. 9–9. doi:10.1145/2422531.2422534.

- [13] M. Magno, T. Polonelli, L. Benini, E. Popovici, A Low Cost, Highly Scalable Wireless Sensor Network Solution to Achieve Smart LED Light Control for Green Buildings, IEEE Sensors Journal. 15 (2015) 2963–2973. doi:10.1109/JSEN.2014.2383996.

- [14] N. Mitton, S. Papavassiliou, A. Puliafito, K.S. Trivedi, Combining Cloud and sensors in a smart city environment, EURASIP Journal on Wireless Communications and Networking. (2012) 247–247. doi:10.1186/1687-1499-2012-247.

- [15] T.P. Yekutieli, Y.J. Grobman, Controlling Kinetic Cladding Components in Building Façades: a Case for Autonomous Movement, in: 19th International Conference of the Association of Computer-Aided Architectural Design Research in Asia CAADRIA, 2014.

- [16] S.Y. Jang, S. Lee, S.A. Kim, Collaborative Responsive Facade Design Using Sensor and Actuator Network, in: Lecture Notes in Computer Science, 2013: pp. 11–18. doi:10.1007/978-3-642-40840-3-2.

- [17] Hopkinson - 1956 - Glare Discomfort and Pupil Diameter, (n.d.).

- [18] Borisuit et al. - 2014 - Effects of Realistic Office Daylighting and Electric Lighting Conditions on Visual Comfort, Alertness and Mood, (n.d.).
- [19] K.G. Sehen, Sehen am Bildschirmarbeitsplatz: Nützliche Tipps für Ihre Tätigkeit am Computer Beruflich und Privat, KGS, Köln. (2001).
- [20] R.G. Hopkinson, Glare Discomfort and Pupil Diameter, *Journal of the Optical Society of America*. 46 (1956) 649–649. doi:10.1364/JOSA.46.000649.
- [21] Y. Lin, S. Fotios, M. Wei, Y. Liu, W. Guo, Y. Sun, Eye Movement and Pupil Size Constriction Under Discomfort Glare, *Investigative Ophthalmology and Visual Science*. 56 (2015) 1649–1656. doi:10.1167/iovs.14-15963.
- [22] A. Borisuit, F. Linhart, J.-L. Scartezzini, M. Munch, Effects of Realistic Office Daylighting and Electric Lighting Conditions on Visual Comfort, Alertness and Mood, *Lighting Research and* (2014) 1–18. doi:10.1177/1477153514531518.
- [23] K.D. Garcia, W.W. Wierwille, Effect of Glare on Performance of a VDT Reading-Comprehension Task, *Human Factors*. 27 (1985) 163–173.
- [24] T. Partonen, J. Lönnqvist, Seasonal affective disorder, *The Lancet*. 352 (1998) 1369–1374.
- [25] R.Z. Goetzel, S.R. Long, R.J. Ozminkowski, K. Hawkins, S. Wang, W. Lynch, Health, Absence, Disability, and Presenteeism Cost Estimates of Certain Physical and Mental Health Conditions Affecting U.S. Employers:, *Journal of Occupational and Environmental Medicine*. 46 (2004) 398–412. doi:10.1097/01.jom.0000121151.40413.bd.
- [26] A. Rodgers, Control of Light: Better light for the Classroom", *Architectural Record*. 79 (1936) 505–509.
- [27] J. Goldemberg, T.B. Johansson, A.K.N. Reddy, R.H. Williams, *Energy for a Sustainable World*, Wiley New York, 1988.

- [28] D.L. DiLaura, *The Lighting Handbook: Reference & Application*, Illuminating Engineering Society of North America, 2011.
- [29] J.Y. Suk, M. Schiler, K. Kensek, Is Exterior Glare Problematic?: Investigation on Visual Discomfort Caused by Reflected Sunlight on Specular Building Facades, in: PLEA, 2016.
- [30] E. Franconi, Y.J. Huang, Shell, System, and Plant Contributions to the Space Conditioning Energy Use of Commercial Buildings, in: *Proceedings for the ACEEE 1996 Summer Study on Energy Efficiency in Buildings*, Asilomar Conference Center, Pacific Grove, CA, 1996.
- [31] E. Lee, L. Fernandes, B. Coffey, A Post-Occupancy Monitored Evaluation of the Dimmable Lighting, Automated Shading, and Underfloor Air Distribution System in The New York Times Building, 2013.
- [32] M. Schiler, E. Valmont, Urban Environmental Glare : the Secondary Consequence of Highly Reflective Materials, in: *PLEA Conference, 2006*: pp. 6–8. http://plea-arch.org/ARCHIVE/2006/Vol11/PLEA2006_PAPER753.pdf.
- [33] J. Allegrini, V. Dorer, J. Carmeliet, Influence of the Urban Microclimate in Street Canyons on the Energy Demand for Space Cooling and Heating of Buildings, *Energy and Buildings*. 55 (2012) 823–832. doi:10.1016/j.enbuild.2012.10.013.
- [34] N.E. Holt, D. Zigmantas, L. Valkunas, X.-P. Li, K.K. Niyogi, G.R. Fleming, Carotenoid Cation Formation and the Regulation of Photosynthetic Light Harvesting, *Science*. 307 (2005) 433–436. doi:10.1126/science.1105833.
- [35] M.J. Dowson-Day, A.J. Millar, Circadian Dysfunction Causes Aberrant Hypocotyl Elongation Patterns in Arabidopsis, *The Plant Journal*. 17 (1999) 63–71. doi:10.1046/j.1365-313X.1999.00353.x.
- [36] Steven Litt, Anish Kapoor’s shiny “C-Curve” Scorches Grass in Distracting Installation at Cleveland Museum of Art, (2015). http://www.cleveland.com/arts/index.ssf/2015/08/anish_kapoors_shiny_c-curve_bu.html (accessed December 10, 2017).

- [37] D.L. Simms, Archimedes and the burning mirrors of Syracuse, *Technology and Culture*. 18 (1977) 1–24.
- [38] J. Theeuwes, J.W.A.M. Alferdinck, M. Perel, Relation Between Glare and Driving Performance, *Human Factors*. 44 (2002) 95–107.
doi:10.1518/0018720024494775.
- [39] R. Gray, D. Regan, Glare Susceptibility Test Results Correlate with Temporal Safety Margin when Executing Turns Across Approaching Vehicles in Simulated Low-Sun Conditions., *Ophthalmic and Physiological Optics*. 27 (2007) 440–50.
doi:10.1111/j.1475-1313.2007.00503.x.
- [40] R. Hart, C. Curcija, D. Arasteh, H. Goudey, C. Kohler, S. Selkowitz, Research Needs : Glass Solar Reflectance and Vinyl Siding, Lawrence Berkeley National Laboratory. (2011) 1–24.
- [41] EIA, U . S . Energy-Related Carbon Dioxide Emissions , 2015, 2017.
https://www.eia.gov/environment/emissions/carbon/pdf/2015_co2analysis.pdf.
- [42] R. Labib, Improving daylighting in existing classrooms using laser cut panels, *Lighting Research and Technology*. 45 (2013) 585–598.
doi:10.1177/1477153512471366.
- [43] A.D.F. Hamlin, *A Text-Book of the History of Architecture*, 1909.
<http://www.gutenberg.org/ebooks/26319>.
- [44] M. Boubekri, *Daylighting, Architecture and Health: Building Design Strategies*, Architectural Press, 2008.
https://books.google.com/books/about/Daylighting_Architecture_and_Health.html?id=e15lq-Ang1sC&pgis=1.
- [45] N. Lechner, *Heating, cooling, lighting: design methods for architects*, Wiley, 2001. <http://books.google.com/books?id=3UykWkxSTGcC>.
- [46] R. Banham, *Architecture of the Well-tempered Environment*, University of Chicago Press, 1984.

- [47] J. Nayak, J. Prajapati, Handbook on energy conscious buildings, Prepared under the Interactive R & D Project. 3 (2006) 03.
- [48] C.L. Robbins, Daylighting. Design and analysis, (1985).
- [49] C.F. Reinhart, Daylighting Handbook-Volume I, 2013.
- [50] K. Rangi, W. Osterhaus, Windowless environments: are they affecting our health, Proceedings of LIGHTING. (1999) 18–19.
- [51] M. Rea, M. Figueiro, J. Bullough, Circadian photobiology: an emerging framework for lighting practice and research, Lighting Research and Technology. 34 (2002) 177–187. doi:10.1191/1365782802lt057oa.
- [52] H.M. Group, Daylighting in Schools. An Investigation into Relationship between Daylight and Human Performance, 1999.
- [53] R. Küller, C. Lindsten, Health and behavior of children in classrooms with and without windows, Journal of Environmental Psychology. 12 (1992) 305–317.
- [54] A.F. Handbook, American society of heating, refrigerating and air-conditioning engineers, Inc.: Atlanta, GA, USA. (2009).
- [55] USGBC, LEED Rating System for New Construction V4, 2014.
<http://www.usgbc.org/ShowFile.aspx?DocumentID=8868>.
- [56] B. Global, BRE Global Ltd, BREEAM New Construction Non-Domestic Buildings Technical Manual, BRE Global Ltd, 2011.
http://www.breeam.org/breeamGeneralPrint/breeam_non_dom_manual_3_0.pdf.
- [57] SLL CIBSE, Code for Lighting Chapter 7 : Construction (Design and Management), in: Butterworth-Heinemann, 2012: pp. 135–142.
<http://books.google.com/books?id=yAzDrxgabNwC>.
- [58] Y.K. Yi, A.M. Malkawi, Association HQE, 2011.
doi:10.1016/j.autcon.2009.03.006.

- [59] Department of Urban Planning, The Pearls Rating System, 2014. <https://www.dpm.gov.abudhabi/>.
- [60] J. Vos, T. Van den Berg, Report on disability glare, CIE Collection. 135 (1999) 1–9.
- [61] J.J. Vos, Reflections on glare, *Lighting Research & Technology*. 35 (2003) 163–175.
- [62] R. Hopkinson, Glare from windows - 3 using the glare index in daylighting design, *Construction Research and Development Journal*. 3 (1971) 23–28.
- [63] M. Jean-Jacques, D. Francioli, P. Rey, Observed variation of lighting conditions versus feelings of visual discomfort in VDT operators: Application of a new model, *Lux Europa*. (1993) 332–339.
- [64] Jan Weinold, evalglare.pdf — Radsite, (2006). <https://www.radiance-online.org/learning/documentation/manual-pages/pdfs/evalglare.pdf/view> (accessed September 7, 2018).
- [65] P. Petherbridge, R.G. Hopkinson, Discomfort glare and the lighting of buildings, *Transactions of the Illuminating Engineering Society*. 15 (1950) 39–79.
- [66] H. Einhom, Unified glare rating (UGR): Merits and application to multiple sources, *International Journal of Lighting Research and Technology*. 30 (1998) 89–93.
- [67] L.H. IES, Reference Volume: Calculation of Visual Comfort Probability (VCP), S. 9 (n.d.) 46–9.
- [68] A.A. Nazzal, A new daylight glare evaluation method: Introduction of the monitoring protocol and calculation method, *Energy and Buildings*. 33 (2001) 257–265.
- [69] M. Tokura, T. Iwata, M. Shukuya, K. Kimura, Experimental Study on a Method for Evaluating Discomfort Glare from Windows, in: 1993.

- [70] G. Ward, Radiance visual comfort calculation, LESO-EPFL, April. (1992). <http://citeseerx.ist.psu.edu/viewdoc/download?doi=10.1.1.51.4937&rep=rep1&type=pdf>.
- [71] U. Nations, World Population Prospects: The 2015 Revision, United Nations Economic and Social Affairs. XXXIII (2015) 1–66. doi:10.1007/s13398-014-0173-7.2.
- [72] K. Jackson, Columbus Under Construction to Become America’s First “Smart City,” (2017). <http://www.foxnews.com/tech/2017/07/10/columbus-under-construction-to-become-americas-first-smart-city.html> (accessed December 10, 2017).
- [73] R.G. Hollands, Will The Real Smart City Please Stand up?, *City*. 12 (2008) 303–320. doi:10.1080/13604810802479126.
- [74] S. Alawadhi, A. Aldama-Nalda, H. Chourabi, J.R. Gil-Garcia, S. Leung, S. Mellouli, T. Nam, T.A. Pardo, H.J. Scholl, S. Walker, Building Understanding of Smart City Initiatives, in: *Lecture Notes in Computer Science (Including Subseries Lecture Notes in Artificial Intelligence and Lecture Notes in Bioinformatics)*, 2012: pp. 40–53. doi:10.1007/978-3-642-33489-4_4.
- [75] D. Evans, The Internet of Things Infographics, (2011). doi:10.5480/1536-5026-34.1.63.
- [76] G. Lilis, G. Conus, N. Asadi, M. Kayal, Towards the Next Generation of Intelligent Building: An Assessment Study of Current Automation and Future IoT Based Systems with a Proposal for Transitional Design, *Sustainable Cities and Society*. 28 (2017) 473–481. doi:10.1016/j.scs.2016.08.019.
- [77] M. Swan, Sensor Mania! The Internet of Things, Wearable Computing, Objective Metrics, and the Quantified Self 2.0, *Journal of Sensor and Actuator Networks*. 1 (2012) 217–253. doi:10.3390/jsan1030217.
- [78] V.L. Erickson, S. Achleitner, A.E. Cerpa, POEM: Power-efficient Occupancy Energy Management System, *Proceedings of the 12th International Conference on Information Processing in Sensor Networks - IPSN '13*. (2013) 203–203. doi:10.1145/2461381.2461407.

- [79] S.C. Kim, Y.S. Jeong, S.O. Park, RFID-Based Indoor Location Tracking to Ensure the Safety of the Elderly in Smart Home Environments, *Personal and Ubiquitous Computing*. 17 (2013) 1699–1707. doi:10.1007/s00779-012-0604-4.
- [80] E. Lee, High-Performance Commercial Building Façades, Lawrence Berkeley National Laboratory. (2006) 133–133.
- [81] P.C. Thomas, S. Moller, HVAC System Size – Getting it Right, Clients Driving Innovation: Moving Ideas into Practice. (2006) 12–14.
- [82] D. Uckelmann, M. Harrison, F. Michahelles, *Architecting the Internet of Things*, Springer Berlin Heidelberg, Berlin, Heidelberg, 2011. doi:10.1007/978-3-642-19157-2.
- [83] Y. Yoshimura, A. Amini, S. Sobolevsky, J. Blat, C. Ratti, Analysis of Pedestrian Behaviors Through Non-Invasive Bluetooth Monitoring, *Applied Geography*. 81 (2017) 43–51. doi:10.1016/j.apgeog.2017.02.002.
- [84] S. Ahn, S. Lee, M. Park, Exploring Absenteeism Control Policies with Awareness of the Effect of Group Norms on Absence Behavior, Using Agent-Based Modeling, in: *Construction Research Congress 2012*, American Society of Civil Engineers, 2012: pp. 1450–1459. doi:10.1061/9780784412329.146.
- [85] D. Shin, A socio-technical framework for Internet-of-Things design: A human-centered design for the Internet of Things, *Telematics and Informatics*. 31 (2014) 519–531. doi:10.1016/j.tele.2014.02.003.
- [86] K. Akkaya, I. Guvenc, R. Aygun, N. Pala, A. Kadri, IoT-based Occupancy Monitoring Techniques for Energy-Efficient Smart Buildings, in: *2015 IEEE Wireless Communications and Networking*, 2015: pp. 58–63.
- [87] P. Suresh, J.V. Daniel, V. Parthasarathy, R. Aswathy, A state of the art review on the Internet of Things (IoT) history, technology and fields of deployment, in: *IEEE*, 2014: pp. 1–8.
- [88] G.J. Pottie, W.J. Kaiser, Wireless integrated network sensors, *Communications of the ACM*. 43 (2000) 51–58.

- [89] L.K. Alazzawi, A.M. Elkateeb, A. Ramesh, W. Aljuhar, Scalability analysis for wireless sensor networks routing protocols, in: IEEE, 2008: pp. 139–144.
- [90] McNeel, RhinoScript Wiki [McNeel Wiki], (n.d.).
<https://wiki.mcneel.com/developer/rhinoscript> (accessed December 10, 2017).
- [91] 800 Bell Street, Houston | 117636 | EMPORIS, (n.d.).
<https://www.emporis.com/buildings/117636/800-bell-street-houston-tx-usa>
(accessed May 10, 2018).
- [92] 2929 Wesleyan - The Skyscraper Center, (n.d.).
<http://www.skyscrapercenter.com/building/2929-wesleyan/15113> (accessed May 7, 2018).
- [93] Museum Tower - The Skyscraper Center, (n.d.).
<http://www.skyscrapercenter.com/building/museum-tower/2700> (accessed May 10, 2018).
- [94] Heritage Plaza - The Skyscraper Center, (n.d.).
<http://www.skyscrapercenter.com/building/heritage-plaza/1079> (accessed May 10, 2018).
- [95] 717 Harwood, Dallas | 42Floors, (n.d.). <https://42floors.com/us/tx/dallas/717-n-harwood-st> (accessed May 10, 2018).
- [96] Rhino for Windows, (1980). <https://www.rhino3d.com/> (accessed August 28, 2018).
- [97] J. Wienold, J. Christoffersen, Evaluation methods and development of a new glare prediction model for daylight environments with the use of CCD cameras, *Energy and Buildings*. 38 (2006) 743–757.
- [98] J.A. Jakubiec, C.F. Reinhart, DIVA 2.0: Integrating daylight and thermal simulations using rhinoceros 3D, DAYSIM and EnergyPlus, *Proceedings of Building Simulation 2011: 12th Conference of International Building Performance Simulation Association*. (2011) 2202–2209.

- [99] C.F. Reinhart, P.-F. Breton, Experimental validation of 3ds Max® Design 2009 and Daysim 3.0, Draft Manuscript Submitted to Building Simulation. (2009).
- [100] G.W. Larson, *Rendering with Radiance: The Art and Science of Lighting Visualization*, Morgan Kaufmann, 1998.
<http://books.google.com/books?id=DUpSAAAAMAAJ>.
- [101] M. Rubin, R. Powles, K. Von Rottkay, Models for the angle-dependent optical properties of coated glazing materials, *Solar Energy*. 66 (1999) 267–276.
- [102] A. Borisuit, J.-L. Scartezzini, A. Thanachareonkit, Visual discomfort and glare rating assessment of integrated daylighting and electric lighting systems using HDR imaging techniques, *Architectural Science Review*. 53 (2010) 359–373.
- [103] J.J. McCann, A. Rizzi, Camera and visual veiling glare in HDR images, *Journal of the Society for Information Display*. 15 (2007) 721–730.
- [104] K. Van Den Wymelenberg, M. Inanici, A Critical Investigation of Common Lighting Design Metrics for Predicting Human Visual Comfort in Offices with Daylight, *Leukos*. 10 (2014) 145–164. doi:10.1080/15502724.2014.881720.
- [105] R. Labib, J.C. Baltazar, Analysis and quantification of visual glare caused by photovoltaic panels installations in urban canyons, (n.d.).
- [106] M. Hirning, G. Isoardi, S. Coyne, I. Cowling, Applying the use of high dynamic range imaging pipelines to discomfort glare research, in: *Proceedings of CIE*, 2010: p. 767e75.
- [107] K.V.D. Wymelenberg, M.N. Inanici, P. Johnson, The Effect of Luminance Distribution Patterns on Occupant Preference in a Daylit Office Environment, *Journal of the Illuminating Engineering Society of North America*. 7 (2010) 103–122. doi:10.1582/LEUKOS.2010.07.02003.
- [108] NSF, Home - XSEDE, (n.d.). <https://www.xsede.org/> (accessed August 29, 2018).

- [109] Skvark, opencv-python, PyPI. (2008). <https://pypi.org/project/opencv-python/> (accessed September 7, 2018).

APPENDIX A

THE XSEDE HIGH PERFORMANCE COMPUTING ENVIRONEMNT

SYSTEM COMPONENT CONFIGURATION	
<i>Intel Haswell Standard Compute Nodes</i>	
Node count	1,944
Clock speed	2.5 GHz
Cores/node	24
DRAM/node	128 GB
SSD memory/node	320 GB
<i>NVIDIA Kepler K80 GPU Nodes</i>	
Node count	36
CPU cores:GPUs/node	24:4
CPU:GPU DRAM/node	128 GB:40 GB
<i>NVIDIA Pascal P100 GPU Nodes</i>	
Node count	36
CPU cores:GPUs/node	28:4
CPU:GPU DRAM/node	128 GB:40 GB

Figure 27 The technical specifications of the XSEDE HPC platform

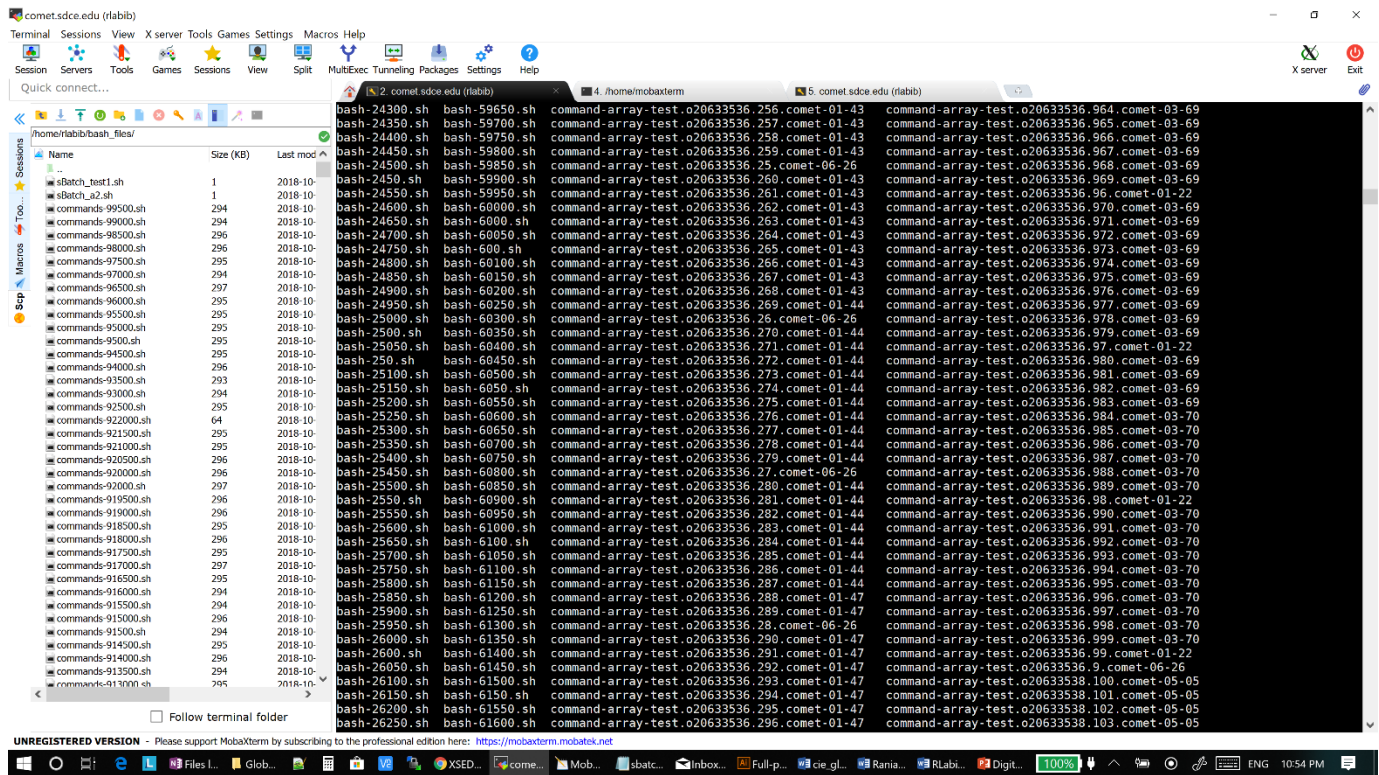


Figure 29 A list of bash files that contain Radiance commands

FAÇADE INTERNET OF THINGS (F+IoT): HUMAN-SENSING FAÇADE-COMMUNICATION APPROACH FOR VISUAL AND THERMAL COMFORT | TG-CDA160011

(INACTIVE)

Allocations

Hide Expired/Inactive Allocations

Show Publications

Principal Investigator: Rania Labib







Resource	Active Until	Used	My Usage	Burn Rate
Oasis Inactive/new	Jul 31, 2017	0.0 / 500.0 SUs  View usage	0.0 SUs	0% of recommended average
Oasis Inactive/supplement	Apr 29, 2019	0.0 / 500.0 SUs  View usage	0.0 SUs	0% of recommended average
Comet Inactive/new	Jul 31, 2017	0.0 / 25000.0 SUs  View usage	0.0 SUs	0% of recommended average
Comet Inactive/supplement	Apr 29, 2019	15287.0 / 23000.0 SUs  View usage	15287.0 SUs	64% of recommended average
Bridges Inactive/renewal	Apr 29, 2019	0.0 / 12000.0 SUs  View usage	0.0 SUs	0% of recommended average
Bridges Pylon Inactive/renewal	Apr 29, 2019	0.0 / 500.0 SUs  View usage	0.0 SUs	0% of recommended average

Figure 30 The computing resources that are available to the author through XSEDE, over 15000 of computing hours were used for the purpose of this research study (shown in the red box), this is equal to about two years of computing time

```
1  #!/usr/bin/env bash
2
3  #SBATCH --job-name="command-array-test"
4  #SBATCH --output="command-array-test.o%A.%a.%N"
5  #SBATCH --partition=shared
6  #SBATCH --nodes=1
7  #SBATCH --ntasks-per-node=1
8  #SBATCH --time=00:05:00
9  #SBATCH --export=ALL
10 #SBATCH --no-requeue
11 #SBATCH --array=0-1000
12
13 command_index=$(( 500*${SLURM_ARRAY_TASK_ID} ))
14 "/home/rlabib/bash_files/commands-${command_index}.sh"
15
```

Figure 31 Example batch job that is submitted to the XSEDE platform, the batch job facilitated running 1000 tasks parallelly on individual computing nodes

APPENDIX B
PYTHON CODE

1- Custom Python script to organize and sort Radiance commands into Linux-based bash files

```
1. import os
2. import sys
3. import shutil
4.
5. iterationsPath = "C:\ladybug\glare"
6. uploadLocation = "/home/rlabib/downloads/glaresimulations/"
7. skyUploadLocation = "/home/rlabib/downloads/simulations/skies/"
8. #skyPath = "C:\ladybug\skylib\climateBasedSkies\Houston_Bush_Intercontinental_TX_USA"
9. skyPath = "C:\ladybug\skylib\climateBasedSkies\Philadelphia_International_Ap_PA_USA"
10. bashFiles = r"C:\Users\RANIA\Desktop\diss_test\glare"
11.
12. skyFileNames = []
13. for root, subFolders, files in os.walk(skyPath):
14.     for file in files:
15.         skyFileNames.append(file)
16.
17. allIterationsPaths = []
18. allIterationsNames = []
19. for item in os.listdir(iterationsPath):
20.     x = os.path.join(iterationsPath, item)
21.     allIterationsPaths.append(x)
22.     allIterationsNames.append(item)
23.
24. i = 1
25. for root, subFolders, files in os.walk(skyPath):
26.     for skyfile in files:
27.         for folder in allIterationsPaths:
28.             folder_index = allIterationsPaths.index(folder)
```

```

29.         for root, subFolders, files in os.walk(folder):
30.             sh_file = open(bashFiles + "/" + "%d.sh" % int(i), 'w')
31.             m = folder.replace("C:\\ladybug\\", uploadLocation)
32.             d = m.replace("\\", "/")
33.             fPath = d + "/imageBasedSimulation/"
34.             sh_file.close()
35.
36.         for file in files:
37.             if file.endswith('Init.bat'):
38.
39.                 with open(os.path.join(root, file), 'r') as fRead:
40.                     all_lines = fRead.readlines()
41.                     fLine1 = all_lines[4]
42.                     rpict =all_lines[5]
43.                     last_line = all_lines[6]
44.                     splitLine = fLine1.split(" ")
45.                     skyName = skyUploadLocation + skyfile
46.                     rpictLine = rpict.split(" ")
47.                     oldOctFileName = splitLine[-1]
48.                     newOctFileName = oldOctFileName.split(".oct")[0] + "_" + skyfile + ".oct"
49.
50.                     rad_index_list = []
51.                     for word_5 in splitLine:
52.                         if ".rad" in word_5:
53.                             rad_wordIndex_5 = splitLine.index(word_5)
54.                             rad_index_list.append(rad_wordIndex_5)
55.                         if ".oct" in word_5:
56.                             oct_wordIndex_5= splitLine.index(word_5)
57.                         if ".sky" in word_5:
58.                             sky_wordIndex_5= splitLine.index(word_5)
59.
60.                     rad_split_word_5 = splitLine[rad_wordIndex_5].split(".")[0]
61.                     oct_split_word_5 = splitLine[oct_wordIndex_5].split(".")[0]
62.                     new_first_rad_split_word1 = splitLine[rad_index_list[0]].split("/")[-1]
63.                     new_second_rad_split_word1 = splitLine[rad_index_list[1]].split("/")[-1]
64.
65.
66.                     line_a = fLine1.replace(splitLine[rad_index_list[0]],new_first_rad_split_word1+ s
kyfile+".rad")

```

```

67.         line_1 = line_a.replace(splitLine[rad_index_list[1]],new_second_rad_split_word1+
skyfile+".rad")
68.         line_1_1 = line_1.replace(splitLine[oct_wordIndex_5],oct_split_word_5 + skyfile+"
.oct" )
69.         line_1_1_1 = line_1_1.replace(splitLine[sky_wordIndex_5], skyName)
70.
71.         for word in rpictLine:
72.             if ".amb" in word:
73.                 amb_wordIndex = rpictLine.index(word)
74.             if ".oct" in word:
75.                 oct_wordIndex= rpictLine.index(word)
76.             if ".unf" in word:
77.                 unf_wordIndex= rpictLine.index(word)
78.
79.         amb_split_word = rpictLine[amb_wordIndex].split(".")[0]
80.         oct_split_word = rpictLine[oct_wordIndex].split(".")[0]
81.         unf_split_word = rpictLine[unf_wordIndex].split(".")[0]
82.         new_rpict_line_1= rpict.replace(rpictLine[amb_wordIndex],amb_split_word + skyfile
+ ".amb")
83.         new_rpict_line_2 = new_rpict_line_1.replace(rpictLine[oct_wordIndex], newOctFileN
ame)
84.         final_rpict_line_3 = new_rpict_line_2.replace(rpictLine[unf_wordIndex],unf_split_
word + skyfile+".unf")
85.         new_Last_line = last_line.replace(last_line.split(" ")[1],unf_split_word + skyfil
e+".unf")
86.
87.         with open(bashFiles+ "/" + "%d.sh" % int(i), 'r+') as the_file:
88.             the_file_lines = the_file.readlines() # old content
89.             the_file.seek(0)
90.             the_file.write('export PATH=$PATH:./home/rlabib/installs/ray/bin\n')
91.             the_file.write('export RAYPATH=./home/rlabib/installs/ray/lib\n')
92.             the_file.write("cd " + fPath + '\n')
93.             the_file.write(line_1_1_1 + '\n')
94.             the_file.write(final_rpict_line_3 + '\n')
95.             the_file.write(new_Last_line + '\n')
96.             for line in the_file_lines:
97.                 the_file.write(line) #old content
98.
99.         if file.endswith('IMG.bat'):

```

```

100.                 with open(os.path.join(root, file), 'r') as lRead:
101.                     commandLine = lRead.readlines()[4]
102.                     rpictLine_1= commandLine.split(" ")
103.
104.                     for word_1 in rpictLine_1:
105.                         if ".amb" in word_1:
106.                             amb_wordIndex_1 = rpictLine_1.index(word_1)
107.                         if ".oct" in word_1:
108.                             oct_wordIndex_1= rpictLine_1.index(word_1)
109.                         if ".unf" in word_1:
110.                             unf_wordIndex_1= rpictLine_1.index(word_1)
111.
112.                     amb_split_word_1 = rpictLine_1[amb_wordIndex_1].split(".")[0]
113.                     oct_split_word_1 = rpictLine_1[oct_wordIndex_1].split(".")[0]
114.                     unf_split_word_1 = rpictLine_1[unf_wordIndex_1].split(".")[0]
115.                     new_rpict_line_1_1= commandLine.replace(rpictLine_1[amb_wordIndex_1],amb_split_wor
rd_1+ skyfile+".amb")
116.                     new_rpict_line_2_1 = new_rpict_line_1_1.replace(rpictLine_1[oct_wordIndex_1], amb
_split_word_1+"_"+skyfile+".oct")
117.                     final_rpict_line_3_1 = new_rpict_line_2_1.replace(rpictLine_1[unf_wordIndex_1],un
f_split_word_1 + skyfile+".unf")
118.
119.                     with open(bashFiles+ "/" + "%d.sh" % int(i), 'a+') as the_file:
120.                         the_file.write(final_rpict_line_3_1 + '\n')
121.                         the_file.close()
122.
123.                 if file.endswith('PCOMP.bat'):
124.                     with open(os.path.join(root, file), 'r') as pRead:
125.                         all_lines_p =pRead.readlines()
126.                         first_line = all_lines_p[4]
127.                         second_line = all_lines_p[5]
128.                         first_line_split= first_line.split(" ")
129.                         second_line_split = second_line.split(" ")
130.
131.                     for word_2 in first_line_split:
132.                         if ".unf" in word_2:
133.                             unf_wordIndex_2= first_line_split.index(word_2)
134.                         if ".HDR" in word_2:
135.                             HDR_wordIndex_2= first_line_split.index(word_2)

```



```

136.
137.         unf_split_word2 = first_line_split[unf_wordIndex_2].split(".")[0]
138.         HDR_split_word2 = first_line_split[HDR_wordIndex_2].split(".")[0]
139.         new_first_line_1= first_line.replace(first_line_split[unf_wordIndex_2],unf_split_
word2+ skyfile+".unf")
140.         final_first_line= new_first_line_1.replace(first_line_split[HDR_wordIndex_2],HDR_
split_word2+ skyfile+".HDR")
141.
142.         for word_3 in second_line_split:
143.             if "temp.HDR" in word_3:
144.                 HDR_wordIndex_3= second_line_split.index(word_3)
145.                 if ".HDR" in word_3 and "temp" not in word_3:
146.                     HDR_wordIndex_4 = second_line_split.index(word_3)
147.
148.                 HDR_split_word3 = second_line_split[HDR_wordIndex_3].split(".")[0]
149.                 HDR_split_word4 = second_line_split[HDR_wordIndex_4].split(".")[0]
150.
151.                 second_line_alt= second_line.replace(second_line_split[HDR_wordIndex_3],HDR_split
_word3+ skyfile+".HDR")
152.                 final_second_line = second_line_alt.replace(second_line_split[HDR_wordIndex_4], H
DR_split_word4+ skyfile+".HDR" )
153.
154.                 with open(bashFiles+ "/" + "%d.sh" % int(i), 'a+') as the_file:
155.                     the_file.write(final_first_line + '\n')
156.                     the_file.write(final_second_line + '\n')
157.                     the_file.close()
158.
159.             i = i+1

```

2- Custom Python script to Upload Bash files to the HPC cluster

```
1.  import paramiko
2.  import sys
3.  import os
4.
5.  host = "comet.sdsc.edu"
6.  username= "rlabib"
7.  password = "*****"
8.  port= 22
9.  ##SSH_COMMAND = "sbatch test.bashrc"
10.
11.  transport = paramiko.Transport((host, port))
12.  transport.connect(username = username, password = password)
13.  sftp = paramiko.SFTPClient.from_transport(transport)
14.
15.  def put(localfile,remotefile):
16.      # Copy localfile to remotefile, overwriting or creating as needed.
17.      sftp.put(localfile,remotefile)
18.
19.  def put_all(localpath,remotepath):
20.      remotepath = remotepath.replace('\\', '/')
21.      # recursively upload a full directory
22.      os.chdir(os.path.split(localpath)[0])
23.      parent=os.path.split(localpath)[1]
24.      for walker in os.walk(parent):
25.          try:
26.              sftp.mkdir(os.path.join(remotepath,walker[0]).replace('\\', '/'))
27.          except:
28.              pass
29.          for file in walker[2]:
30.              put(os.path.join(walker[0],file).replace('\\', '/'),os.path.join(remotepath,walker[0],file).r
eplace('\\', '/'))
31.
32.  put_all("C:\Users\RANIA\Desktop\Test_file", "/home/rlabib")
33.  sftp.close()
34.  transport.close()
```

```
35. print "Done transferring files"
```

3- Custom Python/HTML script to Visualize annual DGP values

```
1. import os
2. import sys
3. import cgi
4.
5. rootdir1 = "C:\Users\Rania\Google Drive\PhD_diss\Glazed_Facade"
6.
7. viewNum_list = ['View Number']
8. month_list = ['Month']
9. day_list = ['Day']
10. hour_list = ['Hour']
11. dgp_list = ['DGP']
12. dgp_key = ['Glare type']
13. list_of_hours = ['6.000', '7.000', '8.000', '9.000', '10.000', '11.000', '12.000', '13.000', '14.000', '15.000', '16.000', '17.000', '18.000']
14.
15. for root, subFolders, files in os.walk(rootdir1):
16.     for file in files:
17.         if file.endswith('dgp'):
18.             with open(os.path.join(root, file), 'r') as fin:
19.                 fileNameSplit = file.split('_')
20.                 viewNumber = fileNameSplit[0]
21.                 html_str = """<html>
22.
23. <body>
24. <script src="https://ajax.googleapis.com/ajax/libs/jquery/1.9.0/jquery.min.js"></script>
25. <script src="https://code.highcharts.com/highcharts.js"></script>
26. <script src="https://code.highcharts.com/modules/data.js"></script>
27. <script src="https://code.highcharts.com/modules/heatmap.js"></script>
```

```

28. <script src="https://code.highcharts.com/modules/exporting.js"></script>
29. <div id="container" style="height: 320px; width: 1000px; margin: 0 auto"></div>
30. <!-- Source: http://vikjavev.no/ver/highcharts-demos/heatmap.csv.php?year=2013 -->
31. <pre id="csv" style="display: none">Date,Time,Temperature\n""
32.
33.         for line in fin:
34.             line_text = line.split(" ")
35.             month = line_text[0]
36.             day = line_text[1]
37.             hour = line_text[2]
38.             dgp_text = line_text[4]
39.             dgp = float(dgp_text)
40.
41.             if str(hour) in list_of_hours:
42.                 data= "2013-"+str(month)+"-"+str(day)+","+str(hour)[:4]+","+str(dgp_text)
43.                 html_str += data
44.             html_str += ""</pre>\n
45.         <script>
46.             $(function () {
47.
48.                 (function (H) {
49.                     var Series = H.Series,
50.                         each = H.each;
51.
52.
53.                     Series.prototype.getContext = function () {
54.                         if (!this.canvas) {
55.                             this.canvas = document.createElement('canvas');
56.                             this.canvas.setAttribute('width', this.chart.chartWidth);
57.                             this.canvas.setAttribute('height', this.chart.chartHeight);
58.                             this.image = this.chart.renderer.image('', 0, 0, this.chart.chartWidth, this.chart.chartHeight).add(this.group);
59.                             this.ctx = this.canvas.getContext('2d');
60.                         }
61.                         return this.ctx;
62.                     };
63.
64.                     Series.prototype.canvasToSVG = function () {
65.                         this.image.attr({ href: this.canvas.toDataURL('image/png') });

```

```

66.         };
67.
68.
69.         H.wrap(H.seriesTypes.heatmap.prototype, 'drawPoints', function () {
70.
71.             var ctx = this.getContext();
72.
73.             if (ctx) {
74.
75.                 // draw the columns
76.                 each(this.points, function (point) {
77.                     var plotY = point.plotY,
78.                         shapeArgs;
79.
80.                     if (plotY !== undefined && !isNaN(plotY) && point.y !== null) {
81.                         shapeArgs = point.shapeArgs;
82.
83.                         ctx.fillStyle = point.color;
84.                         ctx.fillRect(shapeArgs.x, shapeArgs.y, shapeArgs.width, shapeArgs.height);
85.                     }
86.                 });
87.
88.                 this.canvasToSVG();
89.
90.             } else {
91.                 this.chart.showLoading('Your browser doesnt support HTML5 canvas, <br>please use a modern bro
92. wser');
93.
94.             }
95.         });
96.         H.seriesTypes.heatmap.prototype.directTouch = false; // Use k-d-tree
97.     }(Highcharts));
98.
99.
100.    var start;
101.    $('#container').highcharts({
102.        credits: {
103.            enabled: false

```

```
104.     },
105.
106.     data: {
107.         csv: document.getElementById('csv').innerHTML,
108.         parsed: function () {
109.             start = +new Date();
110.         }
111.     },
112.
113.     chart: {
114.         type: 'heatmap',
115.         margin: [60, 10, 80, 50]
116.     },
117.
118.     title: {
119.         text: '',
120.         align: 'left',
121.         x: 40
122.     },
123.
124.     subtitle: {
125.         text: '',
126.         align: 'left',
127.         x: 40
128.     },
129.
130.     xAxis: {
131.         type: 'datetime',
132.         min: Date.UTC(2013, 0, 1),
133.         max: Date.UTC(2014, 0, 1),
134.         labels: {
135.             align: 'left',
136.             x: 5,
137.             y: 14,
138.             format: '{value:%B}' // long month
139.         },
140.         showLastLabel: false,
141.         tickLength: 16
142.     }
```

```
143.     },
144.
145.     yAxis: {
146.         title: {
147.             text: null
148.         },
149.         labels: {
150.             format: '{value}:00'
151.         },
152.         minPadding: 0,
153.         maxPadding: 0,
154.         startOnTick: false,
155.         endOnTick: false,
156.         tickPositions: [6, 8, 10, 12, 14,16],
157.         tickWidth: 1,
158.         min: 6,
159.         max: 18,
160.         reversed: true
161.     },
162.
163.     colorAxis: {
164.         stops: [
165.             [0, '#3060cf'],
166.             [0.2, '#ffffbc'],
167.             [0.6, '#d67d74'],
168.             [0.8, '#c4463a'],
169.             [1, '#c4463a']
170.         ],
171.         min: .2,
172.         max: .8,
173.         startOnTick: false,
174.         endOnTick: false,
175.         labels: {
176.             format: '{value}'
177.         }
178.     },
179.
180.     series: [{
181.         borderWidth: 0,
```

```

182.         nullColor: '#EFEFEF',
183.         colsize: 24 * 36e5, // one day
184.         tooltip: {
185.             headerFormat: 'Temperature<br/>',
186.             pointFormat: '{point.x:%e %b, %Y} {point.y}:00: <b>{point.value} ?</b>'
187.         },
188.         turboThreshold: Number.MAX_VALUE // #3404, remove after 4.0.5 release
189.     }]}
190.
191.     });
192.     console.log('Rendered in ' + (new Date() - start) + ' ms'); // eslint-disable-line no-console
193.
194. });
195.
196. </script>
197. </body>
198. </html>""
199.         html_file_name = "C:\Users\Rania\Google Drive\ABS 2016\Results\Glazed_Facade_HeatMaps\Glazed_
Facade_" + str(
200.             viewNumber) + "_heatmap.html"
201.         f = open(html_file_name, 'w')
202.         f.write(html_str)
203.     f.close()

```


4- custom Python Script inside a Custom-made Grasshopper to calculate the HOY when the sun hits the reflective façade

```
1. # component is made by Rania Labib
2. # Icon credit: flaticon.com
3. """
4. Use with Ladybug bounceFromSurface component to account for obstructing surfaces (i.e. buildings) that might block sunrays from reaching the investigated surface. This component also calculates the intersection of the last bounced ray with an analysis surface(s), this could be helpful when assessing the effect of reflective facades on other facades (analysis surface(s)) for visual comfort and glare studies.
5.
6.     Args:
7.     rays: Connect to rays output from Ladybug's bounceFromSurface component
8.     obstructingSrfs: Breps of buildings and nearby objects that might act as shading surfaces
9.     analysisSrfs : A facade of a building where last bounce of sunrays might intersect with
10.
11.     Returns:
12.     intersectionPts: A list of points of the intersection between the first bounce of rays and the shading breps
13.     newUnobstructedRays: A list of rays that are unobstructed by shading surfaces, such as nearby buildings.
14.     obstructedRays : A list of rays that are blocked by shading surface, such as nearby buildings
15.     lastUnobstructedSegments: A list of line segments that represent the last bounce of unobstructed sunrays
16.     analysisPts: A list of points where the last bounce of unobstructed rays intersect with an analysis facades.
17. """
18.
19. ghenv.Component.Name = "Shading and Reflection Analysis"
20. ghenv.Component.NickName = 'shadingAndReflectionAnalysis'
21. ghenv.Component.IconDisplayMode = ghenv.Component.IconDisplayMode.application
22. ghenv.Component.Category = "Labib"
23.
24. import Rhino as rc
25. import rhinoscriptsyntax as rs
26. import itertools
27. import scriptcontext as sc
28. import ghpythonlib.components as ghcomp
```

```

29. import Grasshopper.Kernel as gh
30.
31. if (rays and rays[0] != None) and (analysisSrfs and analysisSrfs[0] !=None) and runIt == True:
32.     #Explode rays into line segments
33.     notNullRays = []
34.     explodedRays1 = []
35.     explodedRays = []
36.
37.     for r in rays:
38.         if r:
39.             exp_Rays = rs.ExplodeCurves(r)
40.             explodedRays1.append(exp_Rays)
41.             notNullRays.append(r)
42.         else:
43.             pass
44.         #flatten list
45.         for sublist in explodedRays1:
46.             for item in sublist:
47.                 explodedRays.append(item)
48.
49.
50.     numberOfSegments = int(len(explodedRays)/len(notNullRays))
51.
52.     segments = []
53.     for x in range(numberOfSegments):
54.         segment = explodedRays[x][::numberOfSegments]
55.         segments.append(segment)
56.
57.     #Solve lines and obstructing surfaces intersection
58.     intersectionPoints = []
59.
60.     xx = rc.Geometry.Brep.MergeBreps(obstructingSrfs, .0001)
61.
62.     print len(segments)
63.     print len(segments[0])
64.     print numberOfSegments
65.
66.
67.     for l in segments[0]:

```

```

68.     newLine= rs.coercecurve(1)
69.     #newLine = rc.Geometry.Curve.TryGetPolyline(rs.coerce2dpoint(line))
70.     allIntersectionPts = rc.Geometry.Intersect.Intersection.CurveBrep(newLine, xx , .01)
71.     intersectionPoints.append(allIntersectionPts[2])
72.
73.     intersectionPts1 = []
74.     # iterate over the nested list
75.     for arr in intersectionPoints:
76.         # use array if it is not empty
77.         if arr.Count != 0:
78.             # convert array to list and extend new_list
79.             intersectionPts1.extend([arr])
80.
81.
82.     #get index of rays intersecting with obstructingSrfs
83.     intersectIndex = []
84.     notIntersectIndex = []
85.
86.     for i, j in enumerate(intersectionPoints):
87.         if len(j) == 0:
88.             notIntersectIndex.append(i)
89.         else:
90.             intersectIndex.append(i)
91.
92.     newUnobstructedRays = [rays[i] for i in notIntersectIndex]
93.     obstructedRays = [rays[i] for i in intersectIndex]
94.
95.     newSegments= []
96.     for x in range(numberOfSegments):
97.         newList = [segments[x][i] for i in notIntersectIndex]
98.         newSegments.append(newList)
99.
100.         lastUnobstructedSegments = []
101.         for o in newSegments[-1]:
102.             c = rs.coercecurve(o)
103.             lastUnobstructedSegments.append(c)
104.
105.         analysisIntersectionPoints = []
106.         for l in lastUnobstructedSegments:

```

```

107.         for s in analysisSrfs:
108.             lines = rs.coercecurve(1)
109.             newIntersectionPts = rc.Geometry.Intersect.Intersection.CurveBrep(lines,s, .0001)
110.             analysisIntersectionPoints.append(newIntersectionPts[2])
111.
112.             #list of points of intersection between unobstructed layers and the analysisSrfs (i.e. facade)
113.             analysisPts = list(itertools.chain.from_iterable(analysisIntersectionPoints))
114.             intersectionPts = list(itertools.chain.from_iterable(intersectionPts1))
115.             readMe = "Process completed"
116.
117.         else:
118.             readMe= "Provide rays and valid analysis surface(s). Set toggle to True...."
119.             ghenv.Component.AddRuntimeMessage(gh.GH_RuntimeMessageLevel.Warning, "Provide rays and valid analysis sur
face(s). Set toggle to True....")

```

5- Computer vision recognition for HDR image analysis

```

1. import cv2
2. import matplotlib.pyplot as plt
3. import numpy as np
4.
5. filename_image = 'c-11-17-13.tif'
6. filename_mask = 'c-prefered-mask.tif'
7. print 'OpenCV version used', cv2.__version__
8. filename = open("Output_C.txt","w")
9. filename.write("Processing Image : " + str(filename_image) + '\n\n')
10. def get_contour_precedence(contour, cols):

```

```

11.     tolerance_factor = 10
12.     origin = cv2.boundingRect(contour)
13.     return ((origin[1] // tolerance_factor) * tolerance_factor) * cols + origin[0]
14.
15. p_mask_c = cv2.cvtColor(cv2.resize(cv2.imread(filename_mask),(800,800)),cv2.COLOR_RGB2HSV);
16. b_image_1 = cv2.resize(cv2.imread(filename_image),(800,800));
17. cv2.imshow("c_mask_preferred",p_mask_c)
18. cv2.waitKey();
19. b = 0;
20. g = 255;
21. r = 0;
22. target_color = np.uint8([[b, g, r]])
23. target_color_hsv = cv2.cvtColor(target_color, cv2.COLOR_BGR2HSV)
24. target_color_h = target_color_hsv[0,0,0]
25. tolerance = 20
26. lower_hsv = np.array([max(0, target_color_h - tolerance), 10, 10])
27. upper_hsv = np.array([min(179, target_color_h + tolerance), 250, 250])
28. mask = cv2.inRange(p_mask_c, lower_hsv, upper_hsv)
29. cv2.imshow("mask",mask)
30. cv2.waitKey()
31. b_mask = mask;
32. kernel = np.ones((5,5))
33. sharp = cv2.erode(b_mask,kernel, iterations=2)
34. contours, hierarchy = cv2.findContours(sharp,cv2.RETR_TREE,cv2.CHAIN_APPROX_SIMPLE)
35. print ' Number of contours', len(contours)
36. contours.sort(key=lambda x:get_contour_precedence(x, np.shape(b_mask)[0]))
37. label = 1;
38. b_image = b_image_1.copy();
39. temp =np.zeros(np.shape(b_image_1),np.uint8)
40. print ' size of temp',np.shape(temp), np.shape(b_image)
41. out_img = b_image_1.copy()
42.
43. for cnt in contours:
44.     cv2.drawContours(b_image_1,[cnt],0,(255,255,0), 1)
45.     (x, y), r = cv2.minEnclosingCircle(cnt)
46.     x = int(x)
47.     y = int(y)
48.     r = int(r)

```

```

49.     cv2.putText(b_image_1, "{}".format(label), (int(x) - 10, int(y)),cv2.FONT_HERSHEY_SIMPLEX, 0.6, (0, 0, 255), 2)
50.     cv2.drawContours(temp,[cnt],0,(255,255,255), -1)
51.     r = cv2.boundingRect(cnt)
52.     crop_img = b_image[r[1]:r[1]+r[3], r[0]:r[0]+r[2]]
53.     mean = cv2.mean(crop_img);
54.     mean = np.array(mean).reshape(-1,1)
55.     print ' Mean color', mean, np.shape(mean)
56.     if mean[1] < 50:
57.         cv2.putText(out_img, "M", (int(x) - 10, int(y)),cv2.FONT_HERSHEY_SIMPLEX, 0.6, (255, 0, 255), 1)
58.         filename.write("Block number #"+ str(label)+ ' is : ' + 'Magenta'+'\n');
59.     else:
60.         cv2.putText(out_img, "G", (int(x) - 10, int(y)),cv2.FONT_HERSHEY_SIMPLEX, 0.6, (255, 0, 255), 1)
61.         filename.write("Block number #"+ str(label)+ ' is : ' + 'Gray'+'\n');
62.     label = label+1;
63.
64. cv2.imwrite("Block_order_C.PNG",b_image_1)
65. cv2.imwrite("Out_img.PNG",out_img)
66. filename.close()
67. cv2.imshow("preferred",b_image_1)
68. cv2.waitKey()

```